Addis Ababa University

College of Natural and Computational Sciences

School of Earth Sciences

Geophysics Stream

APPLICATION OF INTEGRATED GEOPHYSICAL METHODS TO MAP GEOLOGICAL STRACTURES AND ASSESS THE GROUND WATER POTENTIAL OF THE LEGEDADI-LEGETAFO-AYAT PROSPECTIVE AREA

By: Mequanent Biazen

A Thesis Submitted to the School of Earth Sciences of Addis Ababa University in Partial Fulfillment of the Requirements for the Degree of Master of Science in Exploration Geophysics

Addis Ababa

May, 2015

Addis Ababa University

College of Natural and Computational Sciences

School of Earth Sciences

Geophysics Stream

Application of Integrated Geophysical Methods to Map Geological Structures and Assess the Groundwater Potential of the Legedadi-Legetafo-Ayat Prospective Area

By: Mequanent Biazen

School of Earth Sciences

Approved by board of examiners:

Dr. Balmwal Atnafu	_____	_____
Chairman	**Signature**	**Date**
Dr. Abera Alemu	_____	_____
Advisor	**Signature**	**Date**
Dr. Dessie Nedaw	_____	_____
Co-advisor	**Signature**	**Date**
Professor Tigistu Haile	_____	_____
Internal Examiner	**Signature**	**Date**
Dr. Bekele Abebe	_____	_____
External Examiner	**Signature**	**Date**

Acknowledgements

First and foremost I would like to thank God almighty for giving me this opportunity and help me in every aspect of my life. My hurtful gratitude goes to my advisor, Dr. Abera Alemu for his invaluable, in-depth comments and guidance. It was a pleasure to do this research under his supervision. I owe this thesis also to my co-advisor Dr. Dessie Nedaw.

I would like to thank the WWDSE, Geological Survey and AAWS organizations and all the staffs who contributed for my work. My special thanks go to Mr. Daniel Mamo for his invaluable support throughout this work.

Last but not the least; I would like thank my brother Damtachew Biazen for his special support, prayer and encouragement throughout my study.

Abstract

This MSc thesis work entitled "Application of integrated geophysical methods to map geological structures and assess the groundwater potential of the Legedadi-Legetafo-Ayat prospective area" located in Central Ethiopia, Oromia National Regional State, Finfine Area Special Zone of North Shewa Zone, and Berek Woreda. The objectives of the study are to explore deep high potential groundwater saturated zones and map geologic structural elements which act as a hydraulic barrier that impedes or enhance the movement of the groundwater. The work is being undertaken by Water Works Design and Supervision Enterprise (WWDSE). Mainly the study was studied to solve the shortage of water for the Addis Ababa City. Further, the work is aimed at determining the depth to water table and identification of drilling point through interpretation of the geophysical, geological and borehole data. Geophysical data have been measured, processed and interpreted in one and two dimensions using special software. The results of interpretation indicate that the study area composed of two aquifers, the first is the Upper Basalt aquifer has wide distribution and forms confined and unconfined aquifer system. The thickness of this formation is highly variable from more than 400 meters at Legetafo area to less than 50 meters in Becho plains and the second is Lower Basalt aquifer (LBA) which is composed of tertiary Tarmaber basalt composed of dominantly scoraceous basalt and Amba Aiba basalt. These lineaments can be group into four main systems based on their orientation .These are: NE-SW, NW-SE, N-S/NNE-SSW and E-W trending fracture systems.

Key words: Magnetic anomalies and Pseudo and Geo-electric section; Magnetic and electrical properties of Earth materials.

Table of Contents

List of Tables

List of Figures

List of Appendices

Acronyms

WWDSE	Water Works Design & Supervision Enterprise
VES	Vertical Electrical Sounding
nT	NanoTesla
M.a.s.l	Mean average sea level.
LLA	Legedadi-Legetafo-Ayat
EC	Electrical Conductivity
Km	Kilo meter
UTM	Universal Transverse Meridian
UTME	Universal Transverse Mercator Easting
UTMN	Universal Transverse Mercator Northing
Ω-m	Ohm-meter
AAWSA	Addis Ababa Water and Sewerage Authority
IGRF	International Geomagnetic Reference Field

Chapter One

Introduction

1.1 Background

Water is one of the basic needs to sustain life. Living things such as humans, animals and plants are dependent on water. Our bodies need to ingest water every day to continue functioning. Communities and individuals can exist without many things like shelter, even without food for a period, but they cannot be deprived of water and survive for more than a few days. Because of the intimate relationship between water and life, it plays a vital role in the development of community since reliable supply of water is an essential perquisite for the establishment of a permanent community. Access to clean water is a human right and a basic requirement for economic development. The safest kind of water supply is the use of groundwater.

Ground water plays an important role in Ethiopia as a major source of water for domestic uses, industries and livestock. One of the fundamental conditions for the growth and development of nations like Ethiopia is the certainly the progressive fulfillment of its most urgent water needs. Past and recent studies have shown that the most suitable solution to this problem is undoubtedly the rational utilization of surface water. In fact, due to great extent in territory, which is characterized by sporadic rainfall, the solution is a proper regimen control of the rivers by erecting dams, which can regulate the evaporation and supply water depending on local requirement. However, such interventions require a lot of money. In rural areas where more than 85% of the population lives water storage problems can be solved by proper utilization of groundwater. The first attempt to identify the main aquifers in various parts of Ethiopia, which is located in different geo-petro graphical environments and variable climate, is presented in order to give proper solution for water supply problem in arid and semi arid part of the country (Tamiru Alemayehu, 2006).

Since groundwater normally has a natural protection against pollution by the covering layers, only minor water treatment is required. The largest amount of water on Earth (97.2 %) is contained in the oceans and seas as a saline or salty water but only small amount of it (2.8 %) exist as fresh water on land. This fresh water found on land is distributed as ice caps and glaciers (76.43 %), groundwater and soil moisture (21.96 %), fresh-water lakes (0.32%), saline-lakes (0.29 %) and very small amount of it as

streams channels (0.004 %). The amount of fresh water which is available for domestic, industrial and agriculture purposes is very limited as compared to the total volume of water on the planet earth. Due to the above reasons, the search for ground water is vital as an immediate and sustainable solution to alleviate the scarcity of water for drinking and other domestic uses inmost part of the world as well as in Ethiopia.

In many developing countries there is not only a heavy reliance on groundwater as a primary drinking supply, either collected from shallow depth dug wells or from springs, but also as a supply of water for both agriculture and industrial use. The reliance on groundwater both in the developed and developing countries is such that it is necessary to ensure that there are significant quantities of water and that the water is of a high quality. In addition to being clean through the natural process of filtration while passing through geological formations and thus being suitable for domestic consumption, ground water provides with replenish able and pollution free natural resource. The use of geophysics for both groundwater resource mapping and for water quality evaluations has increased dramatically over the last 10 years in large part due to the rapid advances in microprocessors and associated numerical modeling solutions that facilitated the rapid acquisition and processing of data and their presentation in useful form. The use of geophysics for groundwater studies has also been stimulated in part by a desire to reduce the risk of drilling dry holes and also a desire to offset the costs associated with poor groundwater production. Today, the geophysicist also provides useful parameters for hydro geological modeling of both new groundwater supplies and for the evaluation of existing groundwater contamination. In this respect, the major objectives of this study are to identify potential areas for extraction of groundwater resources within the Legedadi-Legetafo-Ayat (LLA) area. Specifically, the technique employed involves Vertical Electrical Sounding surveys over the wider areas of the plain so as to get a general assessment of its groundwater resource and magnetic method for the identification of fault zones and sheared zones.

1.2 Description of the study area

1.2.1 Location

The Legetafo-Legedadi-Ayat prospective area is located in Oromia National Regional State, Fin fine Area Special Zone of North Shewa Zone, and Berek Woreda. Its catchment is located some 20-40 km east of Addis Ababa city. It is bounded, approximately, between geographic coordinates of longitude

(38^0 52’ 56” – 39^0 09’ 4”) E and latitude of (8^0 58’ 24” - 9^0 10’ 26”) N or in UTM (486961 – 596839) E and (991699 – 1011470) N. The total area of study area is more than 493.2 km^2.

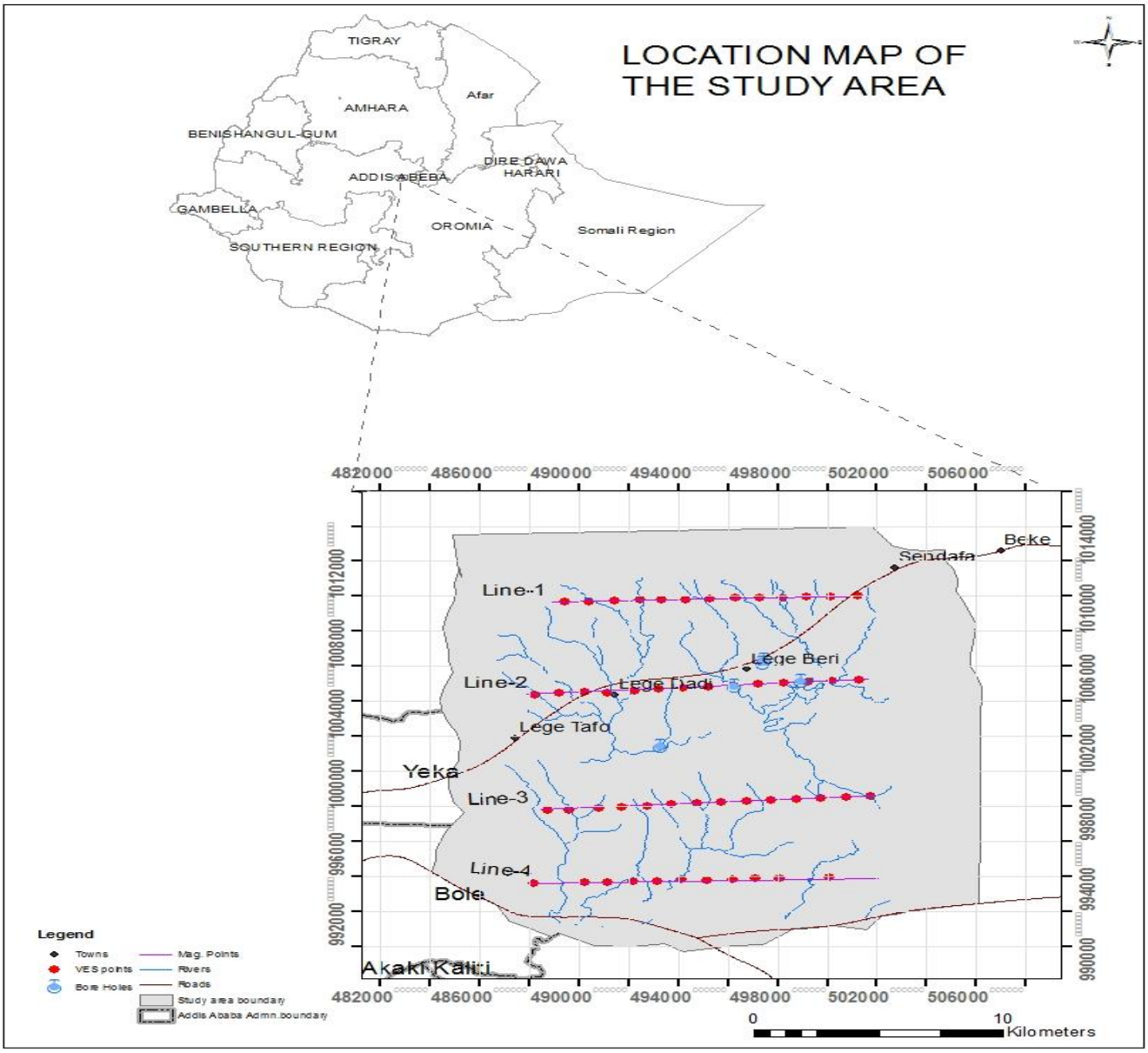

Figure 1. 1 Location of the study area.

1.2.2 Topography

The topography of the study area ranges from flat to undulating plains and hills. Most of the watershed is characterized by flat to undulating plains with altitudes ranging from 2640 and 2320 m above the mean sea level. Topographic map of the area is shown in fig. 2.2 below.

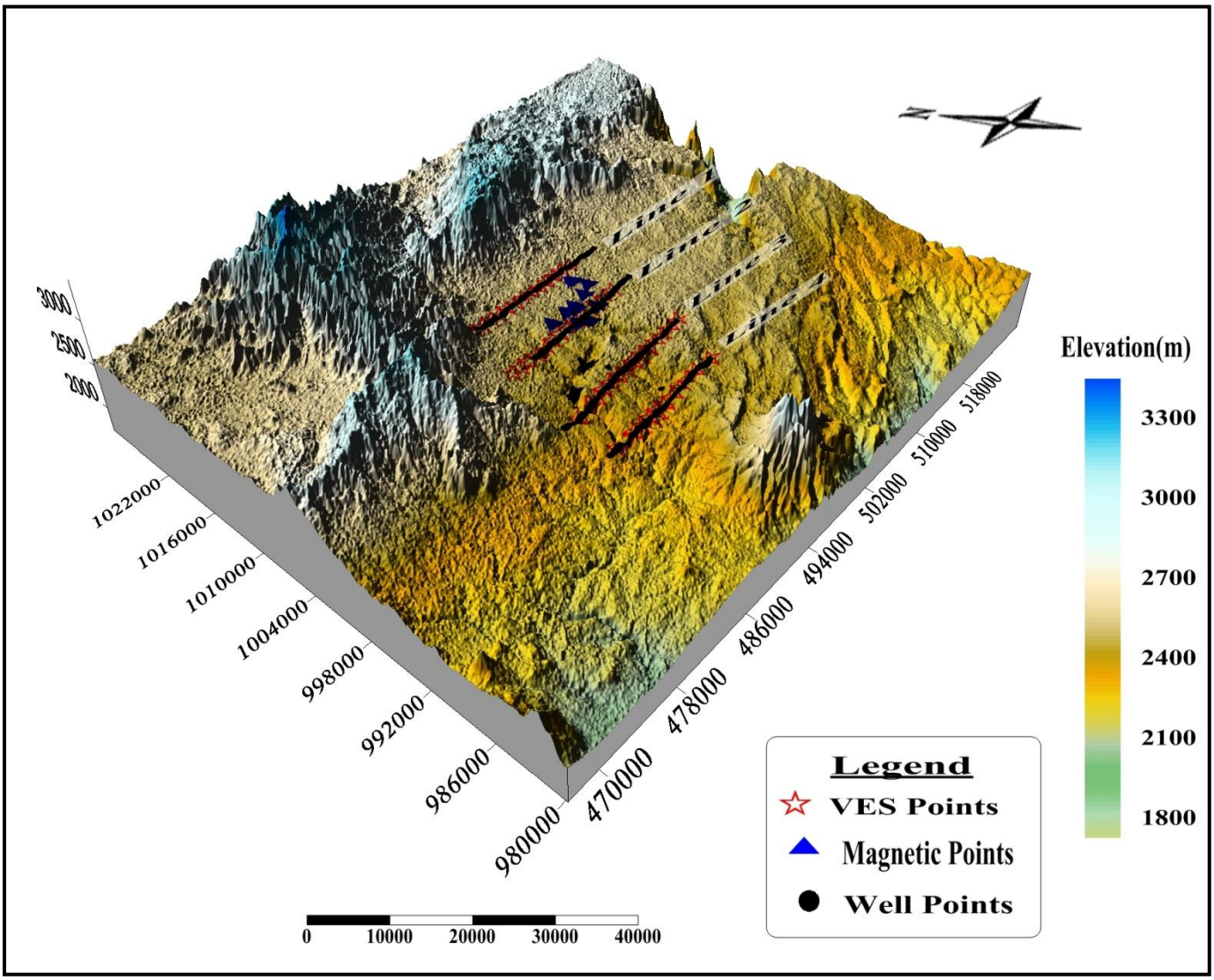

Figure 1. 2 Topographic map of the study area.

1.2.3 Climate

The highest and lowest average maximum temperature over the record periods is 25°C in dry season (March, April and May) and 21°C in the wet season (July and August), while the variation of average monthly temperature values fall in the range of 6°C (November and December) to 11°C (May) throughout the year.

1.2.4 Geology of the area

1.2.4.1 Alaji Rhyolitesand trachyte flows and minor pyroclastic rocks (Nar)

The Intoto mountain range, north of Addis Ababa, trending nearly E-W is built of dominantly compact, massive rhyolites and trachytes flows and subordinate pyroclastic rocks (Justin Visentine et al., 1974; Morton et al., 1979 and others).A K\Ar age of 22.00 Ma (Justin Visentine et al., 1974) indicate that the map unit belong to Alaji Formation .These silicic lavas and pyroclastic rocks form a thick pile along an E-W oriented fissure and uplifted northward (Zanettin and Justine, 1974). The geological map of the area is shown in figure 1.3 below)

At the most western corner of the site area, a relatively small area is underlain by silicic flows and minor pyroclastic rocks belonging to Alaji Formation .The rocks are strongly weathered and jointed .In places deeply weathered to reddish lateritic soil .The rocks are weathering mainly to pinkish-yellow, white and grey .The main jointing sets trend E-W, NE-SW and NW-SE and inclined between 85^0 and 90^0.

1.2.4.2 Termaber Basalts (Ntb)

The Termaber Formation, pre rift volcanic, Middle Miocene age, the Shield Group of Mohr (1968) is represented by various basalts erupted from shield volcanoes ,which range from femic pyroxene – olivine porphyritic varieties to leucocratic plagioclase porphyritic types. Zanettin et al. (1974) pointed out that all varieties from ankarmites through Hawaiities to Mugearie are present, usually flows are easily recognizable and paleosols and scoraceous horizons are in many places seen at the base flows. On the Ethiopian Plateau, the shield volcanoes of the Termaber Formation become progressively younger from north to south (Zanettin et al., 1974). Central type volcanism started in the north almost 26 Ma ago. Termaber-Meghezez Basalts of the Meghezez Mt. northeast of the site area are 13 Ma old.

The most northern segment of the site area is covered by Termaber Basalt strongly fractured and jointed, commonly layered, strongly to moderately weathered, dark gray in color, dominantly aphantic, and aphyric, porphyritic varieties are not uncommon with scattered phenocrysts of plagioclase and olivine and in places rich in large plagioclase phenocrysts, commonly bluish weathering .Volcanic agglomerate pods are common within the basalt flows separated from the flows by paleosoils .Highly vesicular, amygdaloidal varieties are common usually occurring on the top part of the flow. Silicic lava flows and pyroclastic rocks occur in places. The map unit is also exposed in the middle part of the site area in the

Akaki, Legedadi and Lagatafo river gorges as windows .The recently completed test wells (LLA-01and LLA-02) 432 and500 meters depths respectively, located on the basalt were wholly drilled through the Termaber basalt, indicating that the formation here is over 500 meters thick. The artesian well drilled by Addis Ababa Water Supply Authority at Legatafo river bank southwest of LLA -01 encountered the Termaber Basalt flows at around 180 meters depth indicating that the formation continues underneath the overlying silicic formation

The contact between the overlying silicic unit and the underlying Termaber Basalts lies at around 2440 meters in the Legatafo and Legagadi exposures .In this locality the thickness of the overlying silicic formation is in the order of 60 meters .However, the lihologic units reported from the mapping well AMW 8 (WWDSE, 2008) are acidic rocks up to 116 m depth ,basalt up to 170 m(54 m thick) followed by another acidic unit up to 282 m (112 m thick)and Termaber basalt up to 354 m(over 72 m thickness).

The first encountered acidic sequence (rhyolite, tuff can be correlated to the silicic formation (Nazareth Group) and the underlying basalt including the lower acidic member rocks (ignimbrite) encountered possibly belong to same group. According to the current geological studies, however, the mapping well is expected to encounter the Termaber basalts after about 60 meters (2440 meters contour line) and the expected thickness of the overlying silicic sequence is about 60 m rather than 116 meters. The Termaber Basalts rests on the Alaji Formation described before, the rock types extensively quarried for construction purposes.

Two major joints sets, continuous ,open to tight ,barren, trending NE-SW and NW-SE, inclined steeply due SE and NE and places close to 90^0 are common. The dominant joint system strikes from $205^0$to 250^0SW and dip 70^0SE to 90^0.Lesser joint sets strike 30^0NE or 295^0Nw and dip 30^0NW or 65^0NE respectively.

1.2.4.3 Ignimbrites and pyroclastic rocks (Nn*)*

A thick sequence of assorted stratoid silicics ,ignimbrites, unwelded tuffs ,agglomerates ,ash flows and minor rhyolites and trachytes as well as basalt flows cover a significant segment of the rift floor and the rift escarpments and the adjacent plateau margins .This formation is late Miocene to Pliocene age , named as Blachi rhyolites by Justin –Visentine et al. (1974),Nazareth series by Meyer et al.(1975)Nazareth Group by Kazmin et al.(1980) and Nazareth pyroclastics by Tsegaye et al.(2005).

Central type explosive eruptions played a significant role in the formation of the Nazareth Volcanics such as Wechacha, Yerer, Furi volcanoes on the western shoulder of the rift and Chilalo, Kaka, Bada and some others on the eastern shoulder of the rift .Radiometric ages are available for chilalo (3.5 ma – Kuntz et al., 1975) Wechacha (4.5Ma –Miller and Mohr, 1966), Menagesha (3.0Ma- Morton et al., 1979) and Yerer –Morton et al., 1979) and others.

In the site area, the map unit represents the most extensive regional silicic unit resting conformably above the Termaber Basalt flows (Ntb) described before .It is commonly separated from the underlying basalt flows by ½ -1 meter thick paleosoil .It is wide spread all over the site covering about over half of the site area. The formation consists of dominantly intercalation of ignimbrites, unweldded tuffs, ash flows, agglomerate and minor trachytes and rhyolites flows. Each rock type is separated from the overlying and the underlying member by up to 2 meters thick yellowish –brown baked paleosoils. The maximum estimated preserved thickness ranges approximately from 150 to 250 meters .The artesian well drilled by Addis Ababa Water supply Authority at Legatafo river bank encountered over 180m thick salic sequence. The succession is well exposed along the Akaki and Legadadi, Legatafo river gorges and their tributaries. Measured ages in the site area and its surrounding ranges from 11-5.2 Ma (Justin –Visentine et al, 1974; Kuntz et al., 1975; Morton et al., 1979; Kazmin et al., 1979; Charent et al., 1998; W\gebraiel et al, 1990; Mazzarini et al., 1999; Tsegaye et al., 2005 and references cited therein). Mapping borehole AMW-8 encountered over 282m thick Nazreth Group rocks (rhyolite, tuff, basalt, ignimbrite) resting on scoraceous basalt (Ntb).

The ignimbrite sequence is constituted by different flow units consisting of pale-green to pale-yellow, light green, grey, white, welded and crystal rich commenditic and pantelleritic ignimbrites interlayered with other pyroclastic rocks. The ignimbrites commonly form conspicuous marker horizons owing to their relative resistance to erosion as compared to interlayring poorly or less welded pyroclastic rocks .The ignimbrite horizons commonly form steep vertical walls or ridges separated from the less welded pyroclastic units by yellowish-brown paleosols. In most cases the top part is covered by ignimbrites and forms extensive little modified sheet of flat topped topographic features. The rocks are commonly columnar jointed and ridge forming and quarried for various construction purposes.

They are strongly fractured, jointed, dominantly; trending NE-SW and NW-SE and dipping steeply (85^0-90^0) or horizontally layered. The jointing is continuous, tight and barren. E-W and N-S trending Joint

sets are also common. The joint sets dominantly strike from 10^0-85^0 NE and 110^0 to 150^0 SE and rarely E-W or N-S directions .Dip is also predominantly vertical or greater than 85^0.

The most widespread ignimbrites are formed of small flattened glass shards and larger rock fragments which are generally pumiceous, either glassy or partially crystalline. High temperature sanidine, anortohclase, quartz, barkertinite and sodic ferriferous clinopyroxene occur as phenocrysts. All the rocks have a glassy groundmass with minor or less devitrified spots or veins. Extremely fine grained (aphanitic) mesostaseas occur quite frequently, sometimes with eutaxitic and pseudo-fluidal structure easily recognizable from the curving of the fiamme near the phenocrysts. The fiamme vary in color from dark brown to black. The phenocrysts are dominantly feldspars (sanidine and /or anothoclase) and subordinate quartz and plagioclase. They are anhedral, often fractured, almost always unaltered and sometimes deeply corroded and embayed crystals. Mafic minerals are generally rare. A brown fresh amphibole (oxhornblende) occurs locally. Minute emerald green crystals of pyroxenes – aegirine–augite are present. Iron- oxides and zeolites are abundant; rutile, zircon and apatite are less common.

The tuffs are variegated in color, fine to course grained, commonly poorly welded, massive, rarely bedded, strongly weathered, and usually separated from one another and ignimbrite horizons by paleosols.

The ash is white in color, poorly consolidated, thinly laminated or layered and flat lying. The volcanic agglomerate is variegated in color with few centimeters to several meters diameter of commonly ignimbrites, pumice and other rock inclusions. The agglomerate member in places contains spectacular huge inclusions of rocks fragments over two meters diameters embedded and stricking out from the tuffaceous material (groundmass).

1.2.4.4 Olivine –pyroxene phyric basalt lava flows (Qtb)

The most southern corner of the Legadadi- Legatafo site area is covered by highly vesicular, locally amygdaloidal, relatively fresh, porphyritic basalt lava flows with phenocrysts of olivine, pyroxene and plagioclase. The rocks are characteristically grey in color, bouldery exposure and porphyrtic, with large phenocrysts of olivine, pyroxene and plagioclase. It lies on the Nazareth Group rocks –ignimbrites and pyroclastics rocks (Nn) map unit described before. It forms little modified flat topped physiographic feature, strongly jointed, major ones strike NE-SW and dip moderately NW or SE.

The map unit has been correlated or ascribed to the Quaternary Akaki basalt lava flows .For more information refer to the map unit described under South-Ayat –North Fanta Well Field Site Area and South West and West Akaki Well Field Site Area.

It's relatively unmodified geomorphologic expression indicates its recent origin Prominent cinder cones (no collapse craters) lie along its central east-northeasterly axis. The preserved thickness reaches about 130 meters.

Where exposed the Akaki basalt is observed to form columnar flows .Fine grained parts of flows are medium gray and have small irregular intergranular cavities. The basalt is usually porphyritic with phenocrysts by olivine; pyroxene and plagioclase. These typical features distinguish the Akaki basalt from the adjacent Termaber basalt.

The actual age of the basalt is known .The shield developed along a zone of east and north easterly faults that extends far to the east in line with the Main Ethiopian Rift System.

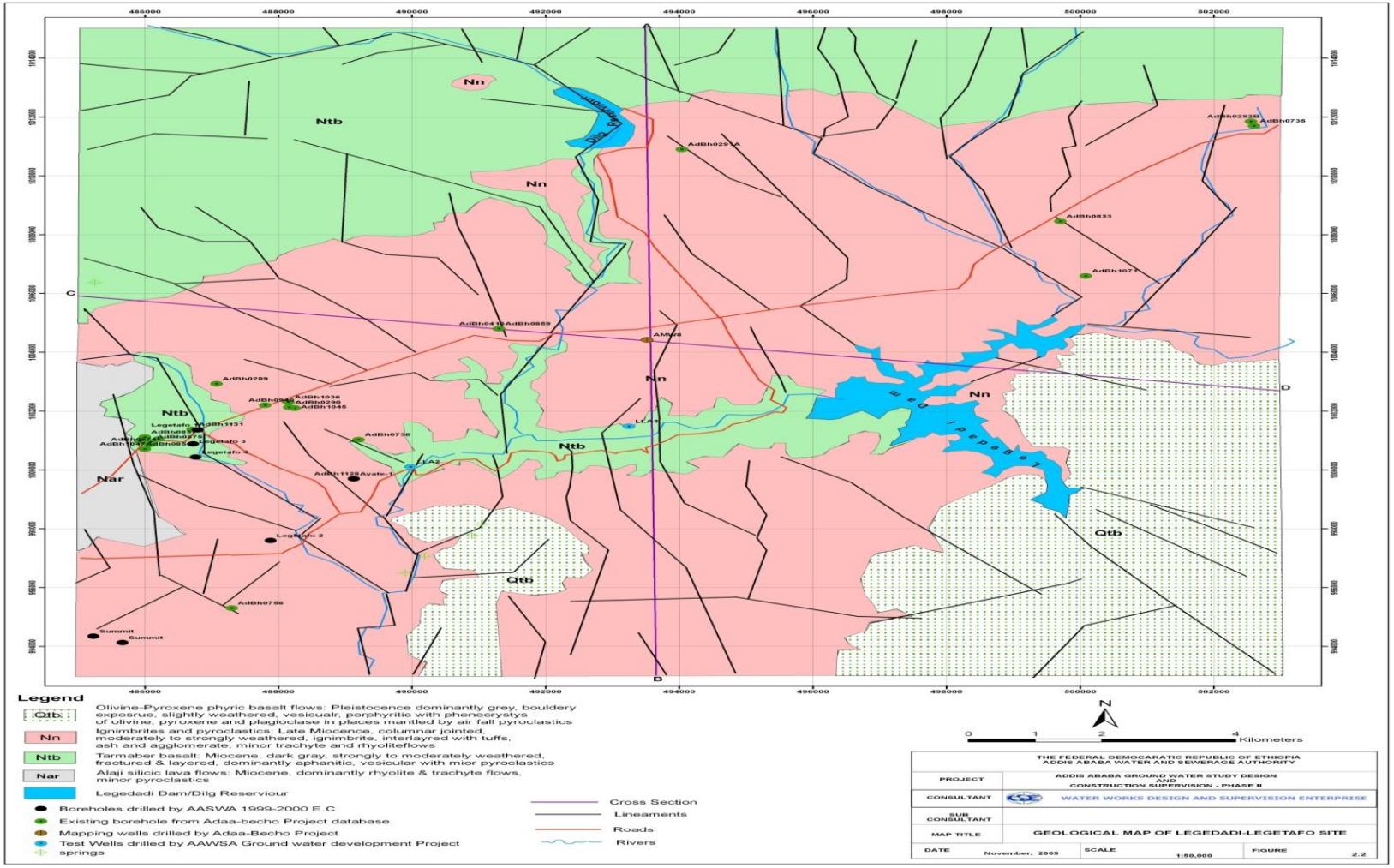

Figure 1. 3 Geological map of the study area (modified after WWDSE, 2008)

1.2.5 Structure

A wide spread brittle deformation comprising fracture systems –lineaments and Joints and minor faults encountered and observed during the course of the field survey and can be recognized and traced from the land sat imageries and topographic maps that cover the site area. A few numbers of faults were encountered during the field work or identified from the land sat imageries studies. This is a primarily because extensional normal faults are concentrated and affected those of the rift complex and to some minor degree the rift margin complex .As already mentioned in the preceding section the site area is located on the western rift margin. The site area is intersected on all scales by prominent linear features and Joints. Only few exposed rock types that underlie the site area are entirely free of joints.

1.2.5.1 Lineaments

Conspicuous linear features can be recognized from the land sat imageries and topographic maps that cover the site area .The features are commonly marked by drainage systems of the site area. It is obvious that the drainage system is mainly controlled by these weak fracture zones .The lineaments range in size from a few kilometers to several kilometers.

These lineaments can be group into four main systems based on their orientation .These are: NE-SW, NW-SE, N-S/NNE-SSW and E-W trending fracture systems.

The NE-SW and NW-SE systems are the major prominent and widespread ones affecting the site area. The orientation of the lineaments corresponds to the regional trend of the Main Ethiopian Rift and Afar Depression respectively. The N-S/NNE-SSW (Figure 1.4 a and b) trending lineament system are less wide spread throughout the entire site area and can be correlated to the Wonji Fault Belt of Mohr (1967) along the axial part of the Main Ethiopian Rift System.

Only few E-W oriented lineaments occur in the site area .These lineaments can be ascribed to the Yerer–Wechacha–Ambo-Tulu Wolele mega lineament system.

1.2.5.2 Jointing

As already intimated in the text, the various rock types that constitute the map units are affected by few millimeters –centimeters to tense of meters long, tight to open, a few centimeters to one meter spacing joint sets .The rocks are affected by several sets of joints generally very closely spaced, and show no

visible displacements of the rocks on either side .The orientation of the joint systems is analogous to the linear features (lineaments) mentioned before. The major ones generally trend NE-SW, NW-SE and subordinate ones trend N-S/NNE-SSW and steeply dipping or vertical (Figure 1.4 a and b)

1.2.5.3 Faults

The mapping well AMW-8 was expected to hit or strike the Termaber basalt at around 60 m below the surface, but on the contrary stroke would be Termaber Formation at a depth of 116 m (116 m preserved thickness of salic rocks, beyond the expected thickness), up to 170 m (54 m thickness) followed by 112 thick another salic rocks and over 72 m thick basaltic unit.

As was intimated in the text before, the mapping well was expected to strike the basaltic unit at around 60 m below the surface because there are already indications that basalt unit is exposed about 60 m below the surface, but on the other hand stroke the map unit at a depth of 116 m, that is around 56 m below the expected depth. If it is the same basalt unit, it is down thrown by over 56m. The Termaber basalt units out crops out as windows in the Legetafo and Legedadi river canyons and disappears underneath the salic pile and reappears in the north–Deri–Sandafa area – below the salic sequence.

The existence of a sort of graben –horst structure is the possible explanation for the occurrence of silica sequence at lower elevations than the underlying basalt flows and complexity of the geology encountered during drilling (see cross sections). Although there are a number of conspicuous lineaments that cross the site area, there is no clear evidence to support the presence of a graben structure. Cross sections drown across the site area–east –west and north west–southeast–show that the silicic sequence is inclined generally due south and occupy pre-existing topographic features and graben structure that is probably why the silicic sequence is usually found to occur at the lower elevation than the underlying Termaber Basalt flows.

This one is currently appears to be the best explanation based on the present level of knowledge of the geological complex of the general area.

It is to be noted that the Nazreth Group (Nn) combrises of not only silica rocks, but also basalt sequences, and the basalt and the ignimbrite encountered at depth possibly belong to Nazreth Group. Two cross sections have been drawn, based on surface and boreholes information.

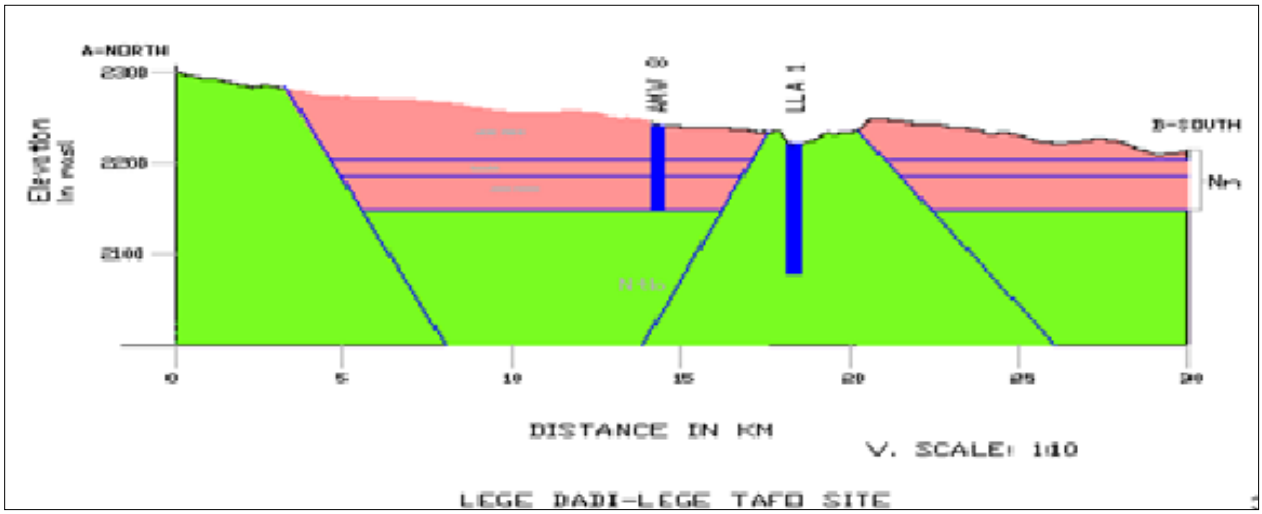

a)

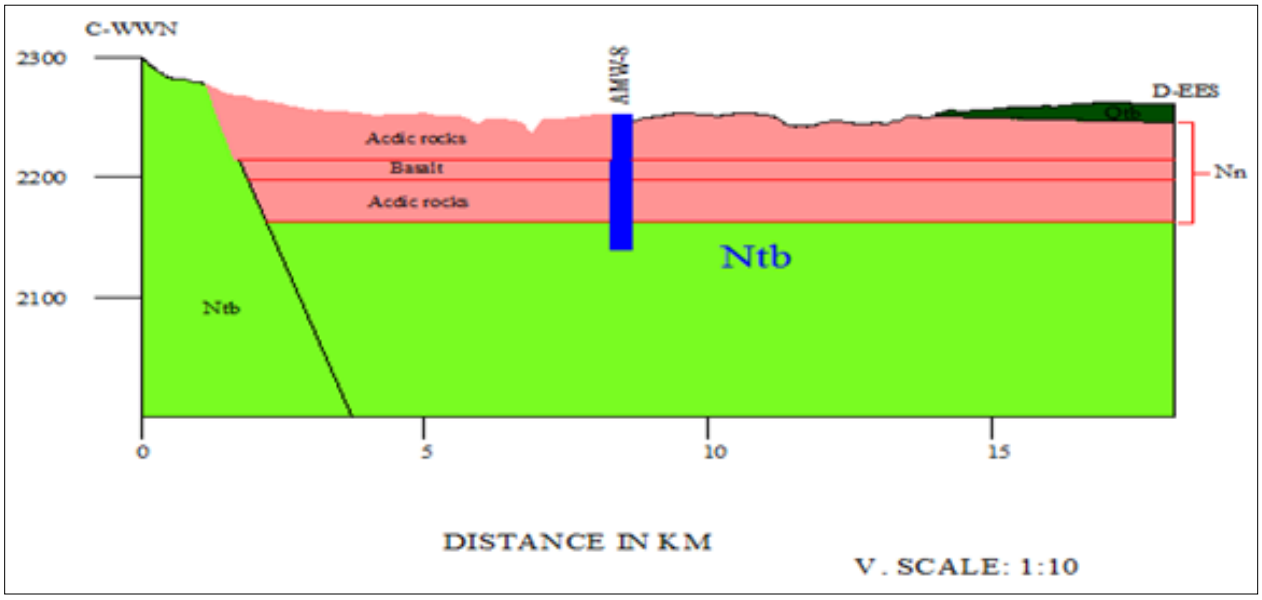

b)

Figure 1. 4 Geological cross section of the area b) along A-B (N to S) b) along C-D (WWN to EES)

1.2.6 Hydrogeology of the area

1.2.6.1 Water Point Data Availability in the prospective Zone

Many of the existing boreholes are available in the western margin of the suggested groundwater prospective zone in the well fields of (LLA-WF01 and LLA-WF03). Borehole data are scarce in the

eastern, south eastern and northeastern margins of the prospective zone particularly almost the entire zone of Well field (LLA-WF02). Most of the wells drilled previously in LLA are less than 300m deep and they are more concentrated in well field (LLA-WF03) close to Legedadi Area. The additional deep test and pilot production wells with depth greater than 300m (WWDSE, 2008) are also distributed closer to Legedadi area. In this study, additional deep test Wells have been proposed in the eastern margin of the prospective zone which includes the whole parts of LLA- WF02.

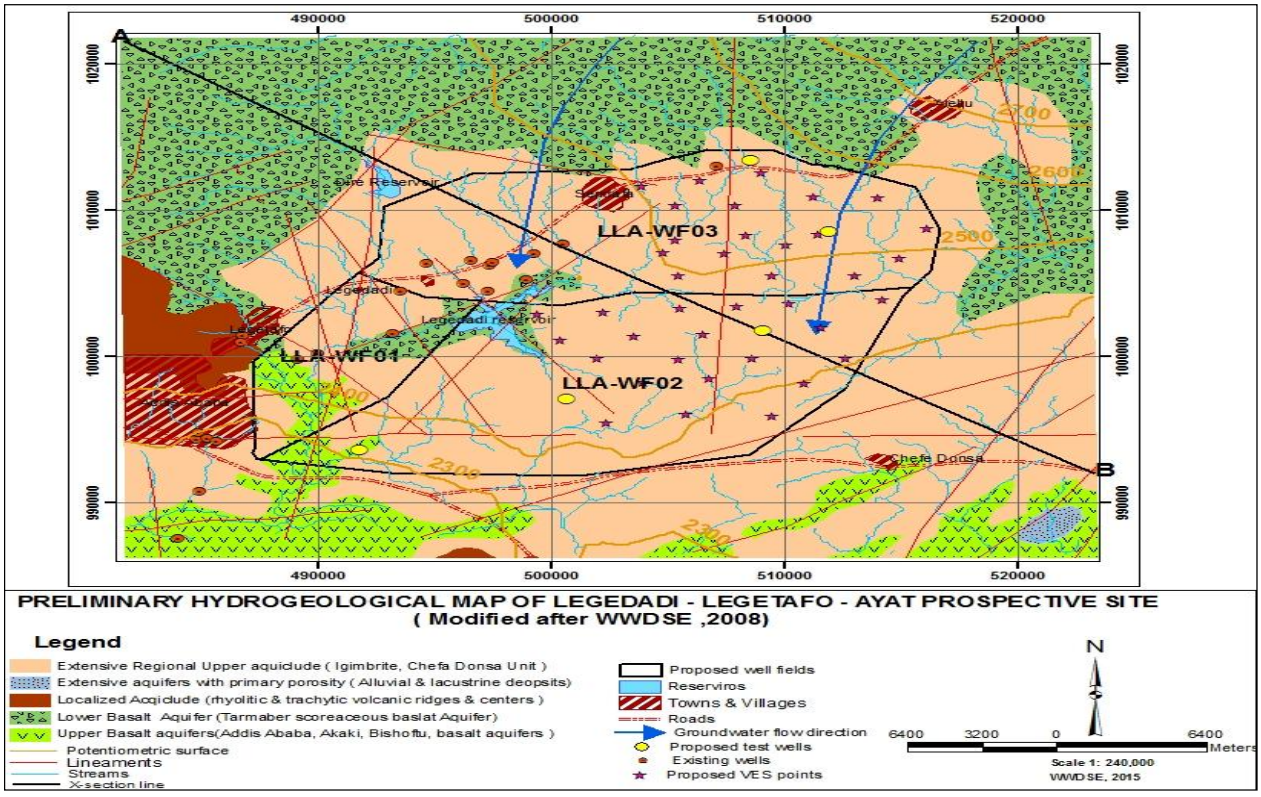

Figure 1. 5 Hydogeological map of the area (Modified after WWDSE, 2008).

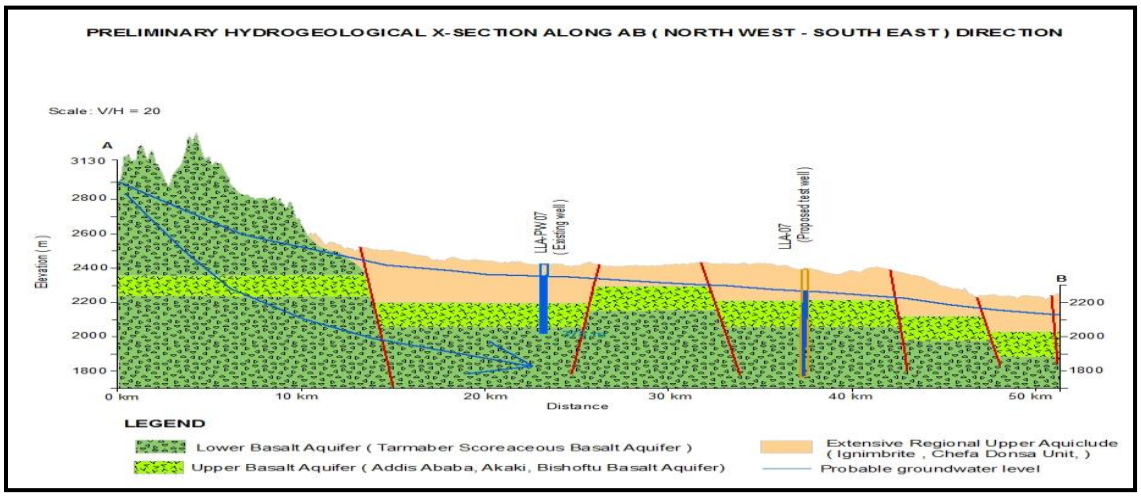

Figure 1. 6 Hydro geological cross section along AB (modified after WWDSE, 2008)

1.3 Statement of the Problem

The area is one of the six special Zones of Oromia regions. The Legedadi Dam is located in the study area. It is one of the water resources of Addis Ababa city. This study also purposely studied to search ground water for Addis Ababa city. This study is intended to solve the water shortage of the city by developing geo-electrical section of the subsurface, which tells us the general aquifer property and groundwater potential beneath the survey area.

1.4 Objectives of the Study

1.4.1General Objectives

The main objective of this project is to characterize the Legetafo-Legedadi-Ayat (LLA) well field, in the northeast of Addis Ababa, and investigate the potential of the area for deep groundwater resource, through the mapping of the subsurface lithologies and identification of geologic structures that could play a role in the storage and movement of groundwater.

1.4.2 Specific Objectives

The Specific objectives of this thesis are the following:-

- ✓ To delineate geologic structures, like faults and lineaments that are important for groundwater occurrence, storage and circulation.

- ✓ To identify subsurface weak zones that could serve as a conduit or barriers for groundwater movement.
- ✓ To determine the depth to water table and to locate potential drilling sites for the extraction of groundwater.
- ✓ Identify the major subsurface geological units in the area and map possible water saturated horizons.
- ✓ Showing the merit of integrated geophysical investigation for evaluating the groundwater resources and its role in establishment of regional models.

1.5 Methodology

To achieve the objectives mentioned above, a number of steps have been completed. These included reviewing different previous works, not only geophysical works (on groundwater exploration and identification of geological structures) but also geological and hydro-geological literatures on the Legetafo-Legedadi-Ayat prospective area. Finally, two different geophysical methods were employed in the study area: Vertical Electrical Sounding (VES) and magnetic surveying methods. Data's of the two geophysical methods where collected along four selected traverse lines. These VES data are analyzed using appropriate software like Win Resist, IpI2win+Ip, Surfer, MapInfo Professional 8.5 and Microsoft Excel while the magnetic data analyzed by using Oasis Montaj and Surfer, Paint and Microsoft Excel software. Consequently curves, maps and models are produced and interpreted to achieve at the general and specific objectives of the work.

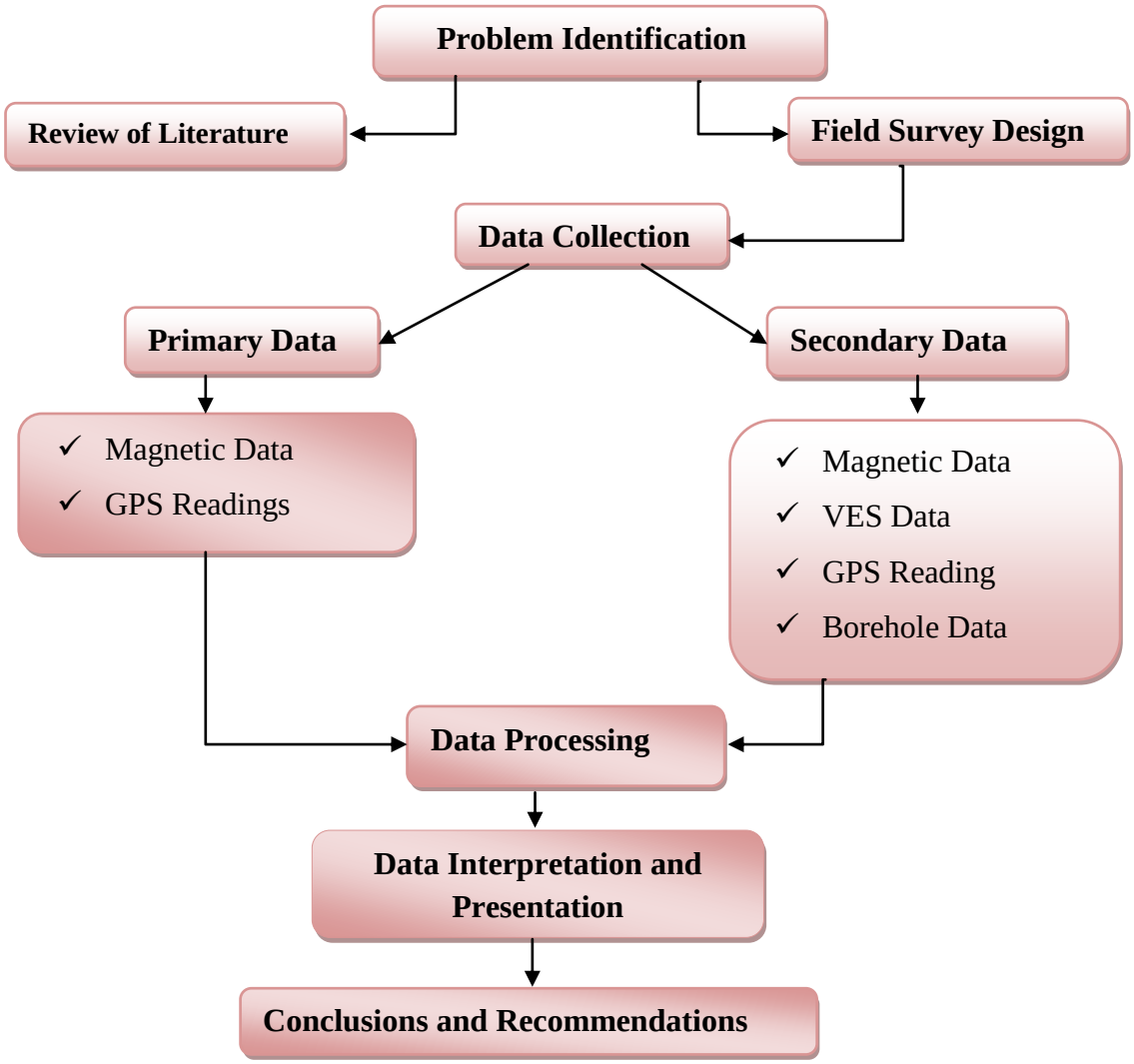

Figure 1. 7 Flow chart of the general methodologies

1.6 Basic Research Questions and Hypothesis

1.6.1 Basic Research Questions

The following are basic research questions raised in this research

- ✓ How far is depth of the water table?
- ✓ How to identify the groundwater table of the area?
- ✓ Where to locate the drilling point?

1.6.2 Research Hypothesis

The characteristics of groundwater aquifer can be delineated by using integrated approach of electrical resistivity and magnetic method.

1.7 Significance of the Study

This study will have a lot of significance from the scientific point of view as well as in solving the problem raised in the society of Addis Ababa and its surroundings. In regard of this the following are the list of the significance of this study:

- It helps as a guidance for the future drilling process
- The material can serve for the department and the company as a source document for the future researchers to continue their research in the similar areas
- It uses as a reference for the study of groundwater in that area
- It develops the researcher's knowledge in the area of groundwater exploration
- It gives information about aquifer zones, its depth as well as the drilling.
- This research work fills the existing gap of detail information and its usage in the geophysical methods in the country.

1.8 Limitation of the Study

Like any other research works, this study has also faced with a number of limitations in this research. The main obstacles were:

• Severe financial and necessary field materials like transport and geophysical instrument,

• Shortage of software for analysis and interpretation of geophysical data,

• Non availability of previous geophysical work on the area, and

• The time bound set for the thesis work coupled with field constraint (transport and instruments).

1.9 Review of Previous Works

Several geological, hydro geological and geophysical studies have been conducted in northeast of Addis Ababa which includes the study area for various purposes. The results of the studies conducted by different authors and organizations are reviewed as follows.

- Regional Hydro geological Studies (scale 1:250,000), 1982

This is a regional study aimed to asses and understands the occurrence, movement and chemical nature of groundwater in the Upper Awash River basin. The Report point outs the existence of four major aquifer zones with different degree of productivity in different part of the basin.

The report concludes that the regional Hydro geological system is not clearly answered due to the lack of subsurface investigation, therefore it suggested further subsurface and detail investigation

- Study of a Groundwater study that includes Addis Ababa and its surrounding (Evaluation of Groundwater Resources Potential Adaa – Becho Plains WWDSE, March 2008)

Addis Ababa and its surroundings are located within Ada'a and Becho Plains Groundwater Basin and this study is the only groundwater basin wide study conducted in the region. The study is based on conceptual model of the basin and carried out review of existing studies, inventory of groundwater sources, collected and analyzed existing surface and groundwater data, generated data from geophysical surveys, test and mapping wells, etc. The basin study shows that the groundwater of Addis Ababa and its surroundings are not limited to Akaki River surface water catchment as stipulated in previous groundwater studies carried out for Addis Ababa Water Supply Projects, but it is part of a wide groundwater basin that extends partly into Abay River surface water basin catchment and covers part of the upper Awash River basin. This was more conceptualized with a drilling of mapping wells in different localities of the catchment. The Hydro geological x-section constructed based on the mapping wells and previously drilled wells shows that the Abay Plateau is the recharge area for the confined aquifer in Upper Awash. The study in general revealed that there are two aquifers in the Becho plain and along west-east direction from Becho-Legedadi section which are separated by ignimbrites and welded tuffs. These are the upper basalt aquifer (UBA) and the regional lower basalt aquifer (LBA).

The Hydro geological section made along Wenoda-Legedadi-Akaki section in the report shows that the upper basalt aquifer has wide distribution and forms confined and unconfined aquifer system. The thickness of this formation is highly variable from more than 400 meters at Legetafo area to less than 50 meters in Becho plains. The Hydrogeological x-section constructed based on the mapping wells and previously drilled wells shows that the Abay Plateau is the recharge area for the confined aquifer in Upper Awash. The study in general revealed that there are two aquifers in the Becho plain and along west-east direction from Becho-Legedadi section which are separated by ignimbrites and welded tuffs. Thses are the upper basalt aquifer (UBA) and the regional lower basalt aquifer (LBA) The Hydrogeological section made along Wenoda-Legedadi-Akaki section in the report shows that the upper

basalt aquifer has wide distribution and forms confined and unconfined aquifer system. The thickness of this formation is highly variable from more than 400 meters at Legetafo area to less than 50 meters in Becho plains.

The Lower Basalt aquifer (LBA) is composed of tertiary Tarmaber basalt composed of dominantly scoraceous basalt and Amba Aiba basalt. The mapping wells drilling at Legedadi (AMW8) has penetrated through lower basalt aquifer. The yield of the well was progressively increasing when the depth of penetration is increased in the formation.

On the groundwater elevation contour map the following initial knowledge is obtained: Entoto and Wechecha –furi ridges acts as local barrier. The recharge at Abay plateau flows to Upper Awash through two main direction i.e. through Becho plain and along Legedadi areas.

Almost 100% of Abay plateau is the recharge area of the lower basalt aquifer in Upper Awash basin including Legedadi Area

- Well Completion Report of Test Wells and Pilot Production Wells at Legedadi – Legatafo – Ayat Groundwater Prospective Site, WWDSE Dec. 2014

For further study, investigation and groundwater evaluation of Legedadi – Legatafo – Ayat Groundwater Prospective Area, Test wells and pilot Production wells were drilled under the supervision of WWDSE .A total of 12 bore holes, 6 test wells and 6 pilot production wells were completed in this phase. The depth of boreholes in the report ranges from 181m to 598m depth and depth to water level ranges from 7.3 m to 33.84m

Chapter Two

Theory of Geophysical Methods

2.1 General

Geophysics is basically the application of the principles of Physics to the study of the Earth (Reynolds, 1997). There are two main aspects of geophysics namely; pure and applied geophysics. Pure geophysics deals with the study of the substantial parts of the planet whilst applied geophysics involves investigating the Earth's interior by taking measurements either at or near the surface of the Earth. The latter is of economic benefit since it aims at exploiting resources for economic use. Many geophysical techniques are employed in geophysical exploration ranging from active to passive methods. This classification depends on their source of energy. Active methods are artificial methods whereas passive methods are natural field methods (Reynolds, 1997).

In active methods, artificially generated signals (electrical or electromagnetic fields) are transmitted into the Earth and the response of the Earth to these signals is measured. Examples of active methods include: electrical resistivity, electromagnetic, seismic, induced polarization and ground-probing radar methods (Reynolds, 1997).

Passive methods on the contrary rely on naturally occurring fields and hence, measure the response of the Earth to these signals. Passive methods can normally give information on active methods. Examples of these methods include; magnetic, gravity, telluric, self-potential and radiometric decay methods (Reynolds, 1997).

There are so many geophysical techniques and a wide range of equipment used in geophysical prospecting. Each of these respond to a particular physical property and the kind of property that a method responds to evidently determines its range of applications. For example, the magnetic method is more appropriate for locating buried magnetic ore bodies due to their high magnetic susceptibility. Similarly, the seismic and electrical methods are preferred for the location of buried water table since they are able to differentiate saturated rock from dry rock by virtue of its higher seismic velocity or higher electrical conductivity (Kearey and Brooks, 2002).

Even though geophysical methods have potential ambiguities of interpretation, they offer a comparatively rapid and cost effective measure of inferring really distributed information on subsurface geology. During subsurface resource exploration, these methods are able to detect and delineate local

features of potential interest which otherwise couldn't have been detected by any realistic drilling operation (Kearey and Brooks, 2002). Some of the geophysical techniques require sophisticated equipment or complex analysis and consequently are inappropriate for use in rural water supply programmes. The two most appropriate methods as far as rural water supply is concerned are the electrical resistivity and electromagnetic (MacDonald et al., 2005). The concepts and operation of these methods are described below.

2.1.1 Electrical Resistivity Method

In geophysical investigations problems such as groundwater exploration, ore prospecting, depth to bedrock determinations, etc., the electrical resistivity method provides a quick and economic means to obtain vital subsurface information. Electrical resistivity methods have been used in a number of groundwater exploration surveys when the resistivity's of the rocks are needed to be inferred. The DC-resistivity method measures the potential difference resulted from the artificial excitation due to a current sent to the ground section. The diagnostic parameter, the electrical resistivity ρ, resulting from measurements at a number of electrode positions, reflects the electrical properties in the ground as a function of depth or lateral distance.

The resistivity of the saturated rocks in the upper part of the earth's crust, decreases with increasing their porosity and the degree of salinity of the saturated fluids. In contrary to the above, the presence of clay and conductive minerals can also reduce the resistivity of rocks which can be resolved by using other geophysical techniques, geological or well information. In resistivity surveying especially in vertical electrical sounding (VES), conduction in rocks is mainly due to pore fluids acting as electrolytes. Water in its pure form is poor conductor but most water contains dissolved salts which facilitate current flow.

The resistivity of geological materials exhibits one of the largest ranges of all physical properties from 1.6×10^{-8} Ω m for native silver to 10^{16} Ω m for pure sulfur. According to that range the resistivity of Earth material differ from one another because of the presence of mineralized zones, zones of water saturation in the subsurface of the Earth. Hence an electrical resistivity method is used to classify the materials due to its properties (Reynolds, 1997). The theory and basic principle of electrical resistivity method was described by different authors (Telford et al, 1990; Dobrin and Savit, 1976; Parasnis, 1962; Robinson and Caruh, 1988; Reynolds, 1997; Gibson and George, 2003) only a short description of this method is included in this thesis.

2.1.2Basic Principle of Electrical (DC) Resistivity method

In resistivity method an electric current is introduced in to the ground by means of two current electrodes, and the potential difference between two pair of potential electrodes is measured. The potential difference between two arbitrarily located points on the surface of a homogeneous isotropic ground is obtained from the fundamental given by the expression below.

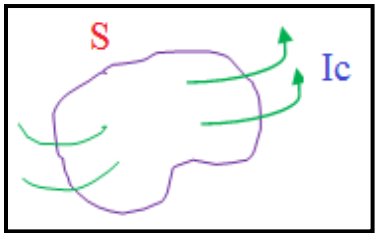

$$(I_c)_s = -\frac{dQ}{dt} \tag{2.1}$$

$$(I_c) = \oint \vec{J}.ds \quad \text{And} \quad Q = \int_v q.dv \tag{2.2}$$

Where "v" is the volume bounded by the surface S.
Substituting the above equations into equation (2.1) and applying divergences theorem, we can get

$$\int_V (\nabla.\vec{J})dv = -\int_V \left(\frac{\partial q}{\partial t}\right)dv \quad \text{Or} \quad \int_V \left(\nabla.\vec{J} + \frac{\partial q}{\partial t}\right)dv = 0 \tag{2.3}$$

Equation (2.3) is valid for any volume so that we can write it as

$$\nabla.\vec{J} + \frac{\partial q}{\partial t} = 0 \tag{2.4}$$

Equation (2.4) is called the law of conservation of charge in differential form and also known as the continuity equation.

For direct current, $\frac{\partial q}{\partial t} = 0$ so that equation (2.4) reduces to the form

$$\nabla.\vec{J} = 0 \tag{2.5}$$

The electric field *E* is conservative field; it can be expressed as a gradient of the scalar potential function V as

$$\vec{E} = -\nabla V \tag{2.6}$$

Where V is measured in volts. From ohm's law; R = V/I, where V and I are the potential difference across the resistor with resistance R (Ω) and the current passing through it respectively. This expression can be written alternatively in terms of the electric field strength E (V/m) and the current density (A/m^2) as

$$\rho = \frac{\vec{E}}{\vec{J}}(\Omega m) \tag{2.7}$$

By taking only their magnitudes, the relation between the current density (**J**) and electric field intensity (***E***) can be given as:

$$\vec{J} = \frac{\vec{E}}{\rho} = -\frac{1}{\rho}\nabla V \tag{2.8}$$

Where ρ is a scalar function of the point of observation and *J* is in the same direction as *E* for isotropic medium. From equations (2.5) and (2.8) we have

$$\nabla\left(\frac{1}{\rho}\right).\nabla V + \frac{1}{\rho}\nabla^2 V = 0 \tag{2.9}$$

This equation is called the fundamental equation of electrical prospecting with direct current.

For homogenous medium, **ρ** is independent of the coordinate axes and equation (2.9) is simplified as

$$\nabla^2 V = 0 \tag{2.10}$$

This is called the Laplace Equation for the potential V.

Therefore, the electrical potential distribution for direct current flow in a homogeneous isotopic medium satisfies the Laplace equation. The above equation has different forms in different coordinate systems.

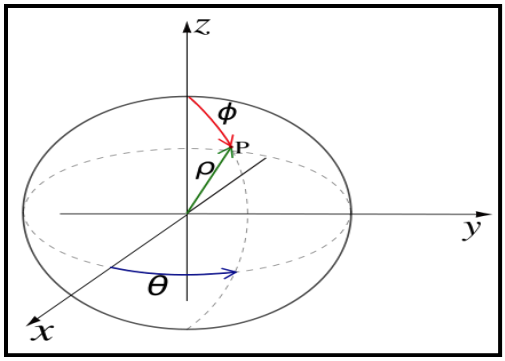

For example, using spherical coordinate system the equation can be expressed as

$$\frac{1}{r^2}\frac{\partial}{\partial r}\left(r^2\frac{\partial V}{\partial r}\right)+\frac{1}{r^2\sin\theta}\frac{\partial}{\partial\theta}\left(\sin\theta\frac{\partial V}{\partial\theta}\right)+\frac{1}{r^2\sin^2\theta}\frac{\partial^2 V}{\partial\phi^2}=0 \quad (2.11)$$

Practically, the DC resistivity survey is conducted with two current electrodes (AB) called source and sink respectively, in which the current I (A) is injected in to the ground and two potential electrodes (MN) where the potential difference ΔV (V) is recorded.

If one considers (DC) source which delivers current I (A) to the homogenous, isotropic earth through the current electrodes, the potential at any point will vary as a function of r where r is the distance from the ground to the current electrodes.
Let us now suppose that a current I be introduced in to an infinite homogeneous medium at a point P. then the potential at a distance r from p will be a function of r and hence Laplace equation can be written as

$$\frac{d^2V}{dr^2}+\frac{2}{r}\frac{dV}{dr}=0 \quad (2.12)$$

Since the potential varies only as a function of r $\frac{\partial V}{\partial\theta}$ and $\frac{\partial V}{\partial\emptyset}$ will be zero.

Current is introduce into the ground by means of two electrodes, i.e., a source and sink; and the potential at any point due to this "bipolar "arrangement is

$$V=\frac{I\rho}{2\pi}\left(\frac{1}{r_1}-\frac{1}{r_2}\right) \quad (2.13)$$

Where r_1 and r_2 are the distance of the point from the source and the sink, respectively.

Consider that a direct current of strength I introduced in to a homogeneous and isotropic earth by means of two point electrodes as shown in the Figure 2.1. The potential difference between the two point P_1 and P_2 on the surface is given by using equation (2.12) as Surface

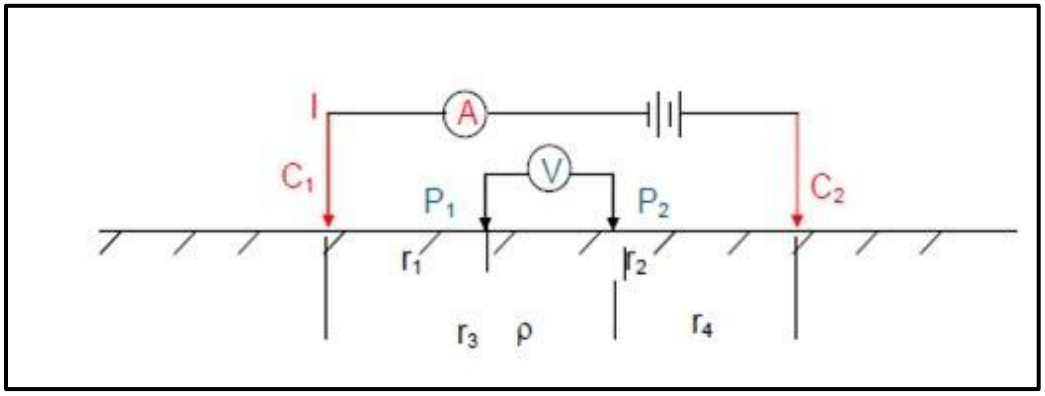

Figure 2. 1 The arrangement of current and potential electrodes in a four-electrode system.

The potential at P_1

$$V_{P_1} = \frac{I\rho}{2\pi}\left[\frac{1}{r_1} - \frac{1}{r_2}\right]$$

Similarly the potential at P_2

$$V_{P_2} = \frac{I\rho}{2\pi}\left[\frac{1}{r_3} - \frac{1}{r_4}\right]$$

The potential difference

$$\Delta V = V_{P_1} - V_{P_2} = \frac{I\rho}{2\pi}\left[\frac{1}{r_1} - \frac{1}{r_2} - \frac{1}{r_3} + \frac{1}{r_4}\right] \quad (2.14)$$

Where the distances r_1, r_2, $r_3$and r_4 are all in meters

Therefore, after re-arranging the distances between the current and potential electrodes according to the well known configurations, we can determine the resistivity of the homogenous ground.

2.1.3 The Apparent resistivity

If the ground is homogenous, the potential difference measured is as a function of the true resistivity of the homogeneous earth and the geometric factor. But in reality the ground is locally in the homogeneous and the potential difference depends on the current applied, the resistivity of the sub surface medium and the geometrical factor (k) determined by electrode array or configurations types. The resistivity calculated from such non homogenous ground is not a true resistivity rather it is called apparent resistivity (ρ_a) which can be related to the parameter as

$$\rho_{aw} = 2\pi a\left(\frac{\Delta V}{I}\right) \tag{2.15}$$

This apparent resistivity has to be interpreted using curve matching or inversion techniques to find estimated resistivity versus depth of the subsurface. This are many type of electrode configurations used in ground surveys of which the most commonly used array are Winner, Schlumberger and the Dipole-Dipole. Since the electrode separation relate to the investigation depth and lateral solution power required, one can choose the best electrode configuration for his planed survey at the initial of his survey .the expression for apparent resistivity in each of the above array types will be different due to the difference in the geometrical factor (K) of each any types.

Take the Schlumberger array in which the electrodes are symmetrically placed a point at the center of the array as shown in the figure below.

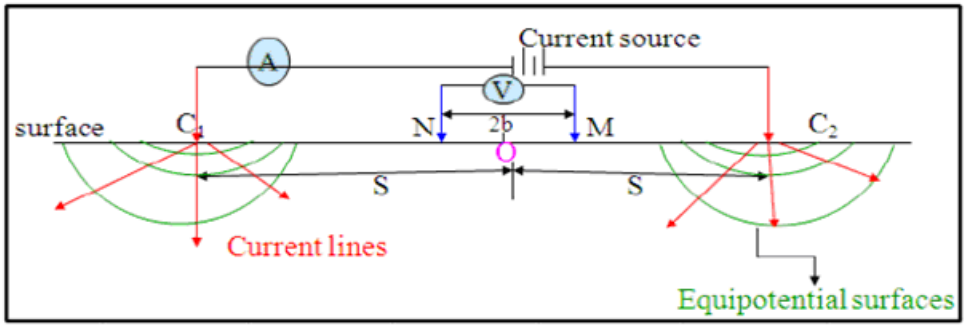

Figure 2. 2 The electrode arrangement for the Schlumberger Array.

Where $r_1 = s - b_1$=s-b, $r = s + b_2$, $r = s + b$ 3 and $r = s - b$ 4, "O" is the center of the array. The potential difference ΔV using equation (2.14) is given by;

$$\Delta V = \frac{I\rho}{2\pi}\left[\left(\frac{1}{s-b} - \frac{1}{s+b}\right) - \left(\frac{1}{s+b} - \frac{1}{s-b}\right)\right]$$

$$\Delta V = \frac{I\rho}{2\pi}\left[\left(\frac{1}{s^2 - b^2}\right)\right] \tag{2.16}$$

$$\rho_a = \pi\left(\frac{s^2 - b^2}{2b}\right)\left(\frac{\Delta V}{I}\right) \tag{2.17}$$

Where the geometric factor

$$k = \pi\left(\frac{s^2 - b^2}{2b}\right) \quad (2.18)$$

2.1.4 Resistivity Sounding Principle (VES)

In resistivity sounding, which is also known as Vertical Electrical Sounding (VES), the positions of electrodes changed with respect to a fixed point (known as the sounding point) and the measured values reflect the vertical distribution of resistivity values on a geologic section.

Vertical electrical sounding (VES) consists of a symmetrical electrode array used to determine the resistivity of the subsurface which is assumed to be horizontally stratified layers. The procedure is used to determine the variations in resistivity in the vertical direction and called electrical drilling or commonly vertical electrical sounding (VES). By expanding symmetrically the distance between current electrodes about a point called the sounding point, while keeping the potential electrodes MN at the same position, provides a sounding curve corresponding to the apparent resistivity versus depth of the location. As the spacing between the current electrode increases, the investigated depth will also increase.

The two most commonly used arrays in electrical sounding survey are the Wenner and Schlumberger arrays. In this work, we have used the data which was collected by using the Schlumberger electrode array techniques. When the Schlumberger array is used, the distance between the potential electrodes is not greater than one tenth of the current electrodes spacing. The advantage of this array is that initially only the spacing between the current electrodes is increased. However, at large current electrode spacing, the measured potential becomes very low and the distance between the potential electrodes is increased. Increasing the potential electrode spacing produces a „step" in the apparent resistivity curve and it is good practice to obtain an overlap between the curve segments by obtaining two readings at different potential electrode spacing for two adjacent current electrode spacing. Segments obtained at larger potential electrode spacing can be shifted in order to produce a smooth curve (Gibson and George, 2003).

In electrical prospecting, to determine the depth and the electrical resistivity of a series of horizontal or nearly horizontal ground current should be transmitted to the ground . In order to solve this problem, we should calculate the potential and the electric field, due to a point source of current, at any point on the surface of a stratified earth. This has advantages because of enables one to use axial symmetry of the

potential filed about the vertical axis through the current source and the additive property of the potential is also be used.

Let as choose a cylindrical system of coordinate with the origin at the point source a direct current located on the surface. The subsurface consists of infinite number of layers separated by horizontal boundary planes, the deepest layer existing to infinite depth ($h_n \to \infty$) and the other layers have finite thickness h_i = h1, h2, h3,…, h_n and resistivity's $\rho_1, \rho_2, \rho_3, \ldots \rho_n$. Each of the layers is electrically homogeneous and isotropic. The derivative of the potential based on the above conditions was first due to Steanescu et al, (1930).

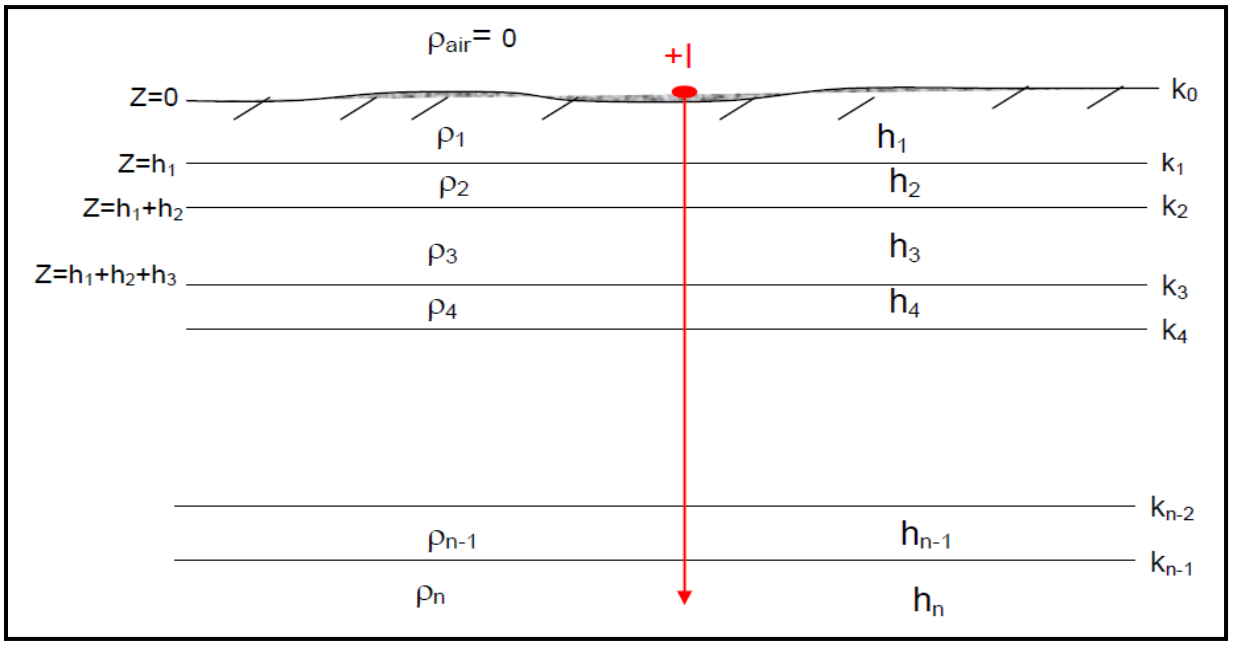

Figure 2. 3 A multi-layer Earth and problem presentation for solution of the potential.

The electrical potential field V for direct current satisfies the differential equation of Laplace, Which is

$$\nabla^2 V = 0$$

$$\frac{\partial^2 V}{\partial x^2} + \frac{\partial^2 V}{\partial y^2} + \frac{\partial^2 V}{\partial^2 z} = 0 \qquad (2.19)$$

The potential field has a cylindrical symmetry with respect to the vertical axis line through the current source .therefore, Laplace equation in cylindrical coordinate is most appropriate.

For a solution symmetrical with respect to the vertical axis $\frac{\partial V}{\partial \theta} = \frac{\partial^2 V}{\partial \theta^2} = 0$ so,

$$\frac{\partial^2 V}{\partial r^2} + \frac{1}{r}\frac{\partial V}{\partial r} + \frac{\partial^2 V}{\partial z^2} = 0 \qquad (2.20)$$

The particular solution of equation (2.20) can be obtained using the method of separation of variables and can be assumed to be of the form

$$V(r,z) = U(r)W(z) \qquad (2.21)$$

Substituting equation (21) to (20) and dividing throughout by the product U(r) W (z) gives

$$\frac{1}{U(r)}\frac{d^2U(r)}{dr^2} + \frac{1}{rU(r)}\frac{dU(r)}{dr} + \frac{1}{W(z)}\frac{d^2W(z)}{dz^2} = 0 \qquad (2.22)$$

This equation is satisfied if and only if

$$\frac{1}{U(r)}\frac{d^2U(r)}{dr^2} + \frac{1}{rU(r)}\frac{dU(r)}{dr} = \lambda^2 \qquad (2.23)$$

And

$$\frac{1}{W(z)}\frac{d^2W(z)}{dz^2} = -\lambda^2 \qquad (2.24)$$

Where λ is an arbitrary constant.

The solution of equation (3.1.24) may be given as

$$W(z) = C_1 e^{-\lambda z} \quad \text{and} \quad W(z) = C_2 e^{+\lambda z} \qquad (2.25)$$

and that of equation (24) is given as

$$U(r) = C_3 J_o(\lambda r) \qquad (2.26)$$

Where J_o is the Bessel function of order zero

The combination of equation (2.25) and (2.26) gives the particular solution of the deferential equation given by equation (2.20), which is

$$V(r,z) = C_4 e^{-\lambda z} J_o(\lambda r) \text{ and } V(r,z) = C_5 e^{+\lambda z} J_o(\lambda r) \quad (2.27)$$

Where c and λ are constants.

Since, by theory of differential equation, every linear combination of the particular solution is also a solution, one can make λ to rough all possible values from 0 to ∞ and allowing the constant "c" to very independence of λ the general solution of equation (2.21) can be obtained as

$$V(r,z) = \int_0^\infty \left[\Phi(\lambda) e^{-\lambda z} + \psi(\lambda) e^{-\lambda z}\right] J_0(\lambda r) d\lambda \quad (2.28)$$

Here $\Phi(\lambda)$ and $\psi(\lambda)$ are arbitrary functions of .the boundary conditions control the special form of these equations .From the basics theory, the potential generated by a single point source of current intensity "I" located at the surface of an electrically homogeneous earth is given by

$$V = \frac{I\rho}{2\pi} \frac{1}{\sqrt{r^2 + z^2}} \quad (2.29)$$

Where ρ is the resistivity of homogeneous Earth.

Equation (2.29) can be written in integral form by using the so-called Lipschitz integral (also called the Weber Integral Formula) in theory of Bessel function as

$$\int_0^\infty e^{-\lambda z} J_0(\lambda r) d\lambda = \frac{1}{\sqrt{r^2 + z^2}} \quad (2.30)$$

So that equation (2.29) gives

$$V = \frac{I\rho}{2\pi} \int_0^\infty e^{-\lambda z} J_0(\lambda r) d\lambda \quad (2.31)$$

Equation (2.31) is also a solution of equation (2.20). Therefore, the combined solution will also be a solution to the equation, that is

$$V(r,z)=\frac{I\rho}{2\pi}\int_0^{\infty}\left[e^{-\lambda z}+\Theta(\lambda)e^{-\lambda z}+\mathrm{X}(\lambda)e^{+\lambda z}\right]J_0(\lambda r)d\lambda \qquad (2.32)$$

Where θ(λ)and χ(λ) are arbitrary function λ. Solutions of equation (2.32) are valid in all the layers of the subsurface. However, necessarily the same in the different layers of the subsurface. Therefore, the potential due to a point source of current at the surface of a horizontally layered earth must in each layer satisfy

$$V_i(r,z)=\frac{I\rho}{2\pi}\int_0^{\infty}\left[e^{-\lambda z}+\Theta_i(\lambda)e^{-\lambda z}+\mathrm{X}_i(\lambda)e^{+\lambda z}\right]J_0(\lambda r)d\lambda \qquad (2.33)$$

This equation is called the Stefanescu Integral, with **I** referring to the several layers of the subsurface.

Boundary conditions

For a potential set up by a single source of current at the surface of a horizontally stratified earth

- At each of the boundary planes in the subsurface, the electrical potential must be the same

$$V_i = V_{i+1} \quad \text{at } z=h_i$$

- The vertical component of the current density must be continuous on each boundary plane (the current density normal to the boundary planes …)

$$(J_i)_N = (J_{i+1}) \quad \text{at } z=h_i$$

$$\frac{1}{\rho_i}\frac{\partial V_i}{\partial z} = \frac{1}{\rho_{i+1}}\frac{\partial V_{i+1}}{\partial z}$$

- At the surface (z=0) the vertical component of the current density J_v (and hence that of the electric field intensity) must be zero everywhere except in the infinitesimal neighborhood around the current source. (in air $J_{air} = 0$ and from condition (2), the vertical component of the current density at depth zero must be zero).near the current source the potential must not approach infinity (must remain finite) as at depth 0, Z =0, as r →0

$$V=\frac{I\rho}{2\pi}\frac{1}{\sqrt{r^2+z^2}}$$

- At infinite depth, the potential must approach zero, i.e. V →0 as Z→∞

2.1.4.1 Electrode configuration

This is determined by the mode of arrangement of the current and potential electrodes. There are different types of electrode arrays that can be used in the resistivity method. These include the Pole-Pole, Pole-Dipole, Dipole-Dipole, Wenner, Schlumberger, Lee Partition, Square, Gradient, Crossed Square array, and others. Generally, two (2) potential and two (2) current electrodes are used in electrical resistivity surveys. An exception to this is the Lee Partition electrode array which uses five (5) electrodes. For this survey, the Schlumberger array method was employed.

2.1.4.2 Schlumberger Electrode Array

This is a collinear array of electrodes in which the potential electrodes are located within the current electrodes. This electrode array is symmetrical because the station of measurement is at the centre of the array.

2.1.4.3 Quantitative VES Interpretation: Master Curves

Layer resistivity values can be estimated by matching to a set of master curves calculated assuming a layered Earth, in which layer thickness increases with depth. (Seems to work well). For two layers, master curves can be represented on a single plot. Master curves: log-log plot with ρ_a / ρ_1 on vertical axis and a / h on horizontal (h is depth to interface)

- Plot smoothed field data on log-log graph transparency.
- Overlay transparency on master curves keeping axes parallel.
- Note electrode spacing on transparency at which (a / h=1) to get interface depth.
- Note electrode spacing on transparency at which (ρ_a / ρ_1 =1) to get resistivity of layer 1.
- Read off value of k to calculate resistivity of layer 2:

The two layer master curve given in figure 2.4 below.

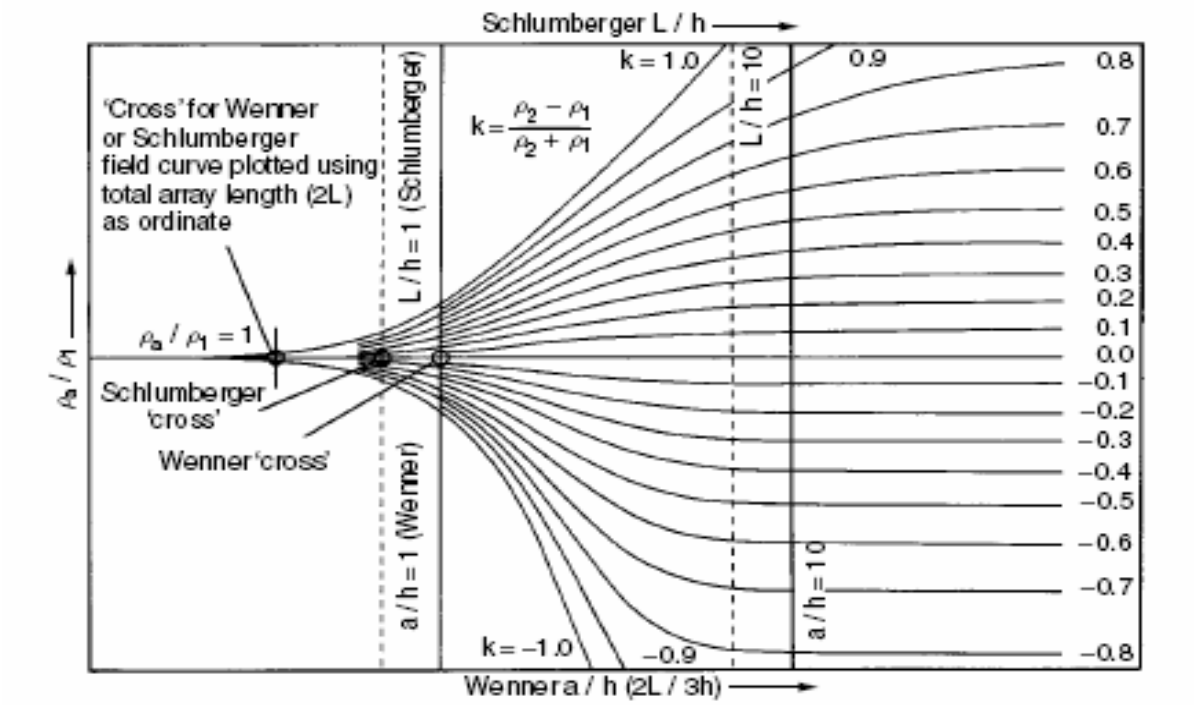

Figure 2. 4 Two layer master curve

2.2 The Magnetic Method

The earth's magnetic field resembles the field of a large bar magnet situated near the center of the earth. Many geological formations, by virtue of their magnetic minerals content, will behave like large buried magnets and will then have a magnetic field associated with them. These local magnetic fields will be superimposed on the magnetic field taken, in the locality of such geological formations, and show deviations from the undisturbed earth's magnetic field. These changes or anomalies could be large or small in magnitude, and could either increase or decrease the earth's main field. Their influences on the main field depend on the geometry, orientation, depth of burial and magnetic properties of the body and the direction and intensity of the inducing earth's field.

Magnetic surveys are used to locate and delineate:

• Magnetic iron ore deposits

• Metallic ore deposits which may have either magnetite associated with them.

• Geological structures like contacts, faults, dykes, etc.

Magnetic surveys are used in groundwater studies to map the depth to the magnetic basement rock and also it provide a valuable aid to litho logical mapping, as the character of a magnetic anomaly is

indicative of the rock. Moreover, it can also be applied in mapping structural features, which often provide a conduit for the accumulation of groundwater and, at times, act as barriers.

2.2.1 Principle of Magnetic Method

2.2.1.1 Magnetic force

The force between two poles of strength m_1, and m_2, situated a distance **r** apart is given by:-

$$F = \frac{m_1 m_2}{\mu r^2}\vec{r} \quad (2.34)$$

Where, r = unit vector from m_1 to m_2

μ = permeability = $\mu_0\mu_r$

μ_r = relative permeability (~ 1 for air and many rocks)

μ_0= permeability of free space =4 π x10^{-7} H/m

r = separation between m_1 and m_2

2.2.1.2 Flux density/Magnetic induction

A magnetic field strength gives rise to a magnetic flux. The magnetic flux density that is the flux per unit area, also called magnetic induction, is denoted by **B,** and the field strength by **H**. The magnetizing force (field strength) gives rise to the flux density, i.e. the cause of the magnetic field is the magnetizing force, thus

$$B = \mu H \quad (2.35)$$

Where, μ is the absolute permeability of the medium (Ω-sec-m^{-1})

H is magnetizing force or field strength (Am^{-1})

B is flux density [Vsm^{-2}] or [Wb-m^{-2}] it is also called tesla [T].

The absolute permeability of vacuum is denoted by μ0, its value in SI unit is: $4\pi \times 10^{-7}$ Ω-sec.-m^{-1}, thus in vacuum the flux density due to a magnetizing force **H** will be

$$B = \mu_0 H \quad (2.36)$$

For most practical purposes, the absolute permeability of air, and even most rocks, may be taken to be μ_0.

2.2.2 The Earth's Magnetic Field

The Earth's magnetic field is akin to that of a dipole situated at the center of the earth with its magnetic moment pointing towards the Earth's geographical south. The Earth's magnetic field vector **F** is completely specified at any point by its elements. Figure 3.4 shows the elements of the Earth's magnetic field.

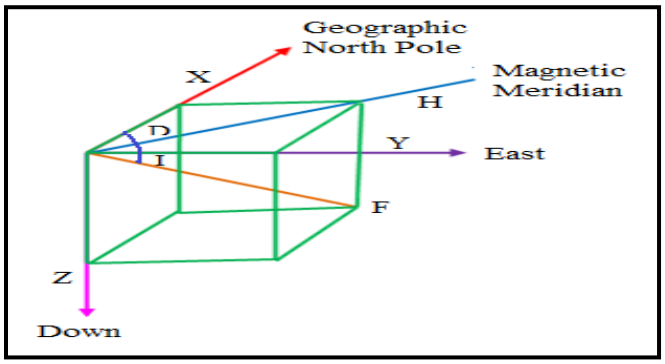

Figure 2. 5 Elements of the Earth's magnetic field

According to figure3.4, the earth's total field is F makes an angle I (the inclination) with the horizontal plan. It can be measured by a dip needle and is also called magnetic dip.

The angel D is the angel between geographic north and magnetic north, or the declination of **H** (here, **H** is the horizontal component of the total field vector, **F**) east or west of true north.

In the northern hemisphere the magnetic field is directed downwards towards the north magnetic pole and in the southern hemisphere it is directed up wards and away from the south magnetic pole. At the magnetic equator the magnetic field is horizontal and at the magnetic poles the field is vertical i.e., the strength of the earth's field varies from 25,000 - 30, 000 nT in the equatorial regions while 60,000 - 70,000 nT, in the polar regions.

The amplitude of total field varies more rapidly along the N-S direction as compared to the east-west. On figure3.3, **Z** is the vertical component of the total field (**F**). It is directed downwards in the northern hemisphere (+ve) and upwards (-ve) in the southern hemisphere. **H**, which is the horizontal component of **F**, is directed towards magnetic north for both the Southern and Northern hemispheres.

2.2.3 Relative permeability, susceptibility and magnetization

For a medium other than vacuum we write $\mu = \mu_r \mu_0$ we get from equation (2.37)

$$B = \mu H = \mu_r \mu_0 H = \mu_0 H + \mu_0(\mu_r - 1) = \mu_0 H + \mu_r k H \quad (2.38)$$

Where, we have put, $k = \mu_r - 1$, that is $\mu_r = 1 + k$

μ_r is a ratio of the two permeability's: $\mu_r = \frac{\mu}{\mu_0}$ and therefore is a pure number. It is called the relative permeability of the medium, and k is called susceptibility; it is also a dimensionless quantity. For a vacuum, $\mu_r = 1$ and $k = 0$.

From eq. 2.38, to obtain in vacuum a flux density equal to the density μH in the medium under consideration, we would need an additional magnetic field strength kH. This additional field strength that may be said to be present at points of space occupied by a medium subject to a field strength H is known as intensity of magnetization M induced by H. The direct relation is given by:

$$M = kH \quad (2.39)$$

Since K is a pure number M is also measured in Am-1. Further B and H are vectors we can state equation 2.39 more generally as magnetic induction (total field within a body) and written as:

$$B = \mu_0(H + M) \quad (2.40)$$

Then, for the x, y and z components of B, in an orthogonal coordinate system, we have

$$\left.\begin{aligned} B_x &= \mu_0(H_x + M_x) \\ B_y &= \mu_0(H_y + M_y) \\ B_z &= \mu_0(H_z + M_z) \end{aligned}\right\} \quad (2.41)$$

Equation (2.41) implies, a magnetic body placed in a magnetic field becomes magnetized by induction. The magnetization (M) is proportional to the inducing external magnetizing force. The constant of proportionality K is the magnetic susceptibility. It is a dimensionless quantity.

Magnetic susceptibility is a measure of the degree to which a material gets magnetized. The larger the susceptibility the greater the intensity of induced magnetization (M) and hence the bigger will be the anomaly produced relative to the Earth's field. The susceptibility of rocks is almost entirely controlled by the amount of ferromagnetic minerals, their grain size, and mode of distribution and hence is highly variable.

2.2.4 Noise and Correction

All magnetic data sets contain elements of noise and will require some form of correction to the raw data to remove all contributions to the observed magnetic field other than those caused by subsurface

magnetic sources. In ground magnetic survey, it is always advisable to keep any magnetic objects like high electric power cable, railway and keys etc., which may cause magnetic noise, away from the sensor. In all magnetic data, diurnal and IGRF correction can be applied. The most significant correction is for the diurnal correction in the Earth's magnetic field. Base station readings taken over a survey period of facilitate the compilation of diurnal correction.

$$DC = \left(\frac{BS_f - BS_i}{t_f - t_i} \right)(t_o - t_i)$$

Where $DC =$ Diurnal Correction

$BS_f =$ Final Base Station Reading $BS_i =$ Initial Base Station Reading

$t_f =$ Observed Time of Final Base Station Reading $t_i =$ Observed Time of Initial Base Station Reading

$t_o =$ Observed Time of each point.

In order to produce a magnetic anomaly, the data have to be corrected to take into account the effect of latitude and, to a lesser extent, longitude. As the Earth's magnetic field strength varies from 25000nT at the magnetic equator to 69000nT at the poles, the increase in magnitude with latitude needs to be taken into account (Reynolds, 1997).Survey data at any given point can be corrected by subtracting the theoretical filed value obtained from IGRF, from the measured value.

2.2.5. Interpretation of Magnetic Data

There are two ways of interpretation: qualitative and quantitative techniques.

2.2.5.1 Qualitative interpretation

For qualitative interpretation the following profile curves and maps were prepared:

- ✓ Profile Curves help to see the changes of the anomalous structure of the subsurface.
- ✓ Statistical Filters such as averaging (Moving average) and median filters used to remove spurious noise or to smooth anomalies to make them more interpretable.
- ✓ Contour Maps have traditionally been a popular way of presenting gridded data. These maps have largely been replaced by images in recent years. Like stacked profiles it can be difficult to choose a single contour interval suitable for all the data. Where recognition of absolute amplitudes of anomalies is important these presentations are important. Many interpreters continue to use contours

because they are superior to images when gradients of anomalies are to be used in determining dips of structures.

- ✓ Analytic Signal transformations combine derivative calculations to produce an attribute that is independent of the main field inclination and direction of magnetization as well as having peaks over the edges of wide bodies. Thus a simple relationship between geometry of the causative bodies and the transformed data are observed.

2.2.5.2 Quantitative interpretation

The essence of quantitative interpretation is to obtain information about the depth to particular magnetic body, its shape and size and details about its magnetization in two possible ways. One is direct, where the field data are interpreted to yield a physical model. The other is the inverse method, where models are generated from which synthetic magnetic anomalies are generated and fitted statistically against the observed data. The degree of detail is limited by the quality and amount of available data and by the sophistication of either the manual methods or the computer software that can be used.

- ➢ Depth estimation based on magnetic method

The depth estimation methods were used to determine the depth of the basaltic intrusions, basement complex and calculated the thickness of the sedimentary section in the studied area. The advantage of these methods is to delineate any geological structures such as faults, dykes-like structures and volcanic basaltic intrusions, etc.

- ➢ 2D Modeling

The 2D modeling method was done to create the type lithology of the area with their respective thickness by constraining with the geo-electric section and the existing boreholes. The model was prepared along the profile and it indicates the faults and fractures of the study area. The model was carried out on GMSYS program on Oasis Montaj software.

Chapter Three

Data Acquisition, Processing and Presentation

3.1 General

The water works design and supervision enterprise (WWDSE) selected an area Northeast of AA and Oromia special zone to be studied in detail for groundwater resources potential based on previous detailed geological and hydro geological and previous VES surveys (WWDSE, 2008).

The choice of geophysical techniques for subsurface investigations should be made judiciously as their success depend, largely, on their suitability to the problem, among other factors. Certain problems are best solved by a particular method than other and thus, require serious consideration. However, the local terrain conditions, access and logistic difficulties, and most importantly availability of instruments and associated cost, impose further constraints on this difficult task. In light of the above mentioned considerations, potential filed methods, namely electrical resistivity technique using Vertical Electrical Sounding (VES) are appraised to achieve some of the objectives of the research work.

In light of the above mentioned considerations, potential filed methods, namely electrical resistivity technique using Vertical Electrical Sounding (VES) are appraised to achieve some of the objectives of the research work.

The geophysical observations have been carried out along four traverse lines. The layout of the geophysical observation points and lines is shown in figure 3.1 below.

Magnetic surveys are frequently employed in mapping regional geological structures owing to their sensitivity to variations in the diagnostic physical parameters (magnetic susceptibility. Cost effectiveness is yet another plus point for the preference. The other method, found to be adequate for problems related to the principal objectives of the work, is that of electrical resistivity technique using Vertical Electrical Sounding (VES).The instrumentation and data acquisition of the magnetic survey and the Vertical Electrical Sounding (VES) geophysical methods performed in this study are explained below.

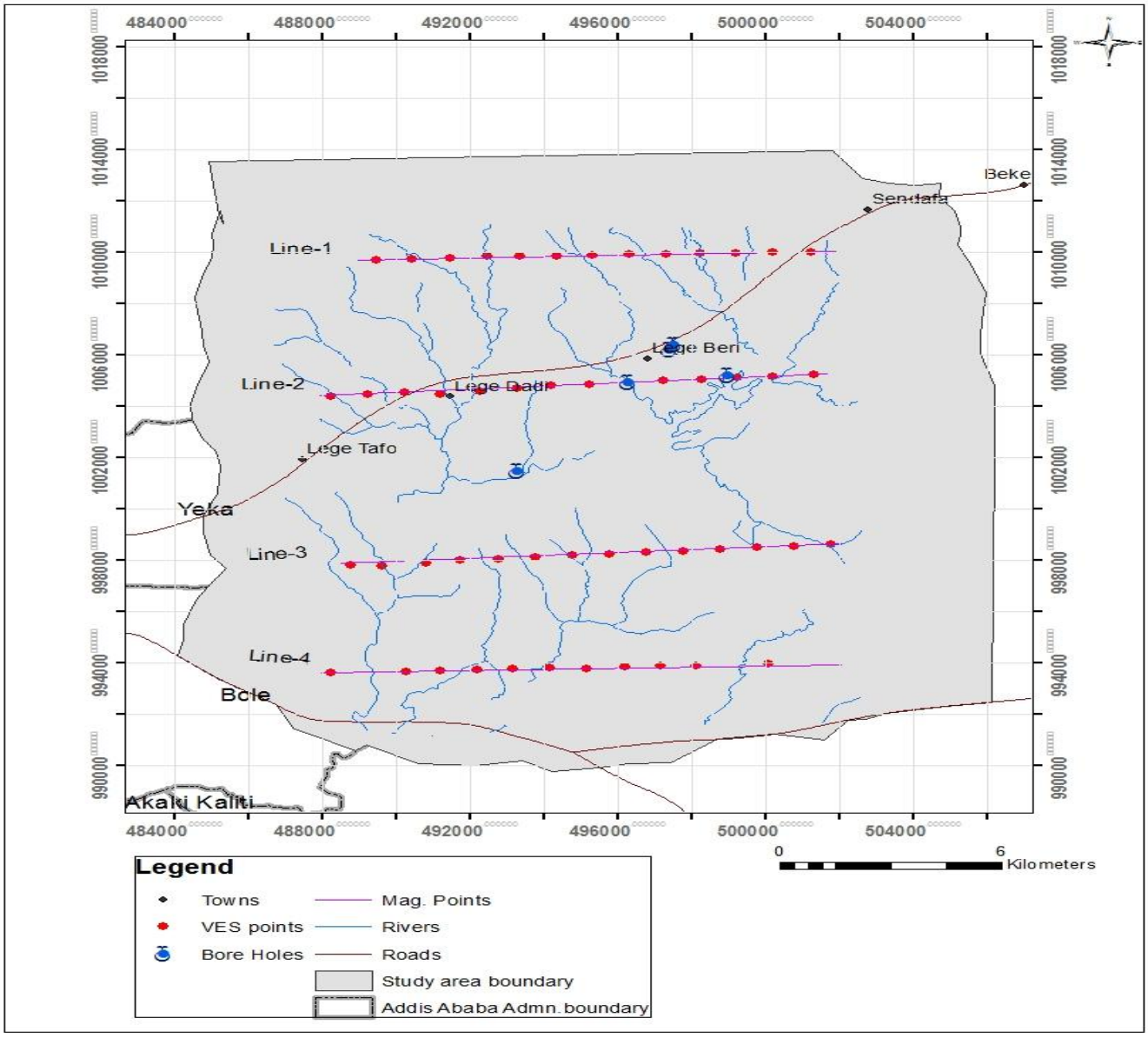

Figure 3. 1 Location map of geophysical survey traverses and boreholes

3.2 Instrumentation and Data Acquisition

3.2.1 Vertical Electrical Sounding

The Vertical Electrical Sounding survey was carried out along four traverse lines oriented approximately southwest -northeast within the area and observations were made at around 0.9km to1km sounding station spacing. A Schlumberger array using current electrode spacing 1500m (AB/2=1500m) was

generally used to the maximum depth of investigation. A total of fifty two (52) VES distributed on four different lines were surveyed in the study area with traverse separation ranging from 4km to 6.5km.

3.2.1.1 Instrumentation

The Vertical Electrical Sounding (VES) survey was carried out using the AGI Super Sting R1 electrical resistivity unit having a maximum current output of 2A.The Schlumberger electrode configuration was used for the Vertical Electrical Sounding measurements in all the investigated lines, with the maximum half-current electrode separation of 1500m.

3.2.1.2 Data Acquisition

A total of fifty two sounding data were used for this thesis work, all the points obtained from Water Works Design and Supervision Enterprise (WWDSE). Generally the resistivity survey was not conducted on a regular grid thus, the spacing of the VES points were not uniform. Rather, they were dictated by the geology, topography and accessibility of the area under investigation. The symmetrical Schlumberger electrode configuration was used for all soundings. The maximum current electrode separation, AB/2=1500m, was chosen based on the depth of interest, (the anticipated depth to the water bearing horizon) and subsurface geology.

3.2.2 Magnetic Survey

3.2.2.1. Instrumentation

The total fields magnetic survey was carried out along all transect lines using G-856AX Portable Proton Precession Magnetometer, which is a versatile and rugged tool for such a survey and, handheld GPS was used for recording the time and position of each stations.

3.2.2.2 Data Acquisition

A total field magnetic survey was carried out along VES lines and readings were taken every 20m along all traverse lines of the VES. A total of two thousand eight hundred ten data were acquired, with transect separation similar to that of the VES, i.e. ranging from 4km to 6.5km. The profiles where oriented about northwest-southeast in order to cross and so to detect the possible structure related to groundwater occurrence. Some of these magnetic data were taken near to the previously drilled boreholes. The total

magnetic intensity, the time, date, station distance and the location of data points were recorded during the field work. In each stations the data was taken three times to take the average keep the quality of the data and taking base station readings at the beginning and end of a 1km interval of the magnetic survey for the profile to overcome diurnal variation.

3.3 Data Reduction, Processing and Presentation

3.3.1 VES Data Reduction, Processing and Presentation

3.3.1.1 Data Reduction

The apparent resistivity values are plotted on logarithmic transparent paper. In processing of the collected data, the apparent resistivity value on the ordinates and the electrode separation (AB/2) on the abscissa. The resistivity measurements were made by progressively increasing the potential electrode distance (MN) for relatively large increment of the current electrode distance (AB/2). In most cases the sounding curve is segmented due to overlap measurement and cannot be interpreted as it is. To have precise interpretations the segmented curves were shifted to the small MN curve points, so that the effect could be quantified and corrections could be made in order to obtain a single smooth curve that could be processed with the computer using "RESIXIP" software (Velpen, 1995)

3.3.1.2 Data processing and presentation

The electrical sounding data collected in the field work were plotted on a bi- logarithmic paper and interpreted by using two layer master curves and auxiliary charts to find out initial model parameters for the thickness and electrical resistivity of the possible layers mapped with survey. These parameters obtained from curve matching techniques arranged and analyzed with litho logical units of existing boreholes were used as initial model in the **WIN RESIST** inversion software which resulted in improved and reliable electrical parameters under the area of investigation as depicted in the interpreted sounding resist curves. Consequently, from the results of these interpreted geoelectric parameters. The depth, thickness and resistivity parameters acquired by the mentioned software program of vertical electrical sounding curves were used to construct geo-electric sections for each VES to show the distribution of different litho logical unit in vertical direction using the software **MapInfo professional** programs. Geo-electric Sections are constructed according to the traverses they positioned. Available litho logical logs from boreholes in proximity of the surveyed traverses have been used for calibration

and further refining the results. Thus, interpreted VES points at existing well sites are employed for calibrating the sounding points with in the area.

3.3.1.3.1 Qualitative Analysis

The aim of interpreting Field VES curves is to determine the thickness and resistivity of subsurface layers in order to obtain the geological picture of the subsurface. Nevertheless, it is mandatory and beneficial to make quick qualitative assessments of the field curves before a detail quantitative interpretation. At early stages of geophysical survey programs, such a practice provides crucial parameters, which may influence the further progress of the data acquisition process. In addition to that, this helps to impart some useful prior knowledge on the geo-electric nature of the area under investigation. On the latter (processing and interpretation) stage, the spatial distribution of electrical parameters can be depicted in the form of plan maps and depth pseudo-sections. In the present case the smoothed field data, from spatially aligned adjacent soundings, have been plotted in the form of pseudo-sections, using the apparent resistivity (ρa) and pseudo depth values (AB/2). Such plot enables to geo-electrically characterize the area both in vertical and lateral directions.

3.3.1.3.2 Quantitative Analysis

The Schlumberger sounding curves, resulted from field measurements were initially analyzed through the classical procedure known as curve matching, using two layer master curves and auxiliary point charts, (Bhattacharya and Patra, 1968). In this preliminary manual interpretation, the number of layers, their thicknesses and resistivity's are obtained. These parameters help to develop a preliminary, conceptual multilayer earth model of the study area.

The layer parameters so obtained have been used as starting models for a computer based modeling and inversion programs. In the present case, the resistivity and thickness values, resulted from the former procedure, were entered as initial models to an iterative-least squares inversion program, RESIST (Velen, 1988), for further refinement and final analysis. The inversion algorithm generates theoretical Schlumberger apparent resistivity curves of the starting models and compares it to the field curve at the given current electrode positions. In case of discrepancies between the two, the program iteratively adjusts the model, until a satisfactory fit is obtained between the observed (field curves) and computer generated theoretical sounding curves. The program terminates based on either pre-determined error criterion (in least squared senses) or at a maximum number of iterations, as defined by the user.

However, due to the well-known problems inherent to the interpretations of VES curves, namely equivalence and suppression, the best-fit model may not necessarily agree with the geology of the area under investigation. Thus, in order to arrive at an accurate and reasonable conclusion, the VES curves were interpreted in light of the knowledge of the local geology and other priories. Moreover, attempts have also been made to correlate and adjust the VES results with geologic log of boreholes, whenever available. Finally, geo-electric sections were constructed by correlating the interpreted true resistivity's and thicknesses of adjacent soundings in order to depict the geo-electric stratifications of subsurface. Such sections, under favorable circumstances and judicious analysis, provide closer pictures of the subsurface geology. The VES curves, Resistivity maps, Pseudo depth sections and geo-electric sections are given from figure 4.1-4.15.

3.3.2 Magnetic Data Reduction, Processing and Presentation

3.3.2.1. Data Reduction

The magnetic data reduction is taken to remove noise from the data that are not related to the geology of the site. This process thereby prepares the dataset for interpretation by reducing the data that contain signal only relevant to the task. During the reduction process data checking and editing, diurnal removal and IGRF removal are performed.

3.3.2.2. Data processing and presentation

The processing of the total intensity map revealed a set of processes such as Observed Total Magnetic Anomaly Map, residual anomaly map, analytic signal map, and 2D modeling construction. All processed map are used for qualitative interpretation. The qualitative interpretation for the constructed magnetic maps, aims to get a clear view of the subsurface structures, estimation of the relative depth of the magnetic anomalies sources. The quantitative interpretation has been used to determine the depth of shallow subsurface structures (faults and dykes), fractures and contacts of the studied area. The analysis and processing were done by specialized computer program (Oasis Montaj V.6.4.2, 2007). All processes of magnetic data are represented by profile curve, maps and 2D models (from figures 4.16-4.24).

Chapter Four

Discussions and Interpretations

4.1 General

As it is mentioned in chapter four the result of vertical electrical sounding (VES) presented in the form of interpreted VES curve, pseudo-depth, slice staked map and vertical geoelectric section. And also the results of the magnetic survey presented as curve and different maps. Residual anomaly map, analytic signal map, TDR map, vertical derivative map, horizontal and vertical gradients of analytic signal map and RTP map, upward continuation map for 2D modeling, Euler deconvolution and 2D model map for qualitative and quantitative interpretation. The results presented and discussed in four profiles.

4.2 Discussions and Interpretation of VES

4.2.1 Interpreted VES Curves

Apparent resistivity versus electrode spacing (AB/2) plotted on a bi-log scale during field work is interpreted using the IPI2Win to obtain the initial model to the inversion software
(Win Resist). It is seen from the interpreted field curves that a very good correlation between the field data and the interpreted model sections are obtained for all VES points. The RMS error of VES's is between1% to 3.7% obtained for the sounding data. Four VES observations were conducted as model resistivity curves selected according to their resistivity and depth. The model VES curves explained briefly below.

4.2.1.1 VES 14 (488215 E, 1004389 N)

The model result of VES 14 is shown in Fig. 4.1. According to the result of VES 14, the depth extent of groundwater occurrence is expected to be between 169–415 meters. Consequently, a well was recommended to be drilled at the location of VES 14, up to a maximum depth of 415 m.

The lithological log succession of the borehole indicates that the aquifer at this location is a sequence of slightly fractured, moderately weathered fractured and slightly fractured basalt flows. The relative degree of saturation of the aquifer can be explained by the magnitude of the resistivity values of the alternating layers of the basalt flow (see model below). The model curve VES 14 shown in figure 4.1

below.

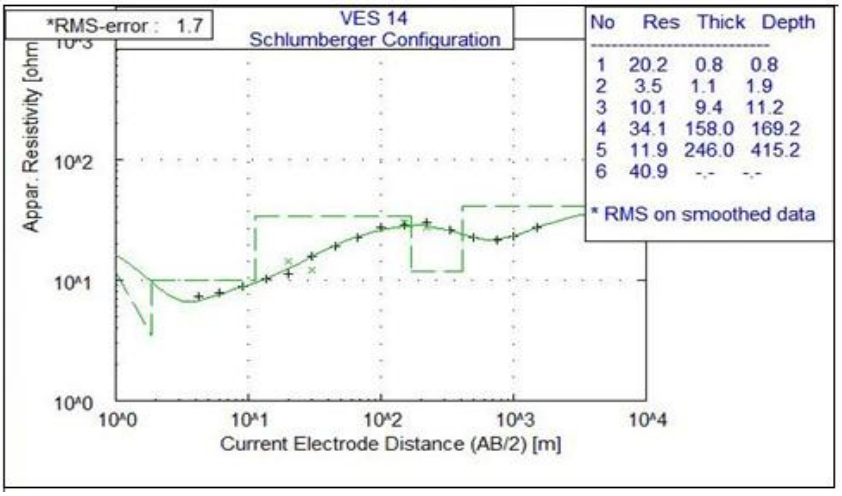

Figure 4. 1 modeling result of VES 14

4.2.1.2 VES 34 (494760 E, 998190 N)

The result of modeling VES 34 is shown in Fig.4.2. Since, the maximum depth of probing at this VES station was 155 m. However, a borehole was drilled around at this location by AL Nile Business Group up to a maximum depth of 432 m.

The lithological description of the borehole suggests that the area is underlain by a sequence of moderately and slightly scoraceous basalts of varying degree of weathering and fracturing. While the upper 150 meter is mainly overlain by massive basalt, the zone between 150 – 250 meter is underlain by varying degree of fractured basalts. The main aquifer at this site is therefore fractured basalts.

The zone between 65 – 155 m is characterized by a resistivity value (28Ω-m) and is expected to be partially water bearing, since it corresponds to the section of the borehole underlain by fractured and decomposed massive basalt. However, the zone below 155 m was characterized by a relatively higher.

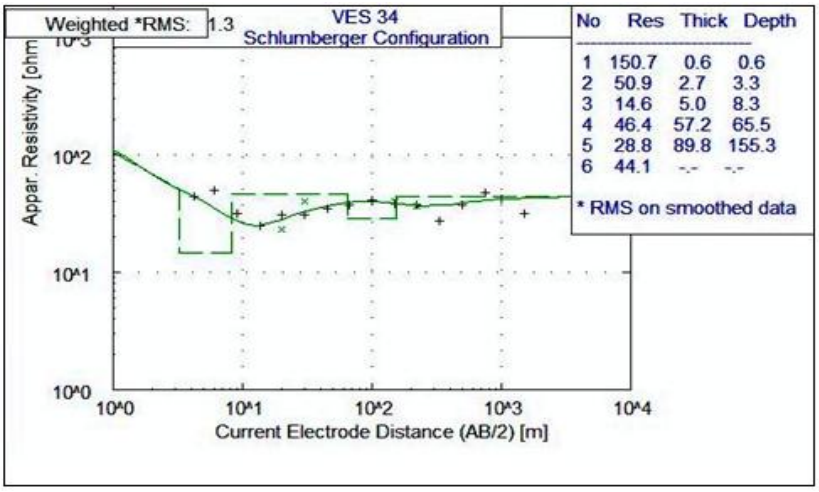

Figure 4. 2 Modeling result of VES 34

4.2.1.3 VES 41 (501752 E, 998607N)

The result of modeling VES 41 is shown in fig.4.3 below. The maximum depth of this modeling VES is 217. The zone between 8 – 217 m is characterized by a resistivity value (30Ω-m) and also expected to be water bearing zone.

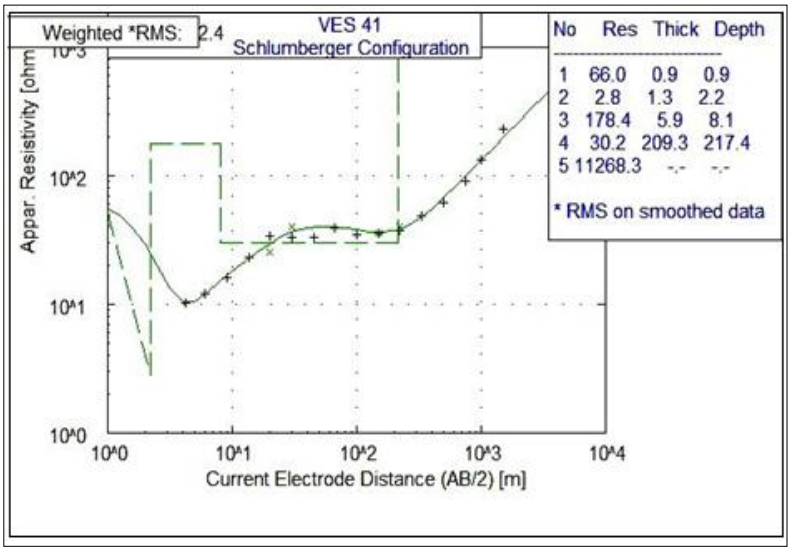

Figure 4. 3 Modeling of VES 41

4.2.1.4 VES 47 (494131E, 993826N)

The result of modeling of VES 47 is shown in Fig.4.4 below. Based on the results of the VES observation at the location, a borehole was recommended to be drilled up to a maximum depth of 250 meter. The maximum depth of this modeling VES is 392m.

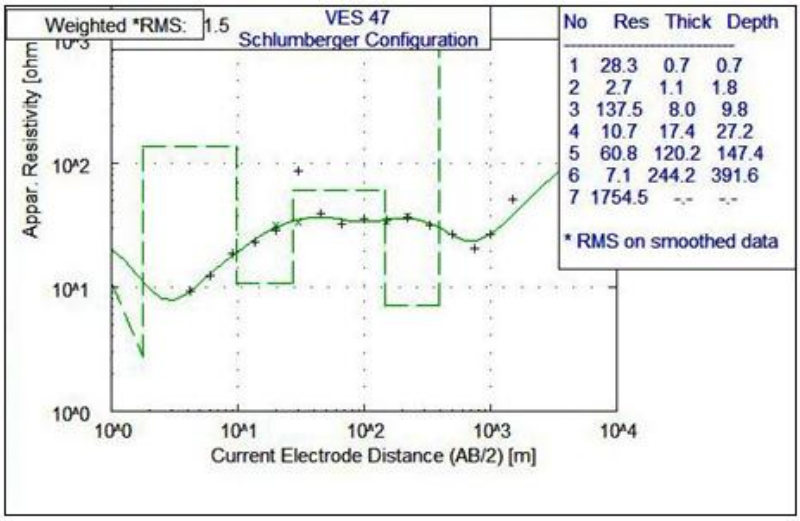

Figure 4. 4 Modeling of VES 47

4.2.2 Sliced-Stacked Section

The apparent resistivity sliced-staked map shown in Figure 4-5 is prepared by two dimensional plan maps for selected AB/2 values of 1.5, 20, 45, 100, 220, 500, 1000, and 1500. All VES points are used for qualitative assessments of the electrical nature of the geologic medium at different depth. The sounding points are approximately evenly distributed from surface to a depth. So it is believed to give a good representation of the ground overall.

The sliced-stacked map shows the relative variation of the apparent resistivity value of the whole area laterally as well as vertically at different depths of the spacing of current electrodes. The apparent resistivity value varies considerably from 0-440Ω-m.

According to the objectives of this thesis work, the most interesting feature of this sliced plot is the low resistivity zone.

The value of the high apparent resistivity value decreases as the depth increases. The value of the low apparent resistivity observed in the west, northwest and northeast parts of the study area.

Relatively high resistivity value is observed in the south part of the area except AB/2 of 45, 100,500 and some parts of AB/2 1000m. In this region's the resistivity value ranges between 160 up to 360 Ohm-m. The high resistivity variation specifically observed at AB/2 of 45,100 and 500m. Fig.4.5 shows sliced-staked section of the four profile lines at different depth of AB/2.

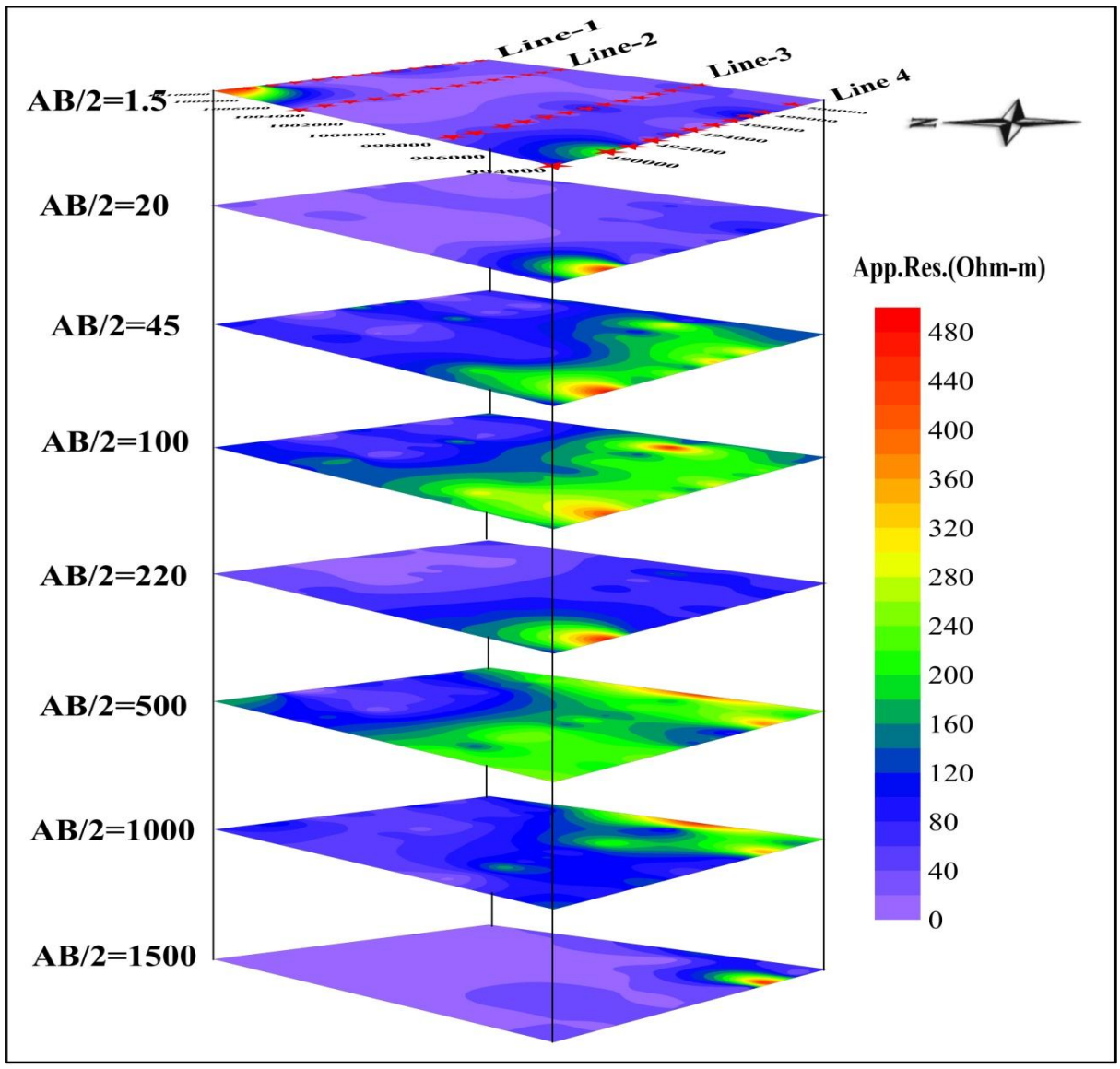

Figure 4. 5 Sliced-Stacked section for different AB/2.

4.2.3 Apparent resistivity Pseudo depth and Geo-electric sections along the selected Lines

From the total of 52 VES, it has been possible to select a number of VES that are well aligned to enable us to construct pseudo depth and geo-electric sections. To this end, 4 parallel lines (Lines-1to Line-4) were chosen. The number of VES on each line and the designation of the VES are given in the following table:

Line No.	VES points lying on the traverse Line	Line length (km)
1	VES 1,2,3,4,5,6,7,8,9,10,11,12 and 13	11.774
2	VES 14,15,16,17,18,19,20,21,22,23,24,25,26 and 27	13.12
3	VES 28,29,30,31,32,33,34,35,36,37,38,39,40 and 41	13
4	VES 42,,43,44,45,46,47,48,49,50,51and 52	11.877

Table 4. 1 VES points on each line and its length

On the average, the VES on each line are found to be spaced at 1km. The apparent resistivity pseudo depth section along the selected lines are mapped from raw data using **Surfer 10** software and the resistivity sounding geo-electric sections along the selected line are constructed from the interpreted layer parameters of each VES points (sample interpretations of the individual VES are shown in (Appendex-2). In interpreting these field curves, a combination of RESIXIP (IPI2Win + IP) and **Win Resist** software were used. The initial model parameters were obtained using the RESIXIP interactive software. These model parameters were then used to invert the field data. Optimal RMS error of less than 4 has been taken to be acceptable.

In the following sub sections, the apparent resistivity pseudo depth and geo-electric sections for each line are presented and discussed separately.

4.2.3.1 Traverse Line-1

This line is oriented in near North West to south east direction. The line has a total length of about ≈11.8km and there are 13 VES (VES 1, 2 …13) with average VES point spacing of about 0.9 km. The

representative pseudo depth and geo-electric sections for the Line are presented in Figures 4.6 and 4.7 and are discussed below.

Pseudo depth section along Line-1

The pseudo depth section constructed for the 11 VES that lie on the survey traverse Line-1 are given in Figure 4.6. According to this figure, there is a slightly lateral variation in resistivity in the top most part of the section with prominent high resistivity top zones mapped around only. This high resistivity zone is not extending to other VES points. Otherwise, the vast region under the section shows extensive coverage of the low resistivity zone. The resistivity ranges (0 to 60Ω-m) of this low resistivity regions are indicative of potential water saturation.

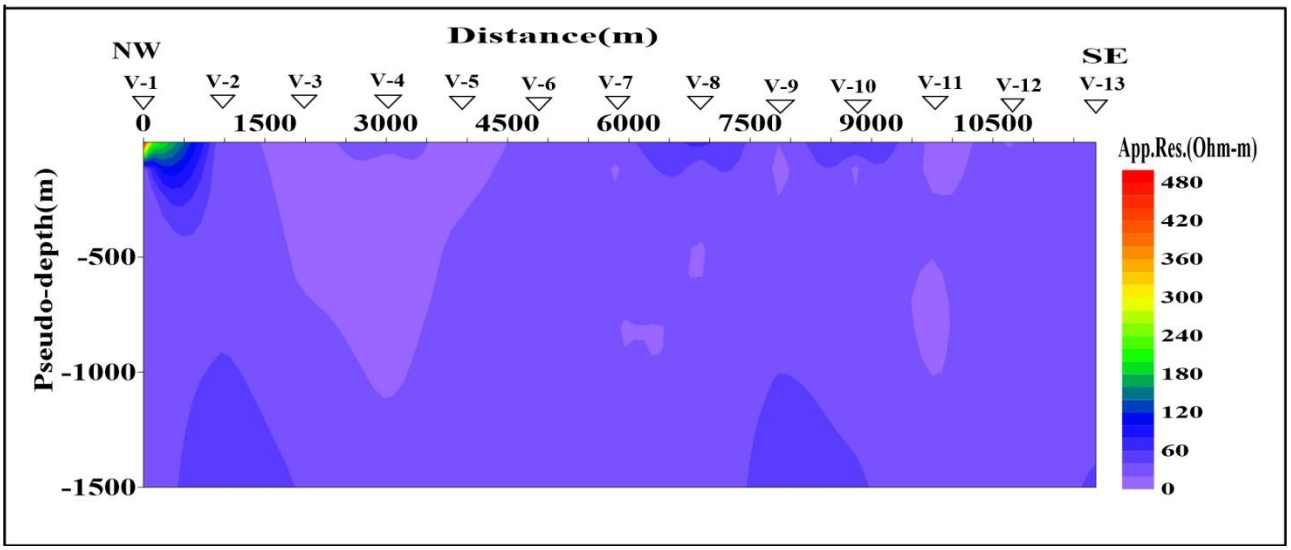

Figure 4. 6 Pseudo depth sections along Line-1

Geo-electric section along Line-1

According to the geo-electric section shown in figure4.7, the uppermost part is represented by widely varying resistivities from 16 to 182Ω-m. The very high resistivity values are generally observed at the relatively elevated zones attributed to moderately fractured and slightly fractured volcanic rocks. The very low resistivity units are associated with decomposed materials, clay and ash while the relatively intermediate to high, resistivity's are interpreted as comprising dry and stiff clay, highly fractured and decomposed volcanic units, tuff and ash and fractured to slightly fractured

volcanic rocks respectively. The thickness of these units is generally below 40m; however, in the extreme case (within the top unit) it reaches 80m. The clayey unit attains maximum thicknesses generally associated with the lower elevated zones and close to inferred geological structures.

As we go deeper we can see clearly distinguished very thick zones of intermediate resistivities with pronounced lateral variations. According to observations of the borehole samples corresponding to BH-LLA-PW6 (Appendix-4) and general geology of the Legedai-Ayat area the various resistivity units underlying traverse line one may be interpreted as comprising:

- Top dry soil(16 -182 Ω-m)
- Moderately weathered and fractured basalt(2-17Ω-m)
- highly weathered basalt(7 -38.9 Ω-m)

As could be discerned from the geo-electric section, the resistivity values for the moderately and slightly fractured and weathered as well as fresh rock units appear relatively lower than expected because of the bulk resistivity effect of the subsurface units.

Moreover, due to limited geological and hydro geological information of the area, it may not be possible to describe with much exactitude, at this moment.

Moreover, zones of very low resistivity's (< 9Ω-m) at depth are interpreted as comprising volcanic rocks highly decomposed in to clay or presence of ash and or tuff. These zones may be less productive and create (possible collapse) problems during drilling.

Furthermore, geological structures are inferred between stations 0 and 11774. These inferred structures need to be checked and their positions be adjusted by Magnetic data for the VES observation interval is too wide to accurately indicate the positions of structures.

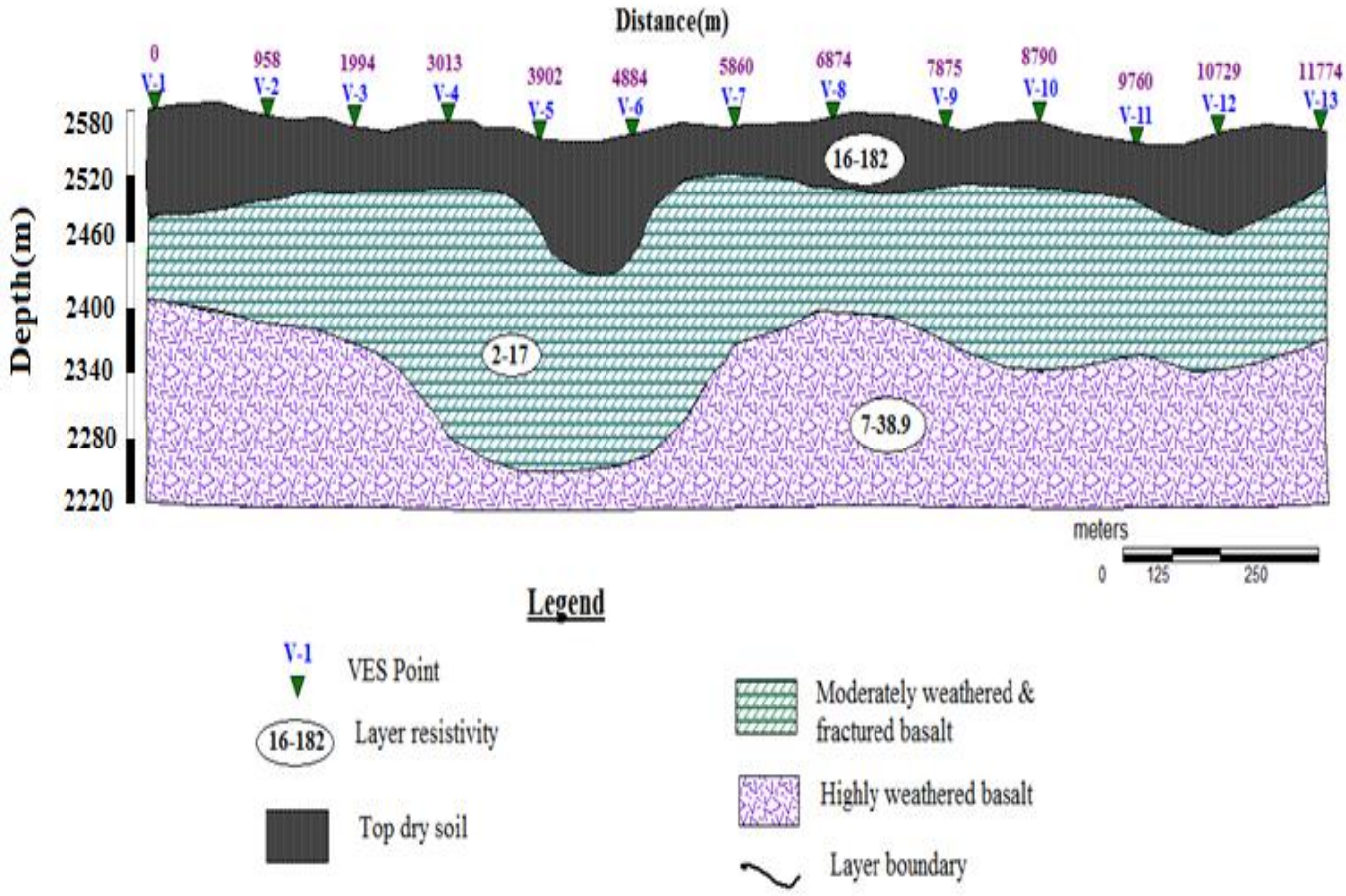

Figure 4. 7 Geo-electric section of traverse line one

4.2.3.2 Traverse Line-2

This line is the survey line is oriented in North West to South East direction running parallel to the other three lines. The line has a total length of about ≈13km and there are 14VES (VES points 14-27) with average VES point spacing of about 0.93km. The representative pseudo depth and geo-electric sections for the Line are presented in Figures 4.8 and 4.9 and are discussed below

Pseudo depth section along Line-2

As the pseudo depth section of this profile shows (Figure 4.8), the top layer mapped for all the 14 VES points is low resistivity. Overall, it is seen that the vast portion of the section is covered by low resistivity zone. The resistivity ranges (6 to 36Ω-m) of this low resistivity region are to be expected for potential water saturated area. As it is observed there is slightly high resistivity in two VES points (VES

24 and VES 27). This high resistivity ranges from 42 to 60Ω-m. In VES 24 the high resistivity is located between a depth of 500m and 100m and in VES 27 the high resistivity value is located between a depth of 750m and 1500m.

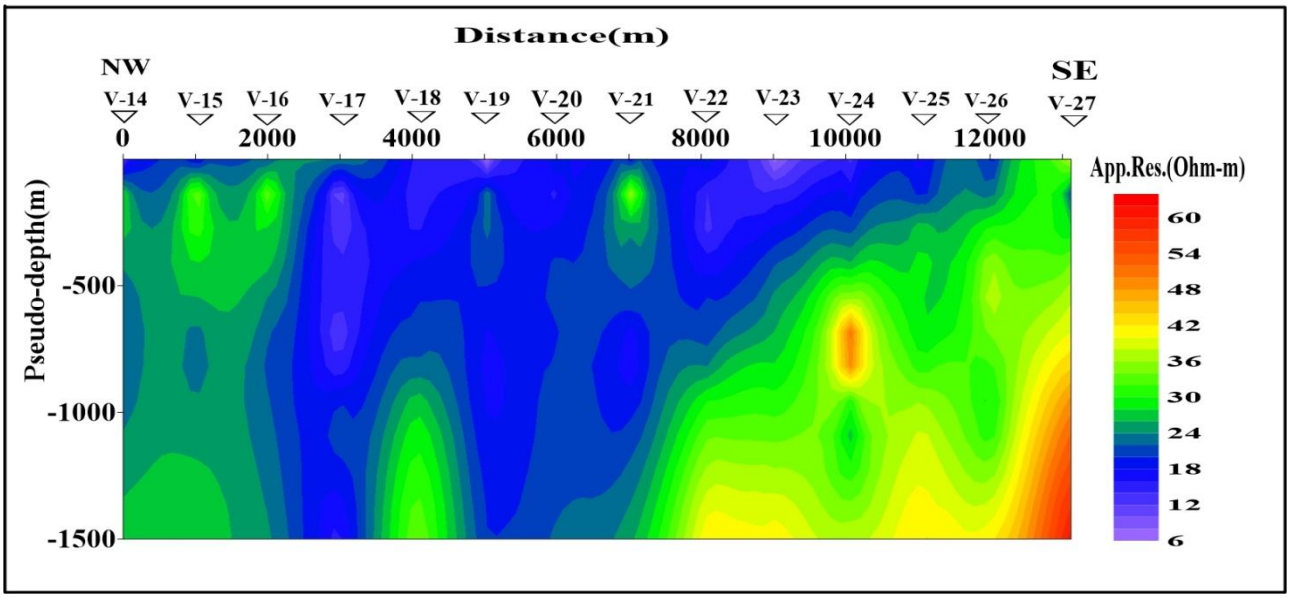

Figure 4. 8 Pseudo depth sections along Line-2

Geo-electric section along Line-2

According to the geo-electric section corresponding to traverse line two shown in figure 4.9, the very low resistivity units (2-40Ω-m) corresponding to the top soil as well as those depicted at intermediate and greater depths to the south west of station 1000 and below station 8087, in the central area are associated with clay, ash and highly decomposed materials.

Most intermediate units are represented by 2.4-14.9Ω-m and 4-17.4Ω-m resistivity's probably related with highly fractured and decomposed rocks and consolidated ash (tuff) and highly to moderately fractured and weathered volcanic rocks (probably water saturated) respectively. In addition, resistivities in the range of 40-100Ω-m are interpreted as comprising moderately to slightly weathered fractured volcanic rock (probably with partial ground water saturation). Zones with very high resistivity's generally above 90Ω-m are observed at depths 300m attributed to the fresh volcanic rocks comprising the bed rock. These are indicated at relatively shallow depth (200-450m), in the central part of the section between station 7038 and 8087 and within a depth range of 120-

250m to the east of station 8087; in the southwestern part of the line the depth to the bedrock exceeds 400m. The maximum depth is expected between stations 7038 and station 11057. The very high bottom resistivity units (> 100Ω-m) are related to slightly fractured and fresh volcanic rocks.

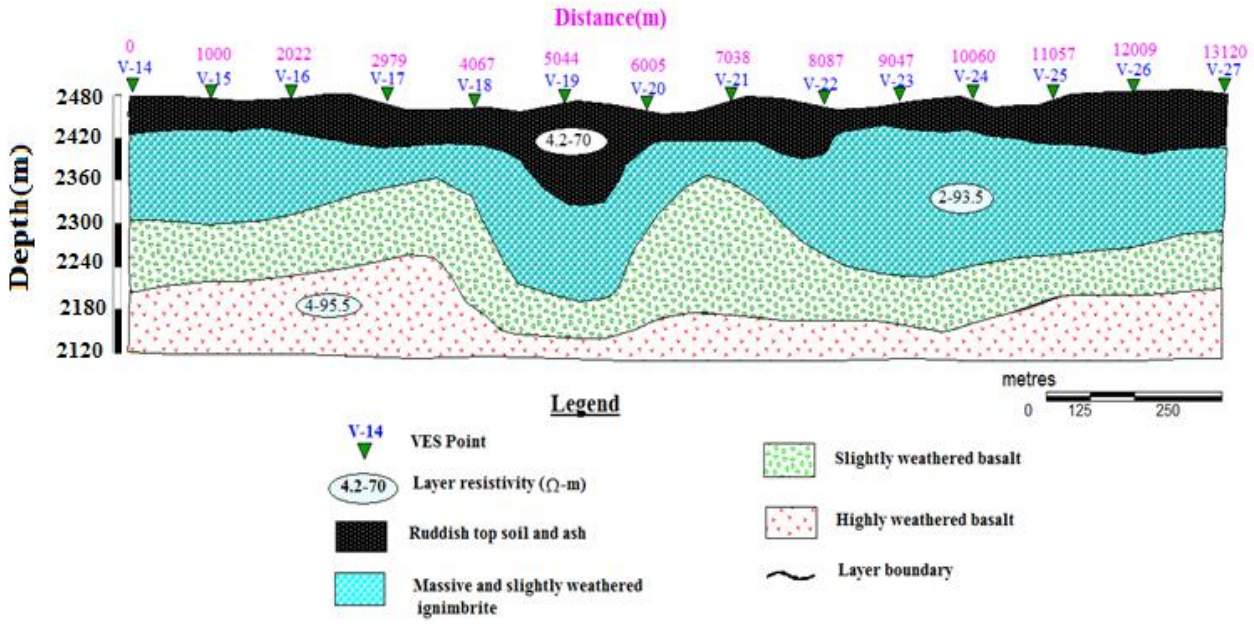

Figure 4. 9 Geo-electric section of traverse line two

4.2.3.3 Traverse Line-3

This line is again oriented in the North West to South East direction and running almost parallel to Lines1, 2 and 4. The line has a total length ≈13km and there are 14VES (VES points 28-41) with average VES point spacing of about 0.9km.

Pseudo depth section along Line-3

Figure 4.10 shows the pseudo depth section constructed for the 14 VES points that lie on this survey traverse Line-3. According to the figure below, very high resistivity zone is found from the top of the region to the bottom of the region mapped around VES-40 and VES-41 with rang of (90 to 240 Ω-m). The resistivity of the remaining VES points has low resistivity ranging from 0 to 80Ω-m. The resistivity ranges of this low resistivity region are indicative of potential water saturation.

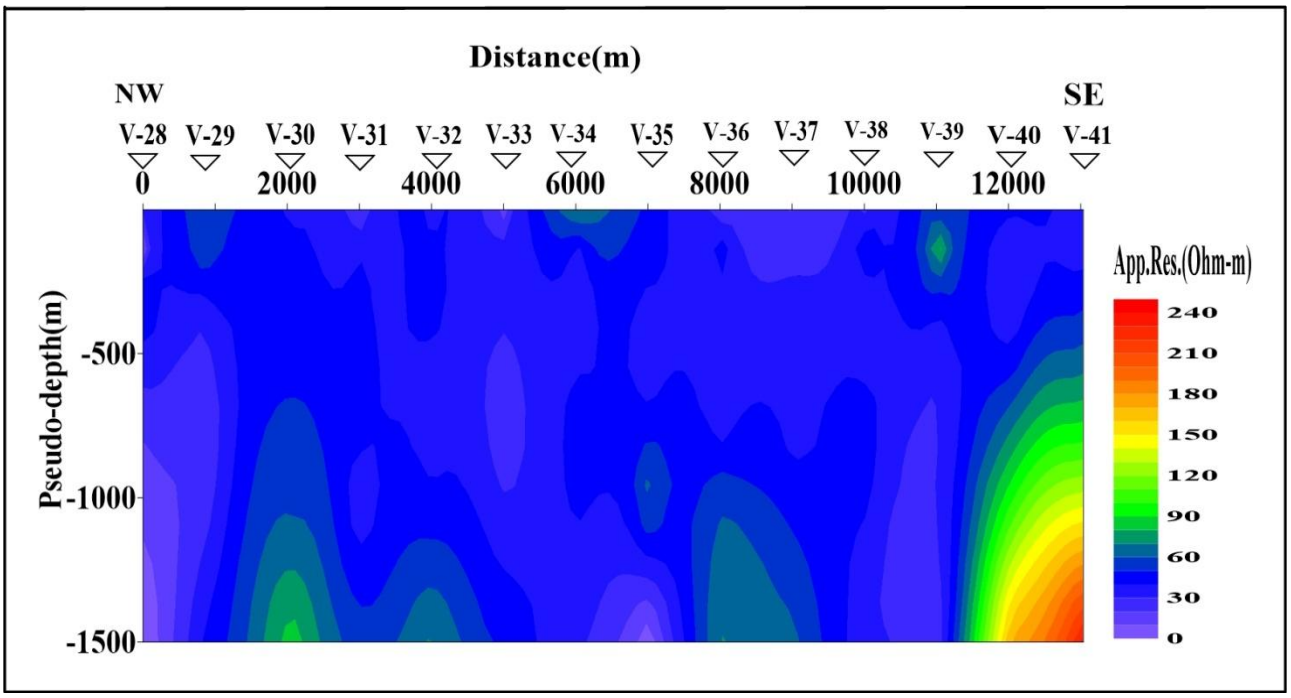

Figure 4. 10 Pseudo depth sections along Line-3

Geo-electric section along Line-3

The geo-electric section of traverse line three shown below in figure 4.11. Wider range resistivity variations are noted within the uppermost unit (16-150Ω-m). Clayey soils, highly decomposed materials and unconsolidated ash are represented by resistivities in the order of 11.8-31Ω-m. The moderately consolidated and compacted clay and highly weathered volcanic rocks have higher resistivity's (13.5-93Ω-m). The very high resistivities within the top unit are attributed to moderately to slightly and fresh volcanic rocks.

At the relatively flatter central and north eastern zones these are underlain by welded tuff with relatively high resistivity. The very thick most intermediate part of line three, to the south west of station 8019, is dominantly represented by resistivity's in the order of 11-35Ω-m while this zone to the east of station 11030 reflects relatively higher and more or less uniformly distributed resistivity's. This northeastern zone is characterized by resistivities of 23-42Ω-m overlying relatively higher 44-49Ω-m resistivities and these in turn are observed overlying a 20-30Ω-m unit. These intermediate resistivity units are interpreted as comprising highly to moderately fractured and weathered volcanic and moderately to slightly fracture rocks.

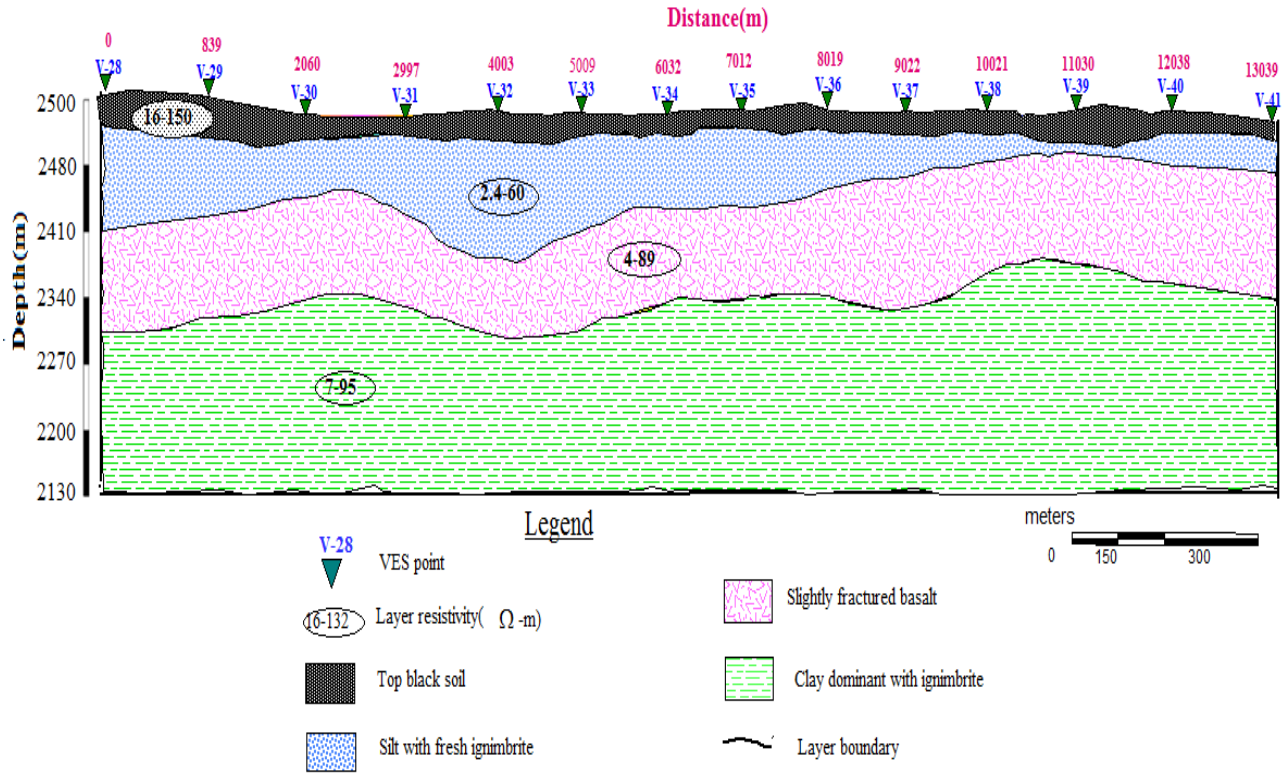

Figure 4. 11 Geo-electric section of traverse line three

4.2.3.4 Traverse Line-4

This line is again oriented in North West to South East direction and almost parallel to the other three traverse lines. The line has a total length of about ≈12km and there are 11 VES (VES points 42-21) with average VES point spacing of about 1km.

Pseudo depth section along Line-4

The pseudo depth section constructed for 11 VES that lie on traverse Line-4 are given in Figure 4.12. According to the figure, there is a lateral variation in resistivity in the top most part of the section with prominent high resistivity top zones mapped between VES-43 and VES-44. This high resistivity zone is not extending to large depth. The vast region under the section shows extensive coverage of the low resistivity zone. The resistivity ranges (0 to 100Ω-m) of this low resistivity region are indicative of potential water saturation. And there is high vertical resistivity variation between VES 50 and VES 52. The resistivity ranges between from 400 to 700Ω-m from a depth of 800m to a depth of 1500m. So, there is no groundwater potential in this VES points.

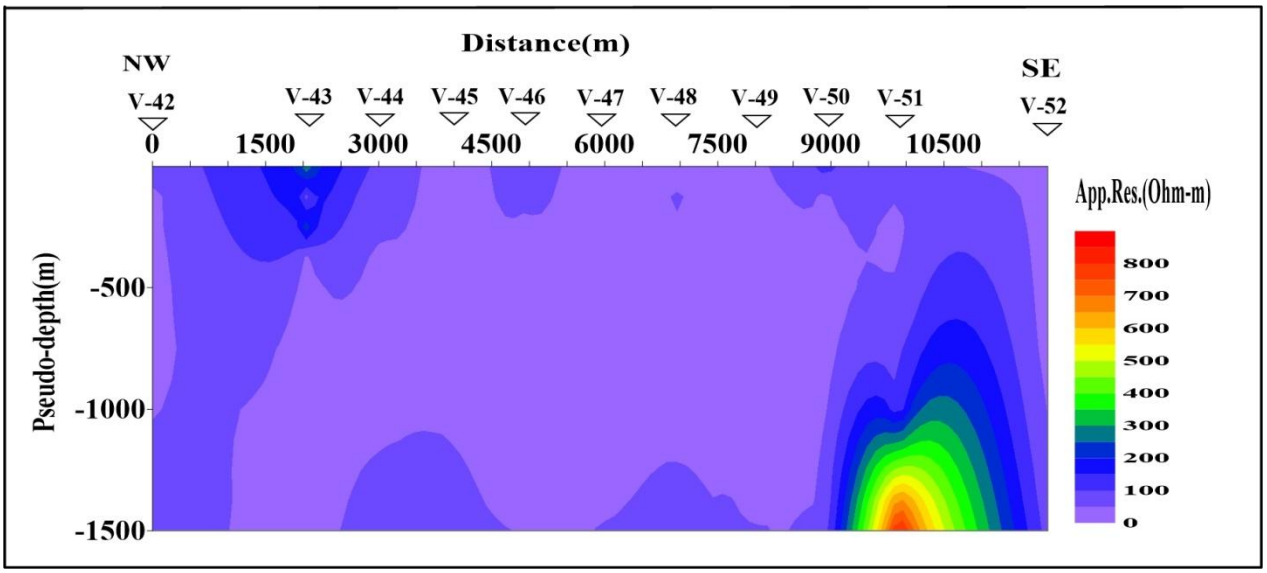

Figure 4. 12 Pseudo depth sections along Line-4

Geo-electric section along Line-4

The geo-electric section of traverse line four is shown in figure 4.13 below. The line passes through a wide quarry area. Wider variations with relatively higher resistivity range are observed at the top of attributed to the occurrence of pyroclastic units, welded tuff, trachytes, ashes, clay and decomposed materials.

The uppermost rock units with very high resistivity values are covered by thin layer of clayey soil on the flatter parts while they are exposed at the steeply sloping zones. The resistivities of these units exceed 200Ω-m for the very fresh and massive ones and lie generally between 3.8 and 250Ω-m for the moderately and slightly fractured rocks. The lower resistivities within the upper most units correspond to highly fractured and decomposed rocks as well as ashes and clay soils.

The degree of fracturing appears to increase with depth.

Since this result is inferred only from VES observations, it has to be confirmed by methods and test drilling prior to any other development program.

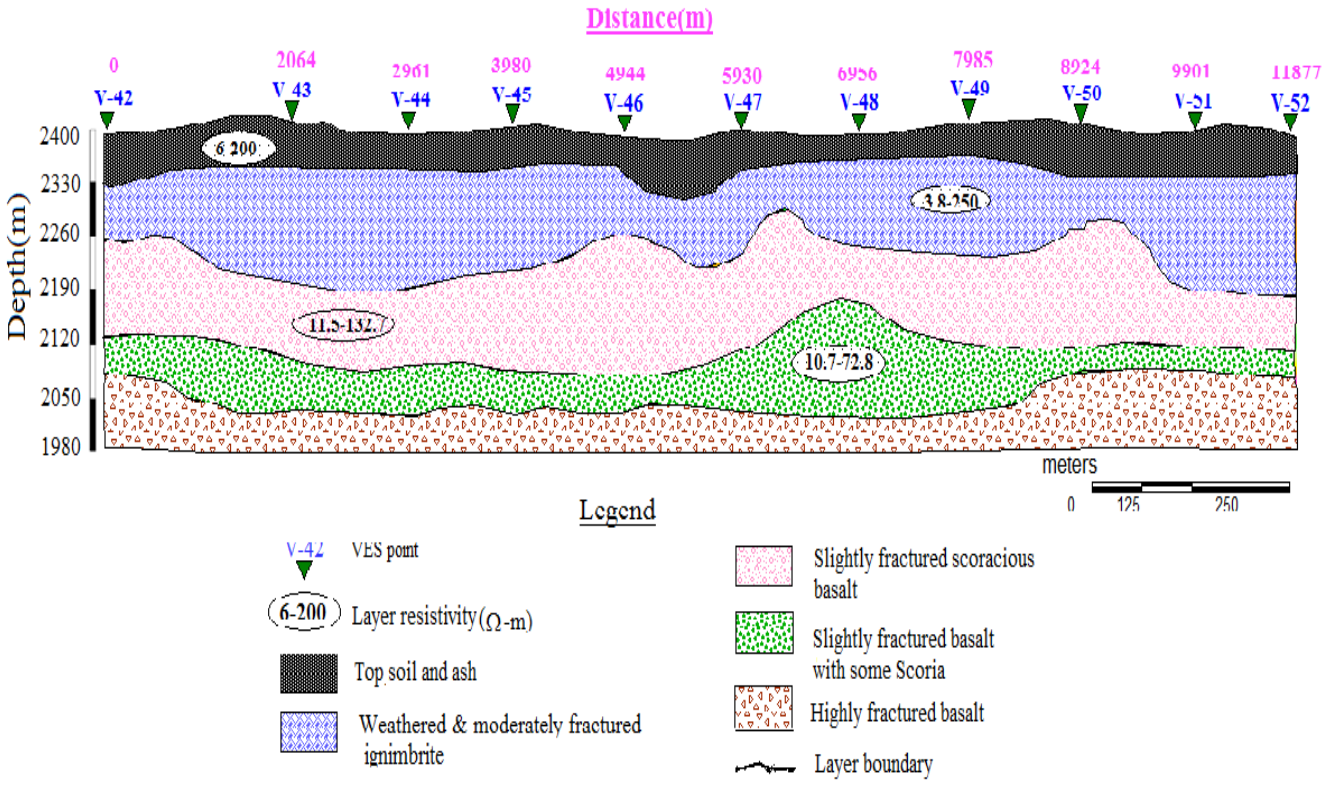

Figure 4. 13 Geo-electric section of traverse line four

4.2.4 Resistivity Maps

The lateral apparent resistivity distribution of the survey area is illustrated in two maps (Fig. 4.14 and 4.15) corresponding to two levels of AB/2=330 and AB/2=500m. The maps are compiled in order to show the resistivity variation around the water table of the study area.

The resistivity distribution at AB/2=330m is shown in Figure 4.14 below. A relatively lower and wider resistivity zone (<36Ω-m) is observed over the northern and some central parts of the study area. A relatively higher resistivity value (36-54Ω-m) is observed over the SW and NE parts of the map. In general, the apparent resistivity distribution at this depth reflects as there is high groundwater potential.

The resistivity distribution at AB/2=500m is shown in Figure 4.15 below. The resistivity distribution for this level revels nearly similar pattern and trend to that of level AB/2=330. This similarity in resistivity distribution signifies that there is a general decrease in heterogeneity of rocks with depth, the heterogeneity in rock masses for AB/2=500m is less than that of AB/2=330. On the other hand, the formation compactness that associates with the decrease in degree of weathering and jointing is in agreement to the rate of variation of resistivity values for the two-depth levels considered. Distribution of the low and high apparent resistivity values for both depth levels appear to have some sort of correlation with the total magnetic anomaly value distributions over the study area (Fig. 4.21) in delineating zones of high groundwater potential.

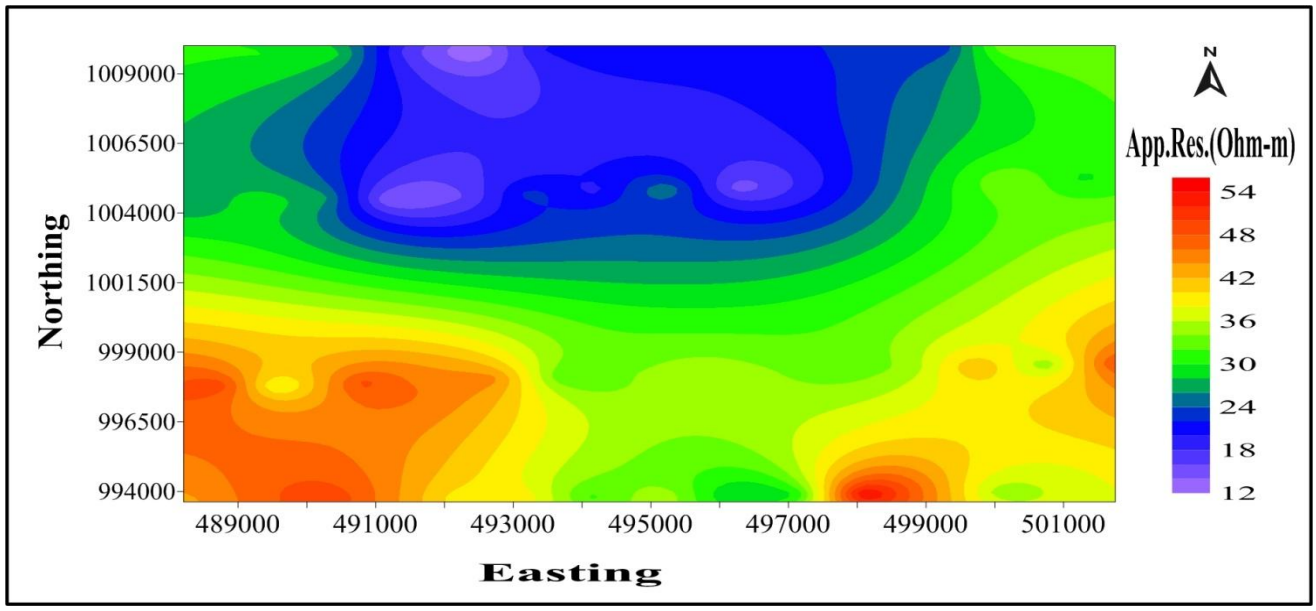

Figure 4. 14 Apparent resistivity map at AB/2=330

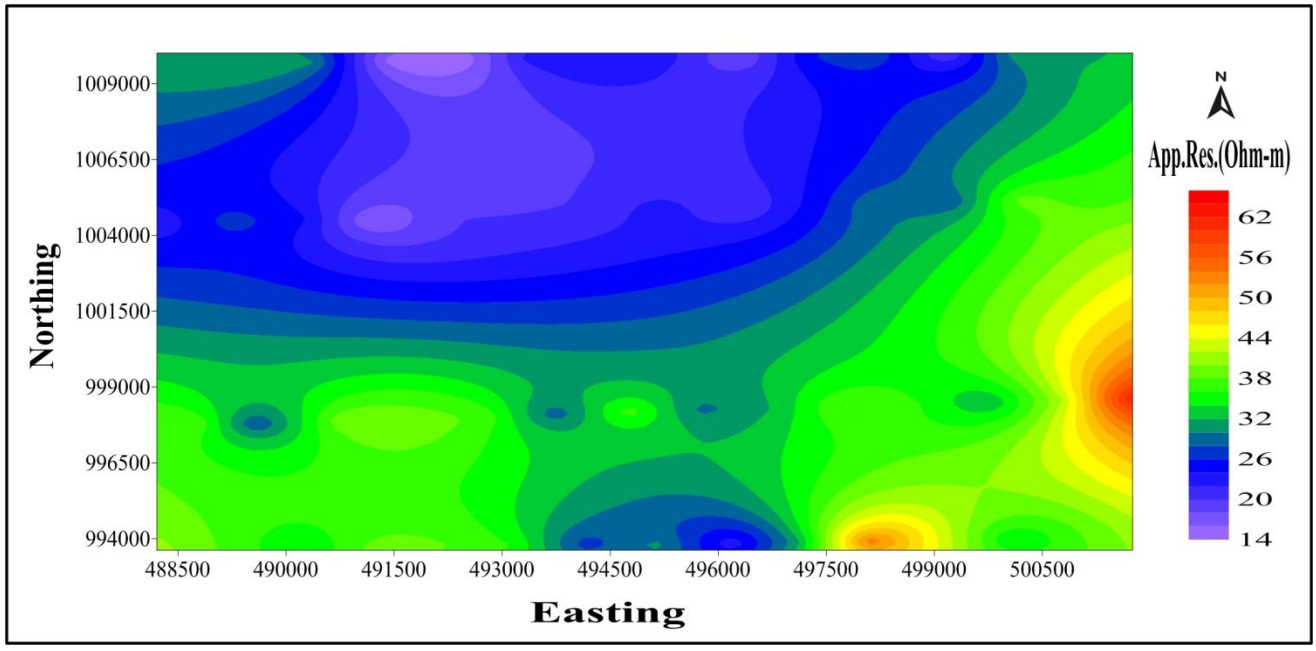

Figure 4. 15 Apparent resistivity map at AB/2=500

4.3. Discussions and Interpretation of Magnetics

4.3.1. Total magnetic field anomaly along profile Line one

Figure 4.16 below shows the total field magnetic profile along line one. The relatively low magnetic anomaly between stations 1500 and 3000 may reflect an underlying low magnetic susceptibility rocks

(acidic rocks). Similarly, the profile also depicts a broad zone of relatively low magnetic response between stations 10000 and 11500, probably corresponding to an underlying thick acidic volcanic rock deposit. On the other hand, the area between stations 11500 and 12500 is characterized by a highly variable, relatively large magnitude magnetic field, which may be due to an underlying basic volcanic flow around this area. The same magnetic anomaly disturbance may also be due to a geological structure crossing the line around these stations (stations 11500 – 12500). In general, the eastern half portion of the profile is relatively dominated by low magnetic anomalies which might suggest that there a geological contact around stations 800 – 8500. It is recommended that interpretations of these general magnetic fields need to be confirmed by detail geological mapping along the lines.

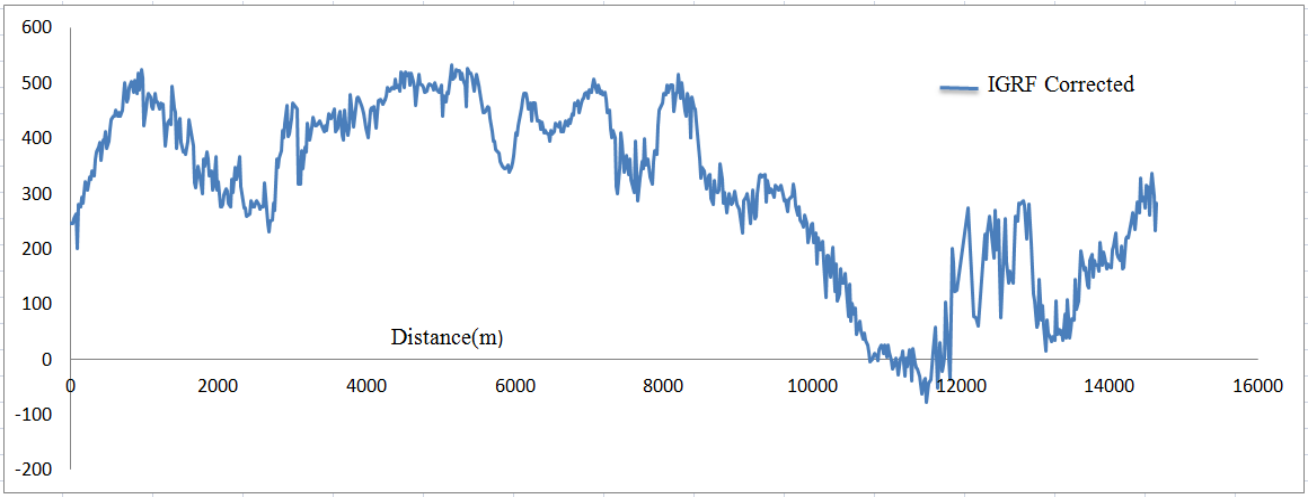

Figure 4. 16 Total magnetic field anomaly profile along line one

4.3.2 Total magnetic field anomaly profile along line two

This profile extends between stations 0 and 16000. The observed magnetic profile seems to indicate a possible geological contact around stations 7000-7500. While the magnetic response west of this possible contact area is variable having relatively higher amplitude, the area to the east is expressed by a relatively quiet (less variable) and of low amplitude total magnetic field. The latter may suggest that these lithological units have slight compositional difference. Moreover, detail interpretation of each side may suggest possible geological contacts/or geological structures around stations 1500, 3250, 4500, 5700 and 6500. Figure 4.17 below shows the total magnetic profile along line two.

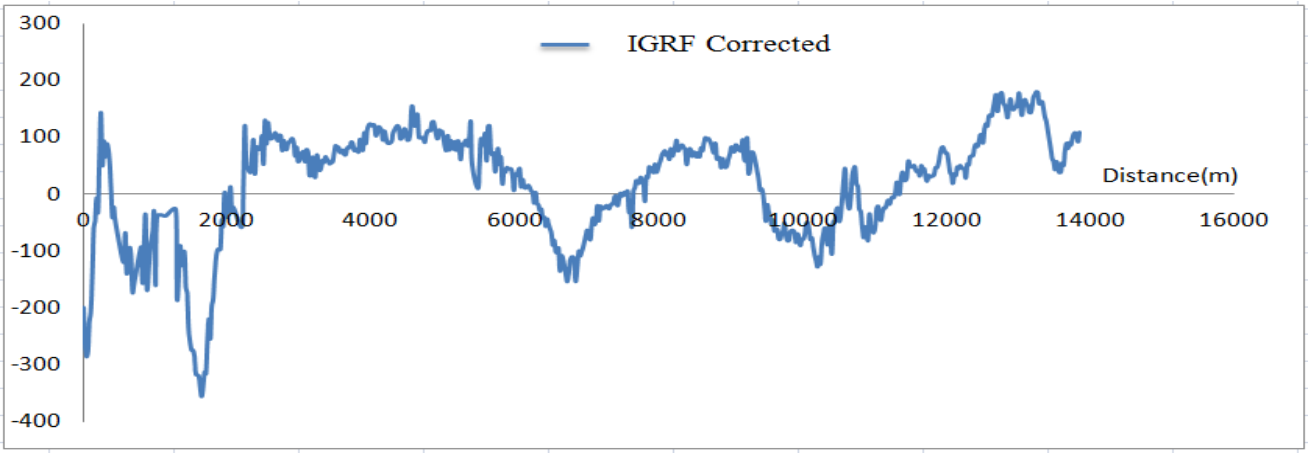

Figure 4. 17 Total magnetic field anomaly profile along line two

4.3.3 Total magnetic field anomaly profile along line three

This profile extends between stations 0 (489434 E, 1009706 N) in the Northwest to station 15422 (504572 E, 1010122 N) in the southeast. According to this profile, the area around stations 0 – 3500 is characterized by highly variable magnetic response with, on average, higher amplitude. The latter high magnetic amplitude (35750 nT) is observed to suddenly drop to a value of about 34500 nT in about 250 m distance (corresponding to a magnetic gradient of 5000 nT/km) which may be interpreted to be due to the presence of a geological structure around these stations. East of Station 4000, the magnetic profile is observed to ascend from a minimum value of about 34700 nT around station 4000 to a maximum value of 35800 nT around station 10500. This trend of the magnetic profile may be interpreted as depicting the depth to the underlying volcanic rocks between stations 4000 and 10500 decreases eastward. In general, the magnetic profile along T3 suggests possible geological structures/contacts around stations 1000, 2800, 3500, 10500 and 11500. The center of a possible major geological structure may be inferred between stations 13500 and 14000.

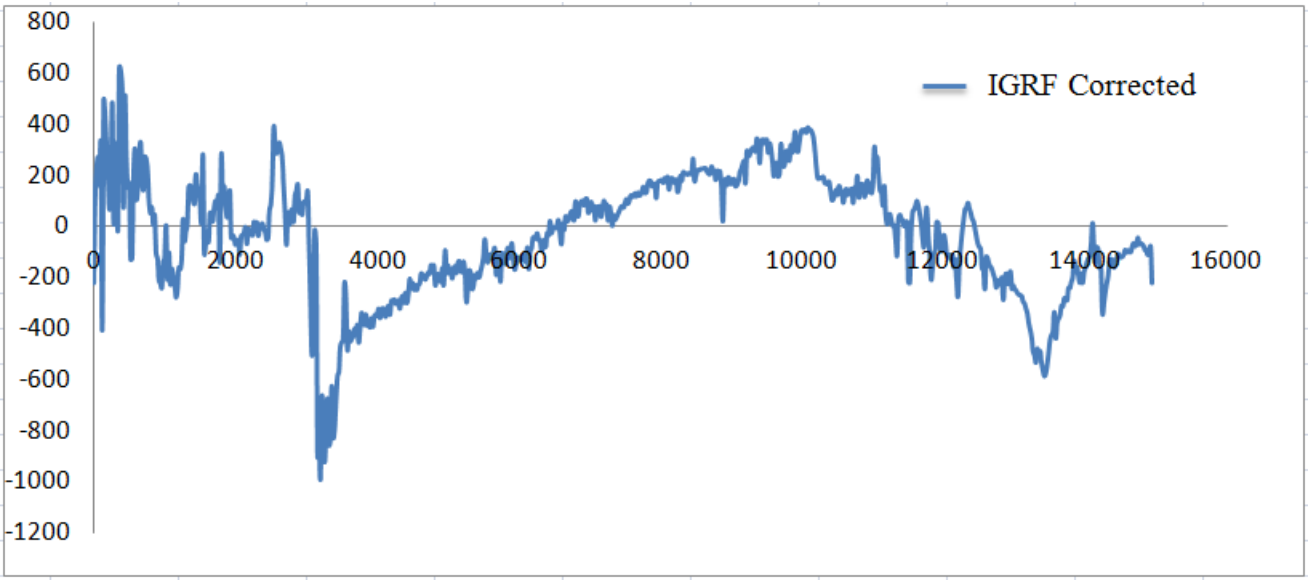

Figure 4. 18 Total magnetic field anomaly profile along line three

4.3.4 Total magnetic field anomaly profile along line four

The magnetic profile along line four (Fig.4.19) has a relatively gentle regional variation with superimposed frequent local variations between stations 0 and 5250. In general the magnetic profile suggests that there are a number of possible geological contacts/structures around stations 1000, 1700 2750, 3750, 4750, 5500, 6000, 7250, 8750 and 10000. Since the amplitude of the magnetic gradient between stations 10000 and 10500 is great (2000 nT/km), a possible regional geological structure is expected around station 10500.

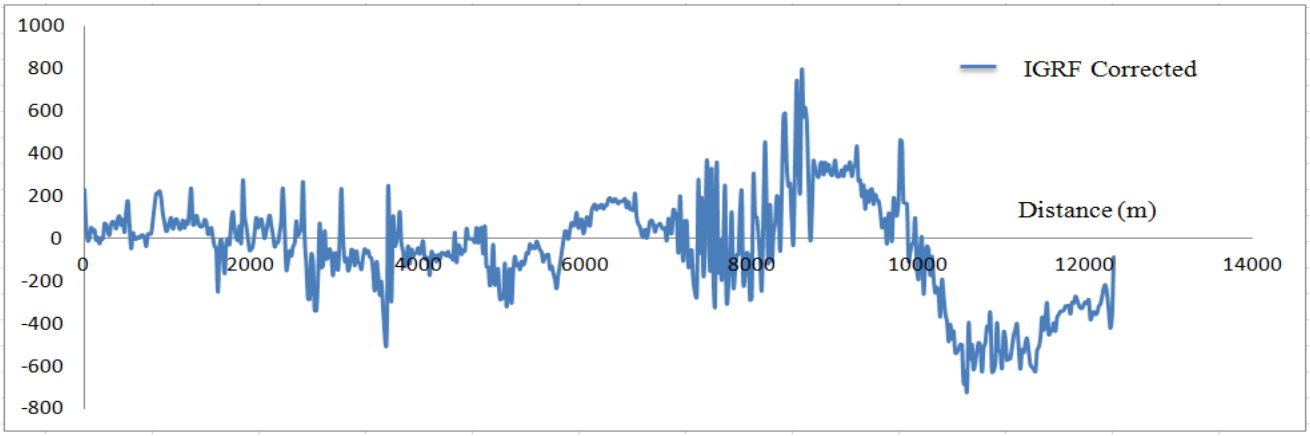

Figure 4. 19 Total magnetic field anomaly profile along line four

4.4 Results and Interpretations of Magnetics

4.4.1 Total Magnetic Field Intensity Map

The total magnetic field anomaly map shows low anomalies in north, northwest and in some parts of south of the study area. The intermediate magnetic anomaly over study area encloses the low magnetic anomaly of northern and eastern part and high magnetic anomaly observed at the western, southeastern and northeastern part of the map. As it is observed in the geological map of the area (Fig.4.20), the high magnetic values correspond to the lineaments that have high magnetic susceptibility values.

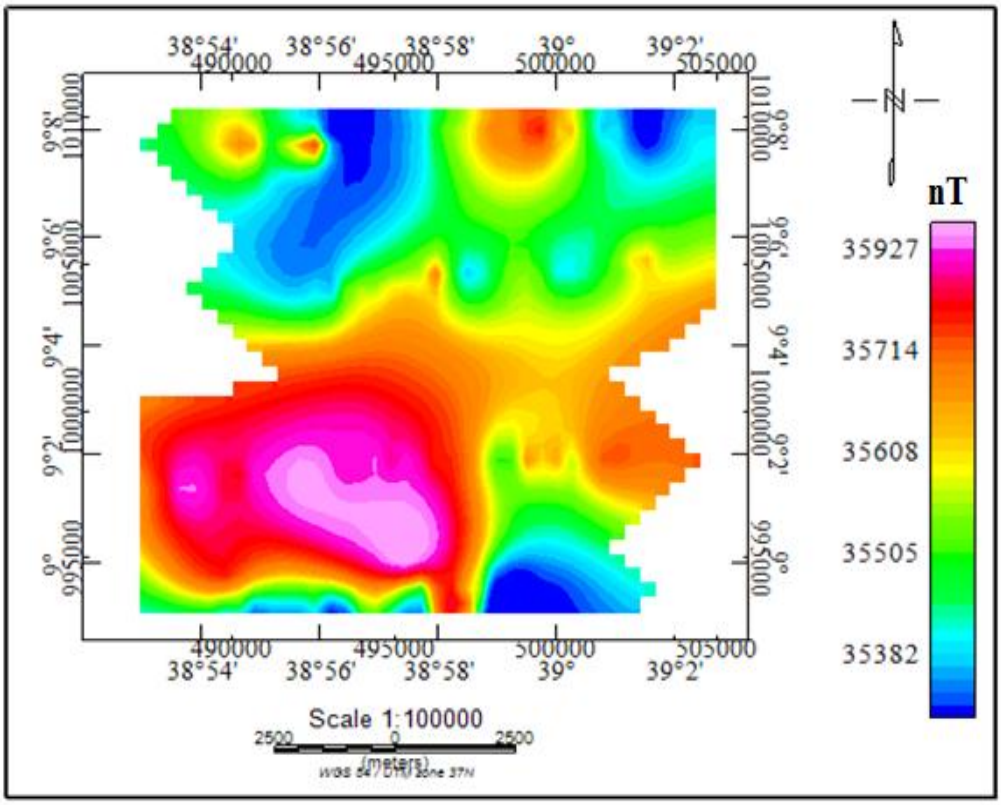

Figure 4. 20 Total Magnetic Field Intensity Map

4.4.2 Total magnetic Field Anomaly Map

The total magnetic field anomaly map was created after subtracting the IGRF value of the area from the observed magnetic value. The map is shown below in Figure 4.21. As shown in the map, the total magnetic anomaly varies from -246 to 430.The residual anomaly is a bipolar (anomalies having positive and negative components) such that the shape and phase of the anomaly depends in part on the magnetic inclination and the presence of any remnant magnetization. This anomaly complexity makes interpretation more difficult because the body and its edges do not necessarily coincide with the most obvious mapped feature. Hence, in order to make accuracy in linear geologic structures, analytic signal has been calculated from residual values and interpretations were made based on this map.

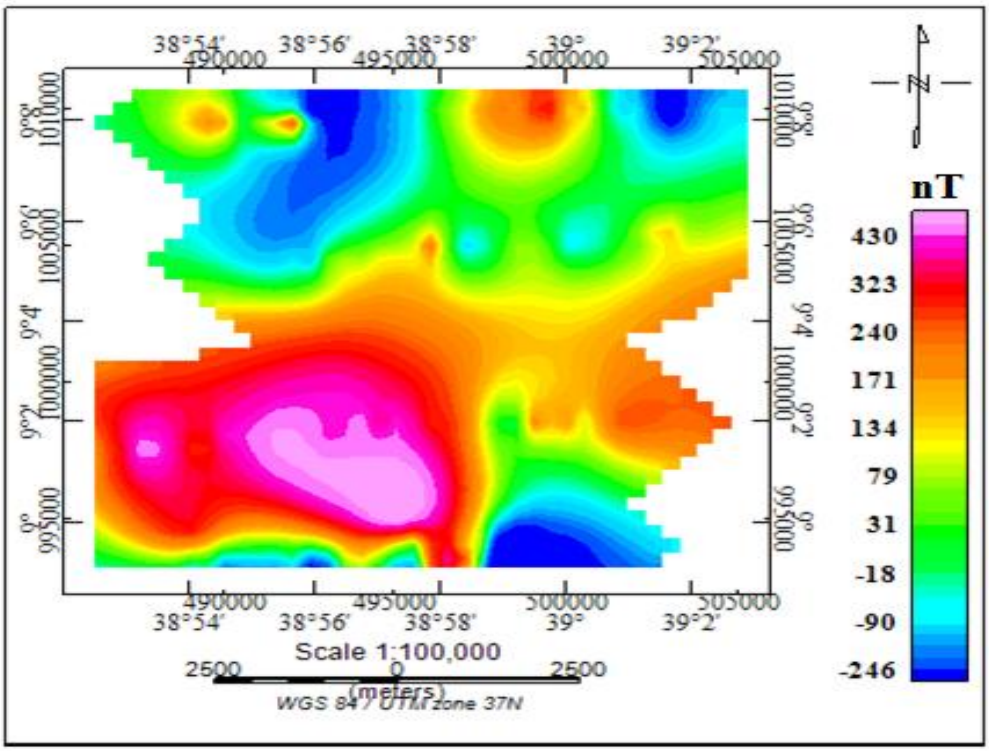

Figure 4. 21 Total magnetic field anomaly map

4.4.3 Signal Analytic Map

Analytic signal map shows the response of anomalous bodies from their upper portions, it is supportive to give a picture of the near subsurface conditions. It is also known that the maximum amplitude is exactly located over a magnetic contact which depends on the locations of the body (horizontal coordinate and depth) but not on the inclinations of

magnetization. The higher values related with geological contacts and the lower values related with weak zones. These zones shown in figure 4.22 also observed in the geological map (Figure 1.3) of the area clearly.

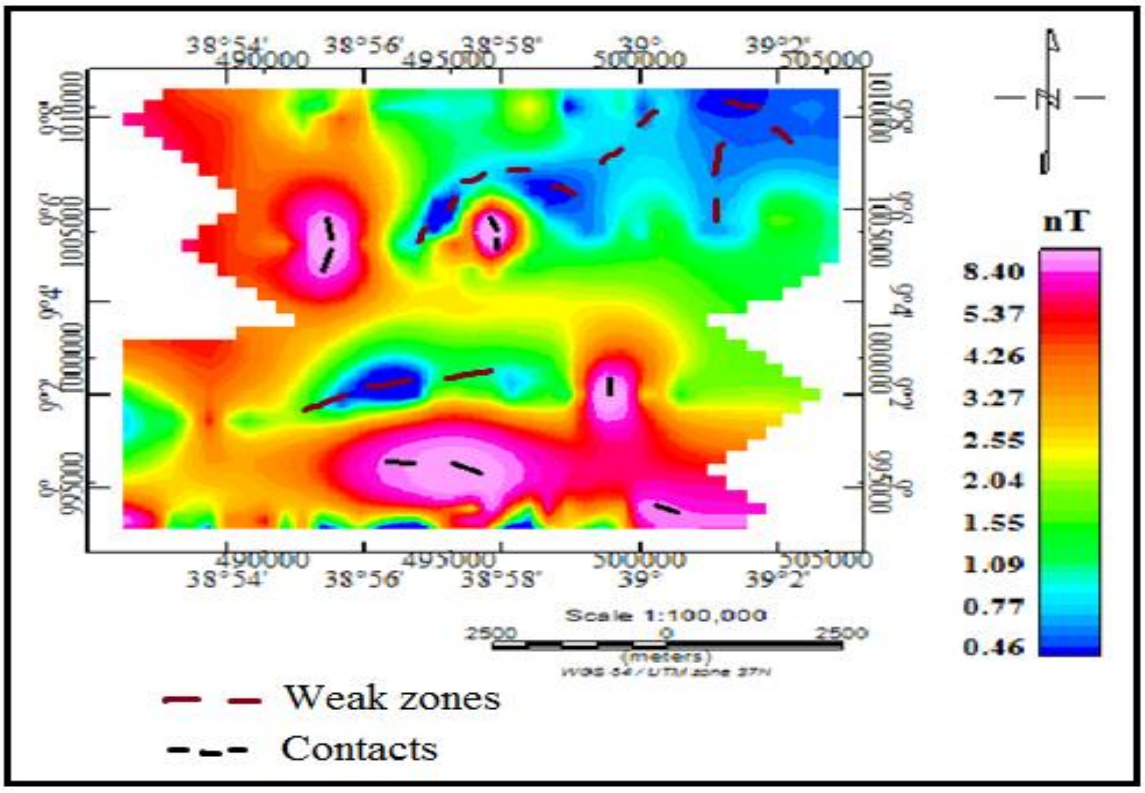

Figure 4. 22 Signal Analytic Map

4.4.4 2D Modeling

The magnetic 2D modeling is done using the GM-SYS modeling of the Oasis montaj software. It is an interactive forward modeling program which calculates the magnetic response from a user defined hypothetical geological model. Any difference between the model response and the observed magnetic field are reduced by refining the model structure. It should be noted that magnetic models are non-unique, i.e. many earth models can produce the same magnetic response, and similarly, several geological lithologies may be interpreted from a given model block's susceptibility properties. It is therefore importance to use as many independent source of information as possible to constrain the model. The modeling of the selected profiles discussed below.

2D modeling of Profile 1

The magnetic 2D model of profile one is prepared from the interoperated from layer parameters of the VES and borehole data (BH-LLA-PW6 and PW1, Appendix 4). The model shows that the existence of geologic structures (faults) below a depth of 180m and extends vertically up to 360m and it is highly fractured basalt. The remanence magnetization varies for each layer. The 2D modeling is given below in figure 4.23.

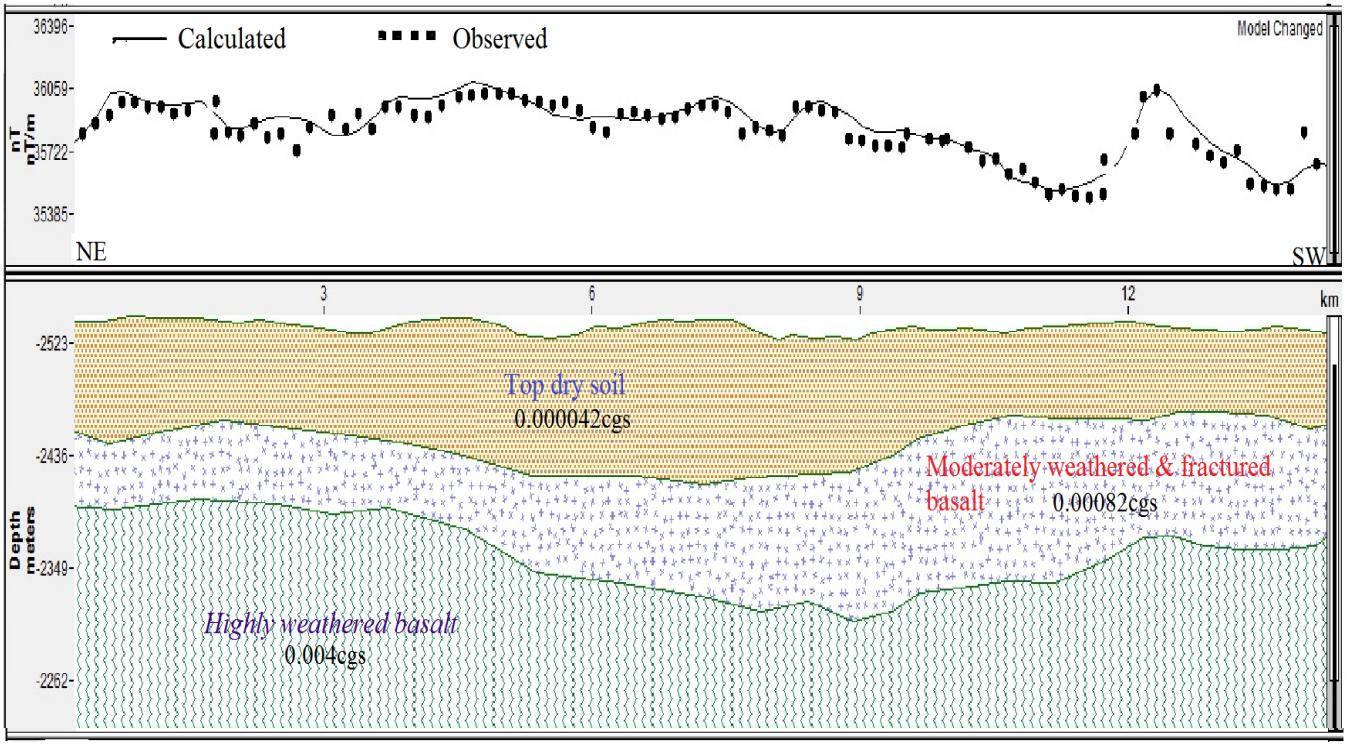

Figure 4. 23 2D modeling of profile one

2D modeling of Profile 2s

The magnetic 2D model of profile two is developed also from the interoperated from layer parameters of the VES of profile two and borehole data (BH-LLA-PW3 and PW4, Appendix 4). The model shows that the existence of weak geologic zones (faults) below 60m and extended up to 340m and it is basaltic intrusion. Like 2D modeling of profile one, the geology of this 2D modeling correlated with the geoelectric section of profile two. The 2D modeling is given below in figure 4.24

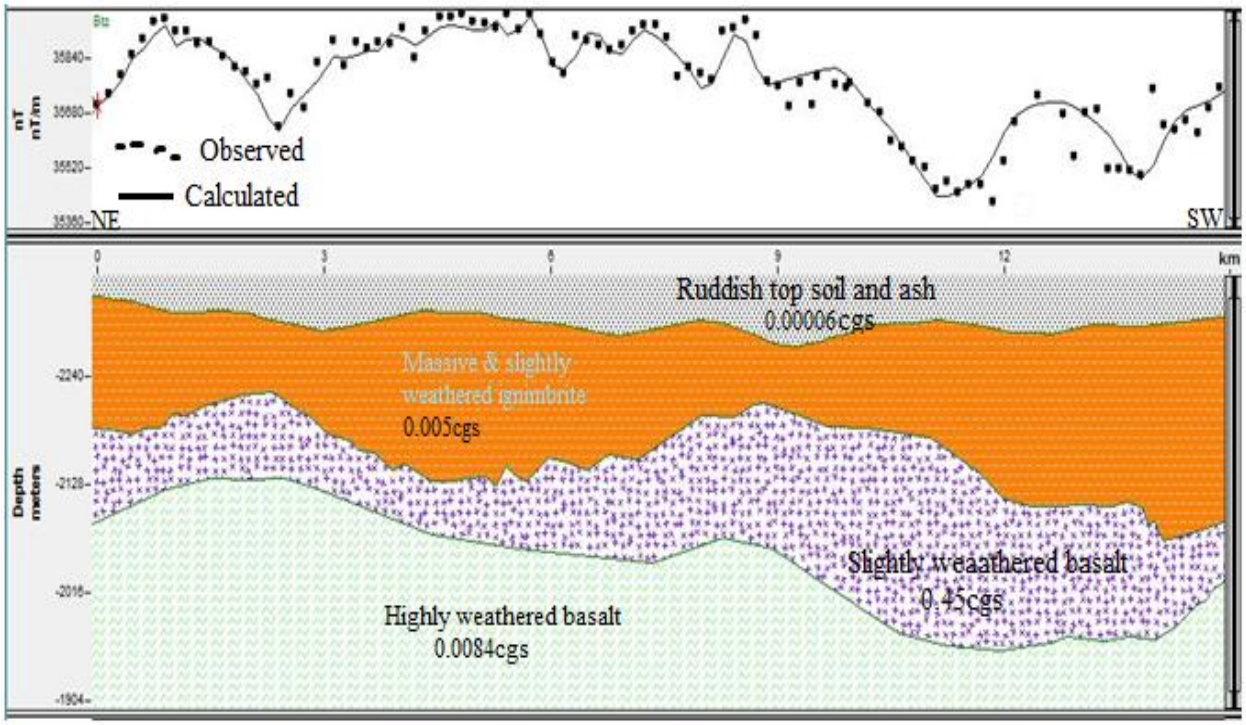

Figure 4. 24 2D modeling of profile two.

Chapter Five

Conclusion and Recommendation

5.1 General

An integrated study involving basically Vertical Electrical Sounding (VES) and magnetic surveys were carried out at the Legedadi-Legetafo-Ayat prospective area. The geophysical surveys: vertical electrical sounding and magnetic surveys were conducted and borehole data were taken from Water Works Design and Supervision Enterprise for better assurance of the electrical surveys.

In the above Chapters of this thesis work, the survey profiles, the instruments employed techniques of data acquisition, interpretation of the results of those different techniques and their relevance to ongoing project and for the scientific community at large has been examined. In this chapter I present the summary of this work and give some concluding remarks about the work.

5.2 Conclusions

According to the results, discussions and interpretations, in general the following conclusions have been drawn using the combination of data presentation approaches:

- The apparent resistivity pseudo-depth sections, the resistivity geoelectric sections and the resistivity maps show the presence of shallow as well as deeper low resistivity horizons. The low resistivity and large thickness of these horizons is an indicator of high groundwater potential in the Legedadi-Legetafo-Ayat prospective area.
- According to the geoelectric section, the logging data and the 2D magnetic maps, the area is highly affected by highly weathered basalt. It the reflection of geological features like faults and fractures. These faults (contacts) and fractures are believed to control the flow of groundwater. The fractures and weak zones are the major controls for the flow of ground water over the area. Most of basaltic rocks (for all traverse lines) are highly fractured and weathered which expected to be the water bearing zones at different depths.
- The geological structures (fractures, faults and contacts) play a great role in the movement and occurrence of the groundwater in the study area. The highly to moderately weathered and fractured

basalts and sand layer contribute more for the recharge and movement of the groundwater through the faults and wake zones.

- Comparison of the electrical and magnetic interpretations with drilled borehole results show that the results of geophysical survey are good correlation with the borehole lithological logging results.
- The main geologic units encountered over the survey area that are likely to bear groundwater are basalts and clays.
- The water table of the study area varies from 20 to 420 meters deep that increases towards the northwest of the study area.

5.2 Recommendations

Based on the outcomes of this study, the following recommendations are forwarded:

- ✓ According to the interpretation of the VES, geoelectric section along traverse Line-2 shows that if BH-2 could preferably be shifted to the near central part of the line between VES-4 and VES-6 the likelihood of extraction of higher volume of groundwater is increased.
- ✓ As seen have seen on result and interpretation part, borehole (BH-3) preferably to sunk on the traverse Line-5 between VES-84 and VES-85.
- ✓ From the geoelectric section along traverse Line-6, borehole (BH-6) should be sunk on the southeastern part of the line between VES-1 and VES-5.
- ✓ Other test boreholes (BH-12, BH-9 and BH-4) are expected to put as it is, but it should be increase the depth to obtain better yield of the boreholes.
- ✓ In order to map the network of fractures and faults and validate the results of this work in respect to mapping of subsurface weak zones in better detail additional geophysical methods- for example like resistivity imaging surveys and magnetic surveys- must be employed only in selected areas.

References

- **Chernet, T., Hart, W.K., Arnson, J.L. Walter, R.C., 1998**; New age constraints on the timing of volcanism and tectonism in the northern Main Ethiopian Rift – Afar transitional zone; Journal of Volcano logy and geothermal research, 80, 267 – 280.
- **Clark and Emerson (1991) and Hunt et al. (1995)**, Magnetic susceptibilities of rocks and minerals
- **Dorbin M. B. (1970)** Introduction to Geophysical Prospecting. New York, Mc Graw Hill.
- **Eyasu Leta, (2014)**. Application of Integrated Geophysical Techniques to Map Deep Groundwater Potential Zones and Geological Structures at Akaki, South-East of Addis Ababa, MSc thesis.
- **Gibson, P.J. and George, D.M., (2003)**. Environmental applications of geophysical surveying techniques. Nova Science Publishers, Inc. New York.
- **Gibson, P.J.and George, D.M., 2003;** Environmental applications of geophysical surveying techniques. Nova Science Publishers, Inc. New York,USA .Pp45-49,137-177.
- **Justine-Visentin et al. (1974)** Miocene and Pliocene Volcanic Rocks of the AddisAbaba–Debr Berhan Area (Ethiopia): Geopetrographic and Radiometric Study. Bull. Volcanol.
- **Kazmin, V., 1972a**. Geology of Ethiopia, Geological Survey of Ethiopia.
- **Kearey, P., and Brooks, M., 2002**, an Introduction to Geophysical Exploration – 2nd ed.: Blackwell Scientific Publications, 254 p.
- **Kearey, P., Brooks, M. and Hill, I., 2002;** An Introduction to Geophysical Exploration, third edition. Blackwell Science Ltd. Oxford, UK .Pp 125-153,183-196.
- **Loke, M. H. and Dahlin, T., (2002).** A comparison of the Gauss-Newton and quasi-Newton methods in resistivity imaging inversion. Journal of Applied Geophysics, **49**: 149-162.
- **Paranis, D.S., 1986**. Principles of Applied Geophysics, fourth edition, Champan and Hall, USA.
- **Parasnis, D.S., 1962:** principle of applied geophysics, 3rd edition. Chapman and hall, London, England. Pp 59-96, 98-129.
- **Reynold, (1997)**. An Introduction to Applied and Environmental Geophysics. John Wiley and Sons limited, England, UK, pp.: 160.
- **Reyonolds, J. M. (1997)** An Introduction to Applied and Environmental Geophysics.

- **Robinson, E.S., and Caruh, C., 1988;** Basic exploration geophysics. John Wiley and Sons Limited, New York, USA. Pp 221-324.
- **Somiah John, (2011)**. Application of Electromagnetic and Electrical Resistivity Methods in Investigating Groundwater Resources of The Sunyani Municipality in The Brong-Ahafo Region of Ghana, MSc thesis
- **Tamiru alemayehu (2006)**, groundwater occurrence in Ethiopia, Addis Ababa University
- **Telford, W.M., Geldart, L.P., Sheriff, R.E., 1990**, Applied Geophysics - 2nd ed.: Cambridge University Press, 770 p.
- **Tewodros Mulugeta, (2011)**. Geophysical Investigation for Groundwater Potential assessment and Mapping Structures at Alidege Plain, South Afar, Ethiopia, MSc thesis.
- **Tibebe Mengesha, (2006)**. Integrated Geophysical Investigation for the Evaluation of Groundwater Resources at Ada'a plain Near Debre-Zeit, MSc thesis.
- **Tigistu Haile, (2014).** Magnetic methods of prospect, unpublished teaching materials.
- **Tigistu Haile, (2014).** Electrical methods of prospect, unpublished teaching material
- **W/Gabriel Giday, Aronson, J.L., and Walter R.C., (1990)**. Geology, Geochronology and Rift Basin Development in the Central Sector of the Main Ethiopian Rift ,Geological Society of America, bulletin ; 102:439-458.
- **WWDSE, (2008)**. Geological investigation report on Legedadi-Legetafo-Ayat, Central Ethiopia. Unpublished report.
- **WWDSE, (2011)**.Geological mapping of groundwater prospect sites, Report, II, Addis Ababa.
- **Zanettin, B. and Justin V. E., (1974)**. The Volcanic of Western Afar and Ethiopian Rift Margins. Padova, Italy, 9: 567–574.
- **Zanettin, B., Justin- Visentia, E, Necolettic M, and piccirillo, E.M., (1980)**. Correlation among Ethiopian Volcanic Formations with Special Reference to the Chronsgiolgical and Stratigaphical problems of the trap series atti convgni lincci, 47: 231-252.

Appendices

Appendix 1 Vertical Electrical sounding (VES) raw data

UTM E	UTM N	Ves no	AB/2(m)													
			1.5	2.1	3	4.2	6	9	13.5	20	20	30	30	45	66	100
489440	1009694	V1	470	123	41.5	27.6	22.7	4.9	23.3	22.4	22.7	24.6	25.5	26.5	25.8	27.6
490397	1009713	V2	27.9	17.6	14.7	11	9.6	9.8	11	12.8	13.4	15.8	16.9	19.2	20.5	23.2
491431	1009770	V3	14.4	4.8	5.1	3.6	3	3	3.1	3.6	5.7	4.1	6.6	8.4	9.9	12.9
492448	1009834	V4	44.7	23.8	23.3	23.4	28.6	25.7	15	8	10.4	5.4	6.3	7.1	9.2	8.3
493337	1009824	V5	10.04	7.5	5.5	5.4	5.8	7.5	9.6	11.7	15.4	15.5	18.4	20.7	19.6	17.5
494318	1009833	V6	22	14	12.9	12.9	11.2	19	22.2	27	38.1	32.4	47.1	49.9	41.9	32.7
495293	1009862	V7	46.7	11.2	7.1	4.7	4.6	5.3	6.7	8.7	9.8	10.4	12.1	13.9	15.2	16.8
496306	1009905	V8	98.5	47.3	39.2	28.6	23.3	27.8	34.4	40.5	41	47	49.3	48.7	37.8	22.3
497307	1009905	V9	31.5	12.8	6.7	5.1	5	5.6	6	6.8	7.3	7.1	7.7	9.1	11	13.3
498220	1009947	V10	112.6	31.9	16.7	10.6	7.8	6.4	6	6.1	7.1	7	8	9.8	11.4	13.3
499190	1009974	V11	15.8	12.3	10.8	9.8	11.2	10.3	9.3	8.6	8.4	8.1	8.1	9.2	11	14.3
500158	1010006	V12	18.7	11.1	10.7	12.4	13.6	14.4	15.5	18.2	17.8	21	20.8	23.2	24.1	26.7
501202	1010009	V13	27.3	13.8	10.2	7.4	7.2	7.1	8.5	11.2	10.2	15.4	14.7	21.1	27.2	33
488215	1004389	V14	12.8	7.8	6.6	7.3	7.8	8.9	10.3	11.3	14.3	12.1	15.9	19.1	22.7	27.1
489212	1004477	V15	14.2	6.7	5.8	6	6.7	8.7	11.9	15.4	16	19.8	21.1	26.2	32.1	36
490230	1004544	V16	14.2	12.1	12.6	16.8	22	27	32.3	33.1	33.5	32.4	32.8	31.5	34.6	36.7
491184	1004471	V17	39.1	25.3	11.2	10.9	9.4	8.3	6.8	6.4	8.4	6.4	8	8.6	9.2	9.5
492265	1004586	V18	16.2	18.7	15.7	14	14.3	14.6	14.4	13.6	18.8	12.7	17.8	15	14.3	14.4
493237	1004689	V19	8.3	7.1	5.4	4.3	3.6	3.7	4.3	5.6	6.9	7.7	9.8	13.9	18.7	23.6
494191	1004796	V20	17.1	11.8	11.6	12.9	16.8	23.2	27.6	32.1	45.4	27.1	38.8	22.3	16.7	15.5
495223	1004845	V21	6.8	9.3	15.8	20.1	24.7	33.4	37.8	38.5	41.6	40	44.1	45.7	40.7	40.6
496269	1004908	V22	21.5	19.2	19.7	18	18.3	18.6	18	18.1	19.2	18.1	19.5	18	15.8	14.5
497226	1004982	V23	7.3	5.6	3.6	3	3	3.1	3.7	4.6	6.4	6.2	8.6	11.4	13.7	14.6
498237	1005047	V24	12.6	9.9	10.1	9.9	12.2	14.5	13.7	20.9	21.1	23.6	24.4	24	23.2	18
499232	1005104	V25	22.2	15.3	11.6	10.4	11	12.1	11.7	11.4	12	9.7	10.3	10.1	11.6	15.4
500181	1005162	V26	24.4	19.3	16.1	11.1	9.5	8	9	11.1	11.5	12.6	13.3	15.6	16.6	21.4

UTM E	UTM N	Ves no	AB/2(m)								
			150	150	220	220	330	500	750	1000	1500
489440	1009694	V1	23.7	28	26.8	29.1	30	31.9	30.6	31.5	32
490397	1009713	V2	25.3	24.1	29.4	28.2	30.4	30.2	38.2	41.3	51
491431	1009770	V3	15.3	14.4	15.6	14.6	17.5	14.9	23	30	38.8
492448	1009834	V4	8.7	9.9	10.2	11.6	12.9	14.5	15.5	16	32
493337	1009824	V5	17.1	16.8	18.2	17.6	19.8	22.5	24.4	28.2	34
494318	1009833	V6	24.5	22.8	21.7	19.7	22.3	24	25.6	29	33
495293	1009862	V7	19.4	18.8	21.4	21.2	22.9	22.7	19.8	20.5	27.4
496306	1009905	V8	20	19.4	22	20.7	23.4	17.8	24.6	21.7	21
497307	1009905	V9	15.6	16.6	18.9	20.2	24.4	26.1	23.2	41.4	54.3
498220	1009947	V10	16.9	17	21.7	22.1	26.5	27.2	24.8	27.5	45
499190	1009974	V11	17.3	17.4	20.1	20.8	23.3	19.9	17.3	19.8	23.8
500158	1010006	V12	30.7	31.3	33.7	34.5	35.2	31.6	26.8	25.6	33
501202	1010009	V13	30.3	29.2	32.8	32.7	35.8	31.6	30.3	32.9	42
488215	1004389	V14	28.8	30.2	27.7	30	26	22.5	21.8	23.4	27.2
489212	1004477	V15	35.4	35.5	33.1	33.6	28.8	26.8	21.9	24.8	28
490230	1004544	V16	33.4	34.1	26.7	27.5	28.4	24.4	21.2	22.3	24.4
491184	1004471	V17	10.2	11.2	12.7	13.5	13.5	15.8	11.1	22.3	14.6
492265	1004586	V18	15	14.4	14.6	14.1	16.8	19.9	20.3	28.7	34.3
493237	1004689	V19	23.5	23.6	22.9	23.2	22	20	17	17.8	20
494191	1004796	V20	14.9	18.1	16.4	19.2	20.6	20.3	19.7	21.2	22.3
495223	1004845	V21	34.7	44.1	25.1	30.9	23.3	23.1	15.3	19.8	25.6
496269	1004908	V22	13.8	14.6	12.8	13.9	14.2	19.8	21	32	42
497226	1004982	V23	15.4	15.1	16.9	16.8	19.8	24.4	26.9	31.5	41.5
498237	1005047	V24	16.5	15.1	19.9	17.5	22.6	30	58.2	24.7	37.8
499232	1005104	V25	21.1	22	26.7	29.3	29.1	28.1	28	37.7	42.2
500181	1005162	V26	24.2	24.3	27.9	28.5	33.1	38.8	32.9	28.6	41.6

UTM S	UTM N	VES no	AB/2(m)													
			1.5	2.1	3	4.2	6	9	13.5	20	20	30	30	45	66	100
501289	1005239	V27	37.9	35.8	38.2	42.2	50.5	59	56.5	46.6	41.5	44.6	39.9	36.7	32.8	23.6
488748	997807	V28	31	18.3	14.4	14.8	15.6	21.5	38.8	29	21.4	43.5	27.5	38.6	46	38.8
489586	997783	V29	58.7	25.9	18	18.9	23.6	31.9	33.4	46.5	44.5	66.2	59.6	54	63.8	64.7
490802	997889	V30	41.1	29.9	20.7	21.2	23.8	20.3	17.8	22.1	26.6	27.2	29.7	31.7	41.5	47.2
491733	997994	V31	26.2	14.6	6.9	4.1	4.7	5.3	7.4	8.75	10.1	14.2	16.1	21.8	27.9	36.7
492737	998051	V32	55.4	34.2	10.3	6.6	6.1	7.8	10.9	15.4	11.4	20.6	16.5	20.8	28	40.6
493740	998116	V33	17.5	9.5	6.8	8.3	11.5	16	20.8	26.3	25.5	33.1	29.2	29.5	34.4	30.1
494760	998190	V34	105	80.4	43.7	44.4	50.3	32	24.9	30.8	23.2	40.2	30.9	34.7	37	40.8
495738	998248	V35	44.8	44.5	62.2	56.2	64.2	58.2	45.7	51.1	37.4	41.6	36.9	43.5	47.8	49.5
496743	998300	V36	14.9	14.6	15	19.3	23.7	25.3	34.7	36.1	30.8	38.5	37.8	45.9	35.3	44.5
497744	998364	V37	15.1	11.5	9.5	10.4	13.9	16	24.4	20.7	26	22	28.4	28.1	29.4	31.4
498741	998421	V38	17.1	18.9	24.7	30.6	41.9	39.7	43.4	50.2	57.5	50.9	61	63.9	59.9	57.6
499747	998489	V39	39.7	33.7	35.1	44.3	51.9	56.6	57.2	65	66.8	62.3	74.4	77	96.6	101.1
500753	998548	V40	59.8	58.9	61.6	55	43.7	30.2	19	18.6	13.7	20.4	14.8	18.7	21.9	30.4
501752	998607	V41	35	15.4	9.8	10.3	12.2	16	23	33.7	25.5	40.5	33.3	33.3	39.1	34.8
488208	993626	V42	83.2	61.8	45	22.5	11.3	10.7	17	30.8	14.9	86.3	18.2	22.6	27.8	33
490271	993664	V43	238.3	186.9	177.8	243.5	247.9	275.9	347.3	677.4	209.1	500	172.8	124.1	97.9	91
491167	993683	V44	131.3	78.3	55.3	35.5	25.1	16.6	17.2	30.1	22.2	72.6	38.8	49.6	54.1	57.2
492185	993732	V45	5.8	5.6	8.1	8.3	9.3	13.3	18.3	24.2	31.9	31.1	41.7	48.6	50	47.3
493148	993753	V46	91.1	88.5	98.8	110.6	130.8	117.7	99.7	83.1	79	74.3	68.9	66.3	65.5	61.4
494131	993826	V47	15.4	11.2	7.4	9.3	12.4	18.5	23.3	28.8	31.7	32.8	87.3	39.3	32.5	35.8
495156	993788	V48	11.7	11.9	13.3	17.2	20	22.2	26.9	31.9	58.7	40.2	76.6	86.1	79.1	65.1
496184	993829	V49	33.4	11	10.6	11.9	14.5	17.8	21.8	28.2	27.7	37.8	37.5	48.8	55.8	48.9
497121	993877	V50	143.8	106.2	96.6	97.5	106.2	108.5	113.4	118.9	86.4	125.2	91.8	82.1	59	41.9
498097	993900	V51	71.5	69.3	84.9	94.2	94.3	86.8	69.4	66.5	72.2	52.9	56.9	50.1	48.9	51.7
500071	993970	V52	31.7	28.6	38.6	40.1	44.1	48.5	51.2	47.2	55.3	39.5	46.1	35.9	30.6	34.5

UTM S	UTM N	VES no	AB/2(m)								
			150	150	220	220	330	500	750	1000	1500
501289	1005239	V27	21.2	22.4	25.1	26.1	31.5	36.8	41.2	50.4	61
488748	997807	V28	0	50	52.9	60.8	47.6	38	21.6	14	0
489586	997783	V29	58.8	61.3	50.4	51.3	32.6	27.7	19.6	23.5	41.6
490802	997889	V30	48.8	59.4	46.6	58.2	48.7	39.8	56.8	56	86.4
491733	997994	V31	39.9	36.3	44.1	41.9	42.7	38.9	45.1	31.5	54.9
492737	998051	V32	44.7	47.3	47.8	50.5	44.7	37.6	35.3	41.65	72.2
493740	998116	V33	35.8	32.5	35.3	31.4	31.8	28.6	23.7	30.1	48.7
494760	998190	V34	38.2	39.9	36.5	37.4	27.7	37.2	47	42	31.4
495738	998248	V35	47	50.8	40.3	46.2	38.8	29.4	45.1	66.5	0
496743	998300	V36	47.6	41.5	39.06	39	34.5	32	33.3	59.3	70.7
497744	998364	V37	27	41.5	21.4	29.2	41.3	38.3	35.3	45.5	62.8
498741	998421	V38	47.04	57.6	37.8	39.4	32.6	36.3	45.1	42	31.4
499747	998489	V39	76.4	90.8	60.5	65.4	41.25	32	29.4	31.5	23.5
500753	998548	V40	31.2	32.3	28.9	31.1	31.9	41.5	68.6	97	172.7
501752	998607	V41	35.8	35.6	40.3	37.3	48.4	62.3	90	133	233.9
488208	993626	V42	36.9	34.8	51	41	41.8	40.8	44.9	47.1	81.5
490271	993664	V43	45	58.2	324	45.8	39.2	33.9	31.8	30.2	38.9
491167	993683	V44	56.3	56	61.4	50.8	47.7	38.6	33.3	36.6	75.3
492185	993732	V45	43.3	49.9	38.7	44.1	40.7	38.1	39.2	46	61.7
493148	993753	V46	54.6	55	44.3	45	40.4	36	35.2	31.3	49.7
494131	993826	V47	35.1	33.6	37.6	36.2	31.5	27	20.3	26.7	51.7
495156	993788	V48	49.8	57.5	44.3	48.2	38.7	30.6	46.6	35.6	73.2
496184	993829	V49	39.1	42.3	33.9	36.9	30.8	22.5	22.3	30	52
497121	993877	V50	31.4	32.3	30.4	30.8	30.6	31.5	33.2	46.3	70.3
498097	993900	V51	54.3	59	42.3	47.9	46.9	53.8	98.3	105.7	847
500071	993970	V52	38.2	39	36.6	38.4	34.7	33.8	34.1	48.1	78.7

Appendix 2 Interpreted VES Curves

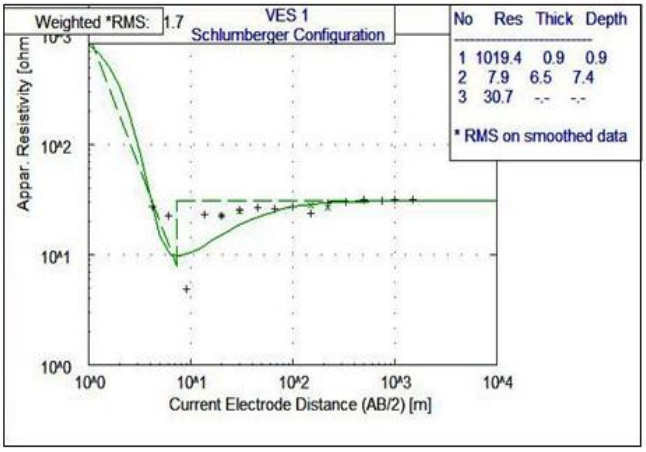

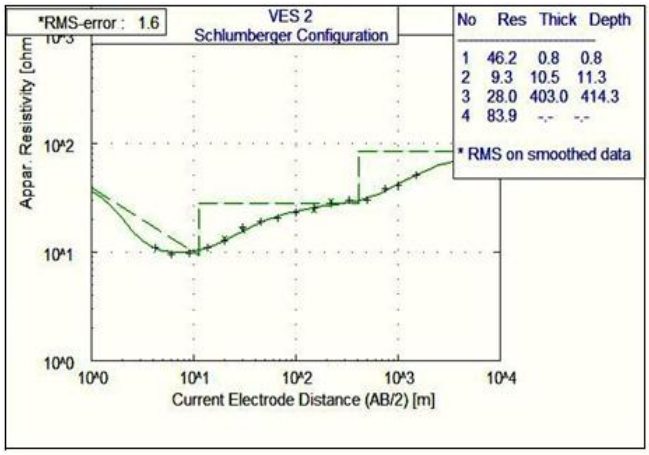

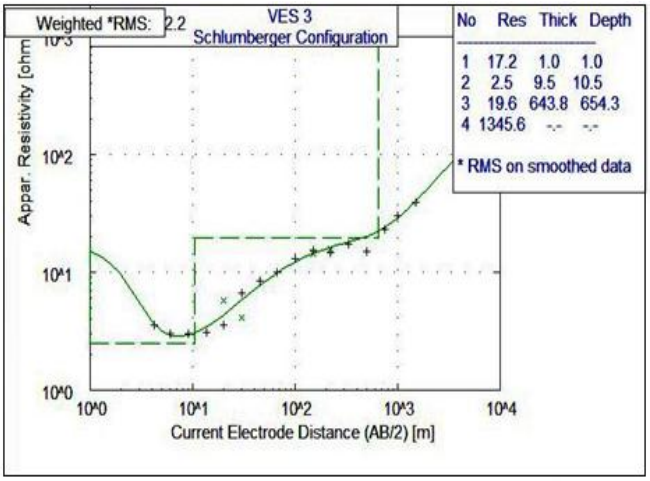

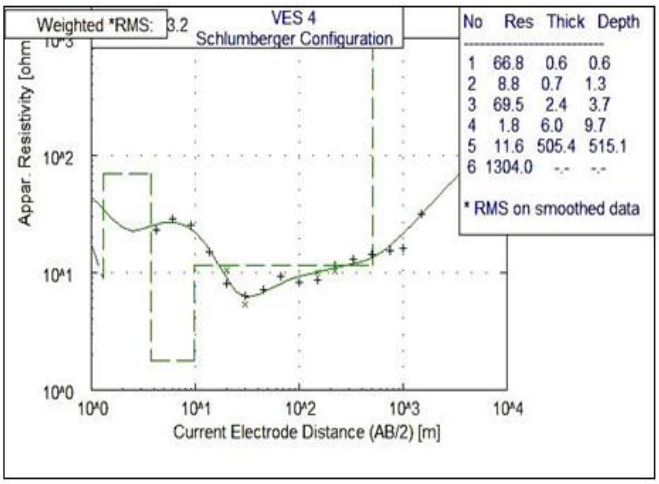

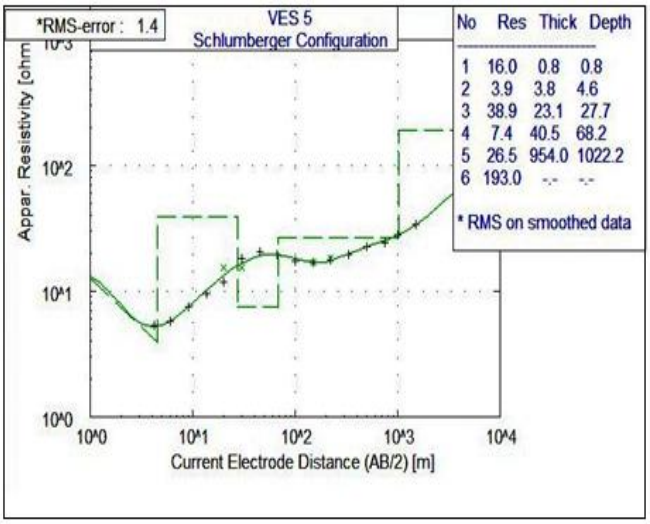

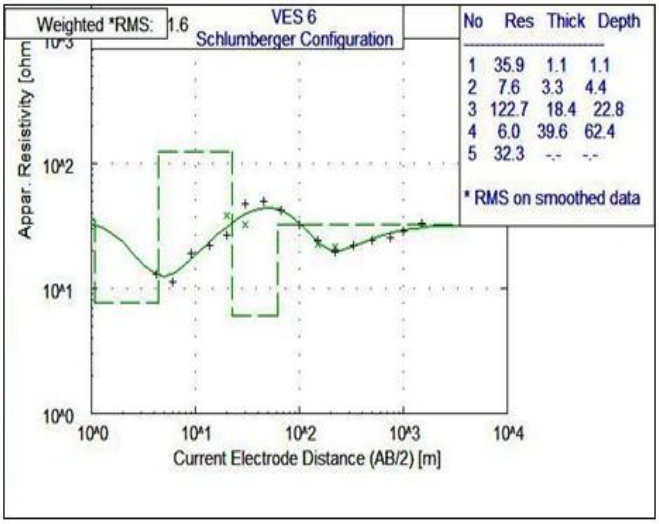

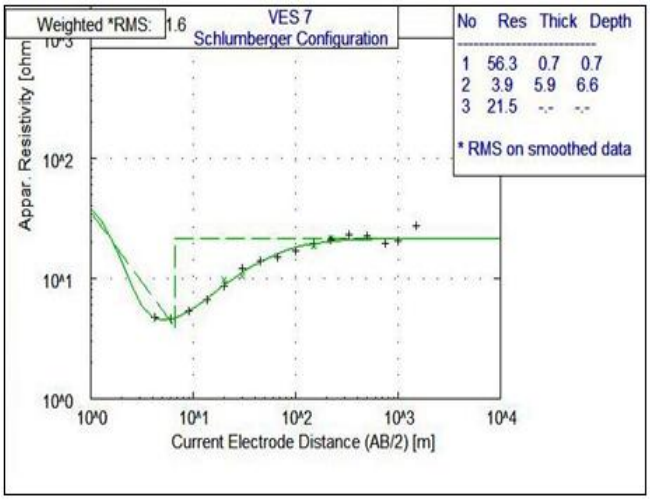
Weighted *RMS: 1.6
VES 7
Schlumberger Configuration
No Res Thick Depth
1 56.3 0.7 0.7
2 3.9 5.9 6.6
3 21.5 -.- -.-
* RMS on smoothed data
Appar. Resistivity [ohm]
Current Electrode Distance (AB/2) [m]

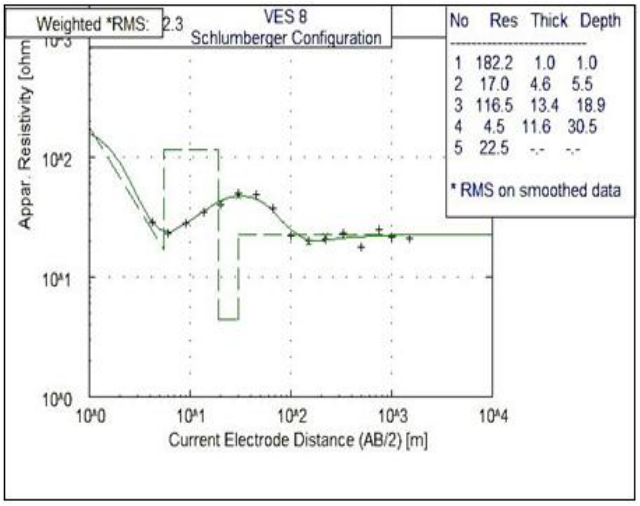
Weighted *RMS: 2.3
VES 8
Schlumberger Configuration
No Res Thick Depth
1 182.2 1.0 1.0
2 17.0 4.6 5.5
3 116.5 13.4 18.9
4 4.5 11.6 30.5
5 22.5 -.- -.-
* RMS on smoothed data
Appar. Resistivity [ohm]
Current Electrode Distance (AB/2) [m]

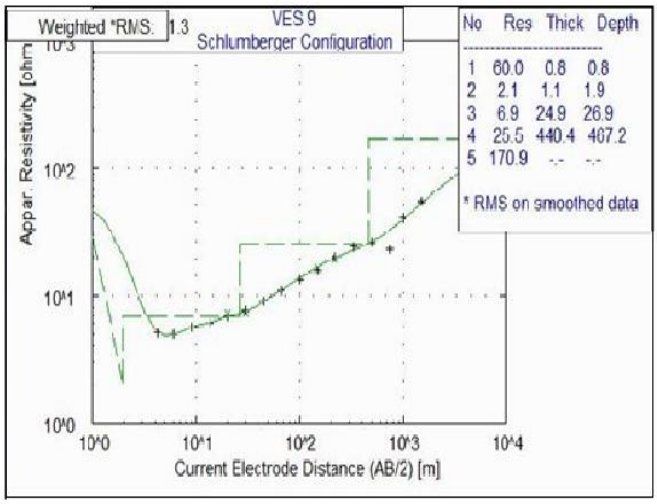
Weighted *RMS: 1.3
VES 9
Schlumberger Configuration
No Res Thick Depth
1 60.0 0.8 0.8
2 2.1 1.1 1.9
3 6.9 24.9 26.9
4 25.5 440.4 467.2
5 170.9 -.- -.-
* RMS on smoothed data
Appar. Resistivity [ohm]
Current Electrode Distance (AB/2) [m]

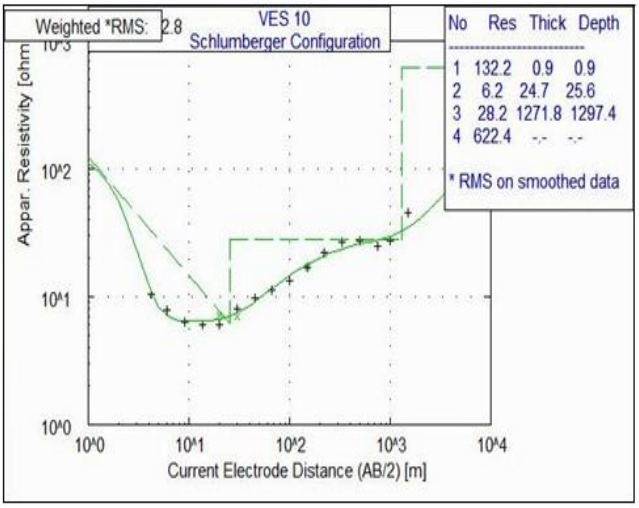
Weighted *RMS: 2.8
VES 10
Schlumberger Configuration
No Res Thick Depth
1 132.2 0.9 0.9
2 6.2 24.7 25.6
3 28.2 1271.8 1297.4
4 622.4 -.- -.-
* RMS on smoothed data
Appar. Resistivity [ohm]
Current Electrode Distance (AB/2) [m]

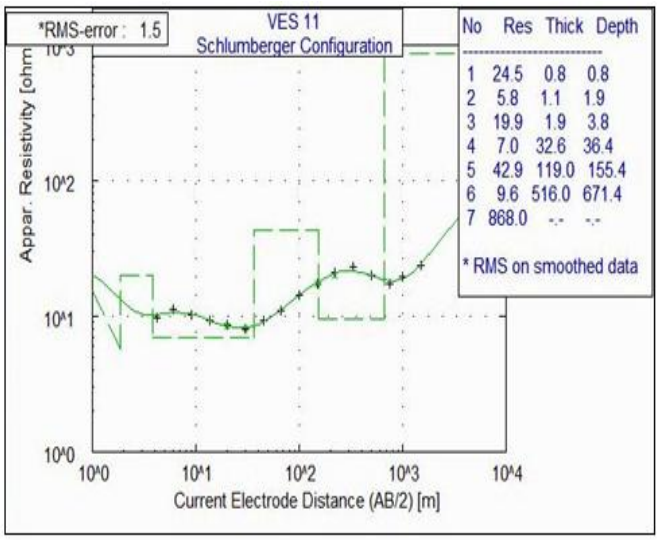
*RMS-error : 1.5
VES 11
Schlumberger Configuration
No Res Thick Depth
1 24.5 0.8 0.8
2 5.8 1.1 1.9
3 19.9 1.9 3.8
4 7.0 32.6 36.4
5 42.9 119.0 155.4
6 9.6 516.0 671.4
7 868.0 -.- -.-
* RMS on smoothed data
Appar. Resistivity [ohm]
Current Electrode Distance (AB/2) [m]

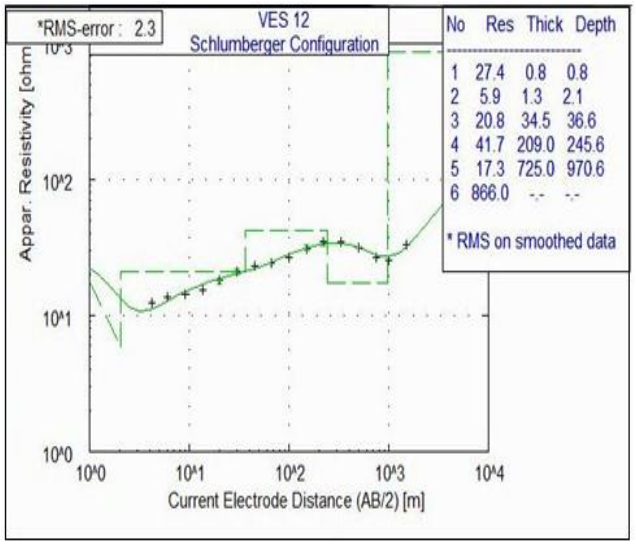
*RMS-error : 2.3
VES 12
Schlumberger Configuration
No Res Thick Depth
1 27.4 0.8 0.8
2 5.9 1.3 2.1
3 20.8 34.5 36.6
4 41.7 209.0 245.6
5 17.3 725.0 970.6
6 866.0 -.- -.-
* RMS on smoothed data
Appar. Resistivity [ohm]
Current Electrode Distance (AB/2) [m]

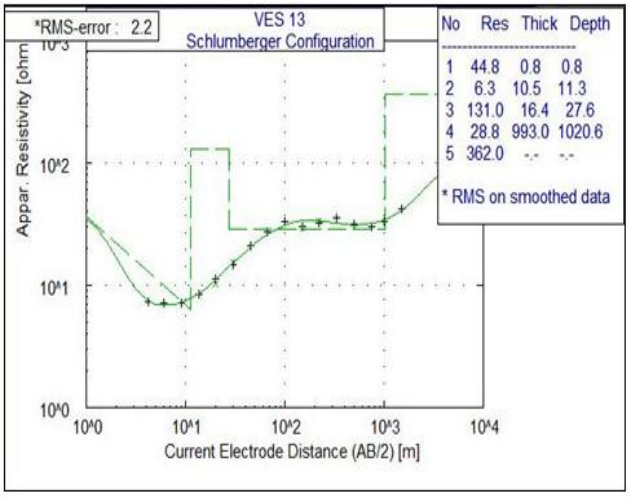
*RMS-error : 2.2
VES 13
Schlumberger Configuration
No Res Thick Depth
1 44.8 0.8 0.8
2 6.3 10.5 11.3
3 131.0 16.4 27.6
4 28.8 993.0 1020.6
5 362.0 -.- -.-
* RMS on smoothed data
Appar. Resistivity [ohm]
Current Electrode Distance (AB/2) [m]

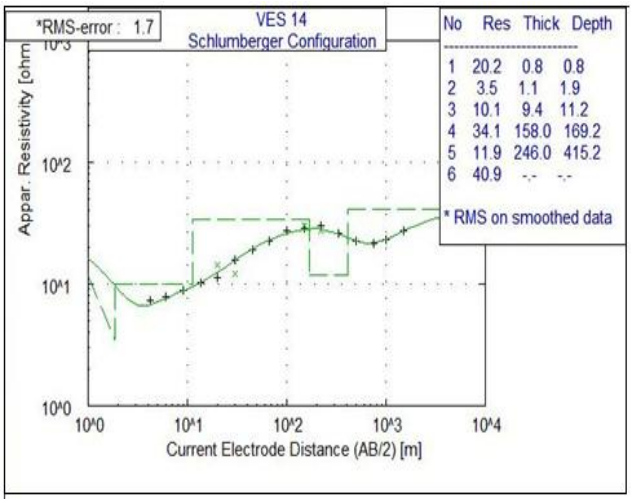
*RMS-error : 1.7
VES 14
Schlumberger Configuration
No Res Thick Depth
1 20.2 0.8 0.8
2 3.5 1.1 1.9
3 10.1 9.4 11.2
4 34.1 158.0 169.2
5 11.9 246.0 415.2
6 40.9 -.- -.-
* RMS on smoothed data
Appar. Resistivity [ohm]
Current Electrode Distance (AB/2) [m]

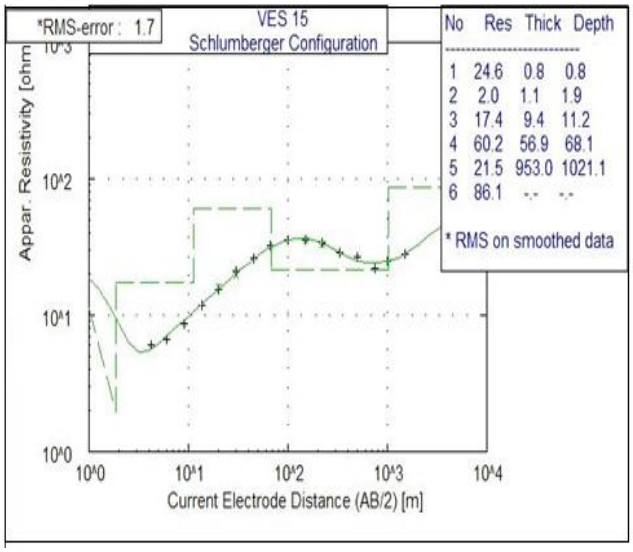
*RMS-error : 1.7
VES 15
Schlumberger Configuration
No Res Thick Depth
1 24.6 0.8 0.8
2 2.0 1.1 1.9
3 17.4 9.4 11.2
4 60.2 56.9 68.1
5 21.5 953.0 1021.1
6 86.1 -.- -.-
* RMS on smoothed data
Appar. Resistivity [ohm]
Current Electrode Distance (AB/2) [m]

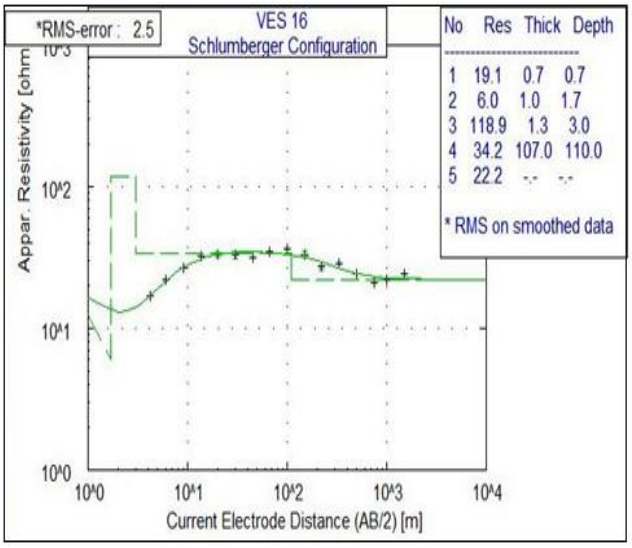
*RMS-error : 2.5
VES 16
Schlumberger Configuration
No Res Thick Depth
1 19.1 0.7 0.7
2 6.0 1.0 1.7
3 118.9 1.3 3.0
4 34.2 107.0 110.0
5 22.2 -.- -.-
* RMS on smoothed data
Appar. Resistivity [ohm]
Current Electrode Distance (AB/2) [m]

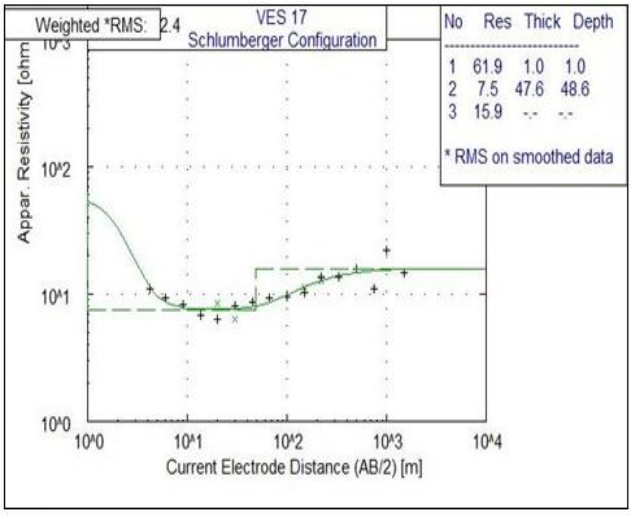
Weighted *RMS: 2.4
VES 17
Schlumberger Configuration
No Res Thick Depth
1 61.9 1.0 1.0
2 7.5 47.6 48.6
3 15.9 -.- -.-
* RMS on smoothed data
Appar. Resistivity [ohm]
Current Electrode Distance (AB/2) [m]

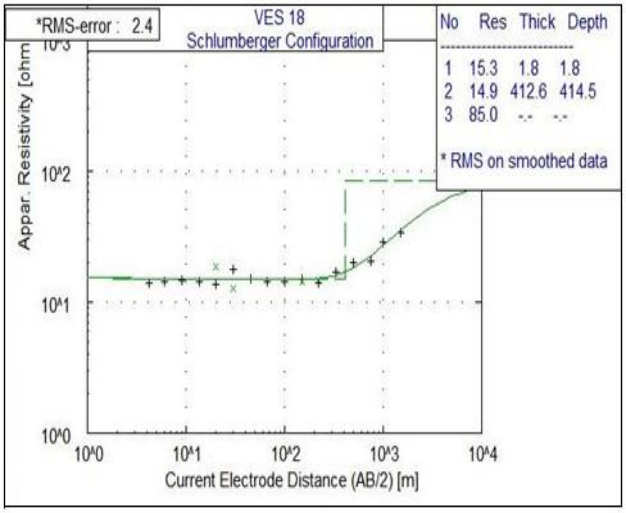
*RMS-error : 2.4
VES 18
Schlumberger Configuration
No Res Thick Depth
1 15.3 1.8 1.8
2 14.9 412.6 414.5
3 85.0 -.- -.-
* RMS on smoothed data
Appar. Resistivity [ohm]
Current Electrode Distance (AB/2) [m]

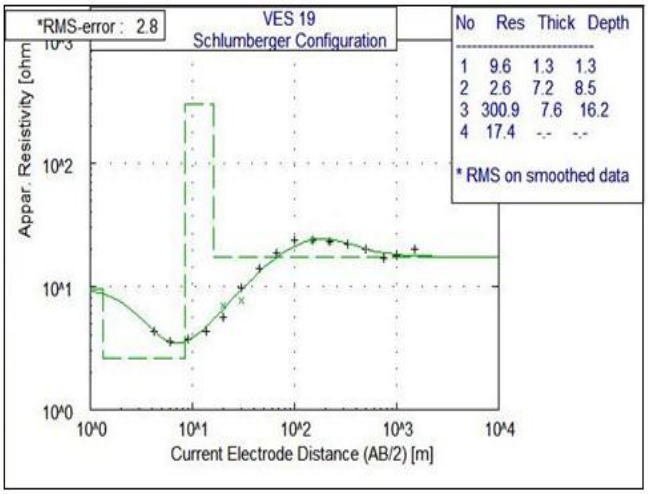
*RMS-error : 2.8
VES 19
Schlumberger Configuration
No Res Thick Depth
1 9.6 1.3 1.3
2 2.6 7.2 8.5
3 300.9 7.6 16.2
4 17.4 -.- -.-
* RMS on smoothed data
Appar. Resistivity [ohm]
Current Electrode Distance (AB/2) [m]

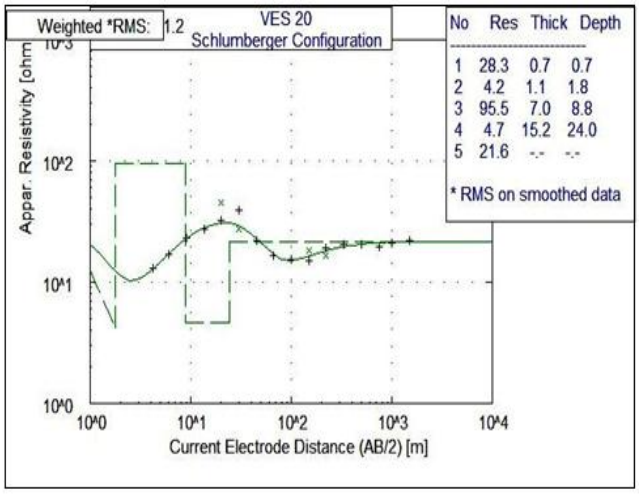
Weighted *RMS: 1.2
VES 20
Schlumberger Configuration
No Res Thick Depth
1 28.3 0.7 0.7
2 4.2 1.1 1.8
3 95.5 7.0 8.8
4 4.7 15.2 24.0
5 21.6 -.- -.-
* RMS on smoothed data
Appar. Resistivity [ohm]
Current Electrode Distance (AB/2) [m]

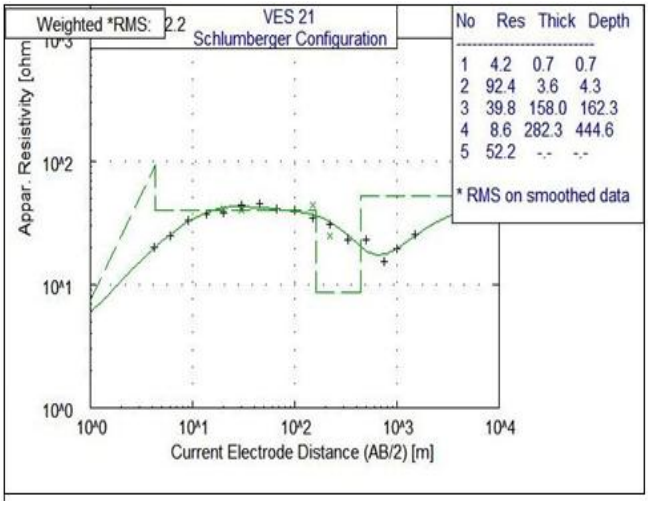
Weighted *RMS: 2.2
VES 21
Schlumberger Configuration
No Res Thick Depth
1 4.2 0.7 0.7
2 92.4 3.6 4.3
3 39.8 158.0 162.3
4 8.6 282.3 444.6
5 52.2 -.- -.-
* RMS on smoothed data
Appar. Resistivity [ohm]
Current Electrode Distance (AB/2) [m]

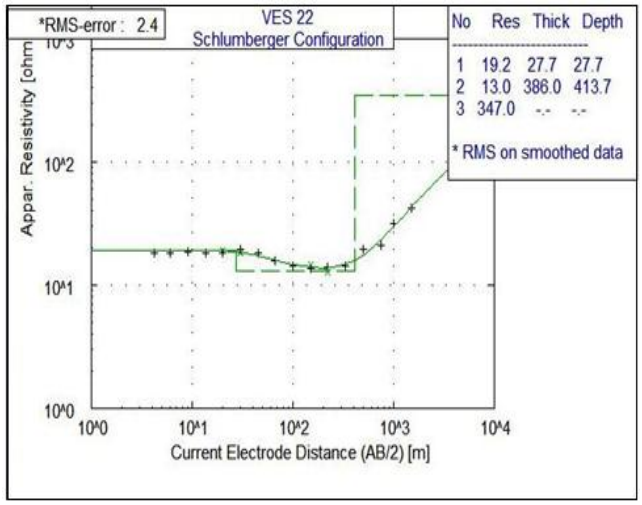
*RMS-error : 2.4
VES 22
Schlumberger Configuration
No Res Thick Depth
1 19.2 27.7 27.7
2 13.0 386.0 413.7
3 347.0 -.- -.-
* RMS on smoothed data
Appar. Resistivity [ohm]
Current Electrode Distance (AB/2) [m]

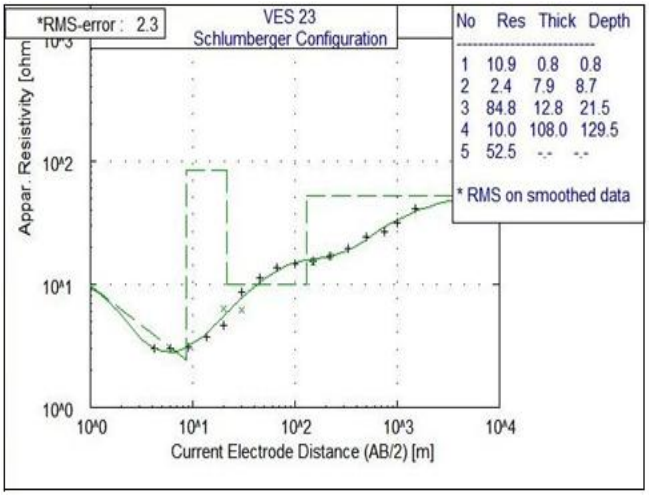
*RMS-error : 2.3
VES 23
Schlumberger Configuration
No Res Thick Depth
1 10.9 0.8 0.8
2 2.4 7.9 8.7
3 84.8 12.8 21.5
4 10.0 108.0 129.5
5 52.5 -.- -.-
* RMS on smoothed data
Appar. Resistivity [ohm]
Current Electrode Distance (AB/2) [m]

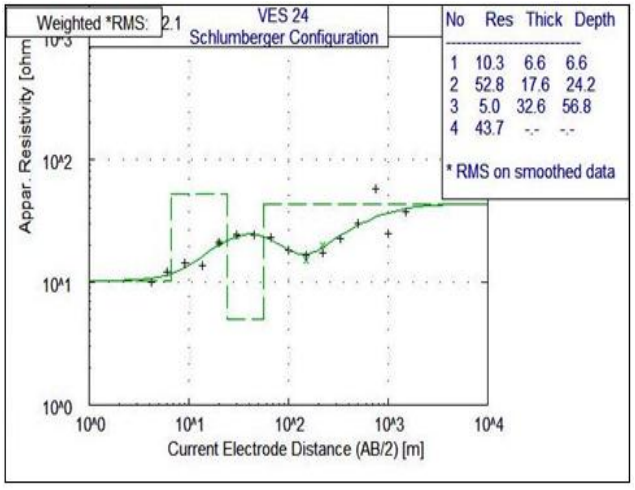
Weighted *RMS: 2.1
VES 24
Schlumberger Configuration
No Res Thick Depth
1 10.3 6.6 6.6
2 52.8 17.6 24.2
3 5.0 32.6 56.8
4 43.7 -.- -.-
* RMS on smoothed data
Appar. Resistivity [ohm]
Current Electrode Distance (AB/2) [m]

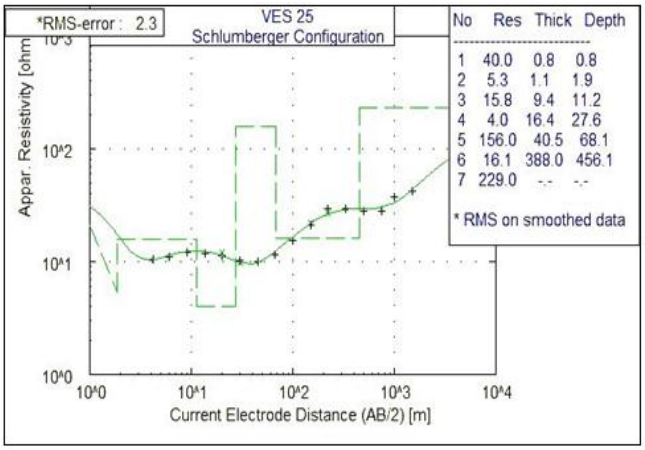
*RMS-error : 2.3
VES 25
Schlumberger Configuration
No Res Thick Depth
1 40.0 0.8 0.8
2 5.3 1.1 1.9
3 15.8 9.4 11.2
4 4.0 16.4 27.6
5 156.0 40.5 68.1
6 16.1 388.0 456.1
7 229.0 -.- -.-
* RMS on smoothed data
Appar. Resistivity [ohm]
Current Electrode Distance (AB/2) [m]

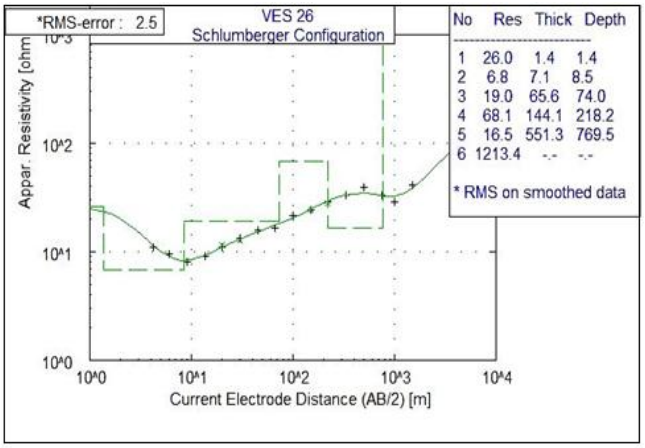
*RMS-error : 2.5
VES 26
Schlumberger Configuration
No Res Thick Depth
1 26.0 1.4 1.4
2 6.8 7.1 8.5
3 19.0 65.6 74.0
4 68.1 144.1 218.2
5 16.5 551.3 769.5
6 1213.4 -.- -.-
* RMS on smoothed data
Appar. Resistivity [ohm]
Current Electrode Distance (AB/2) [m]

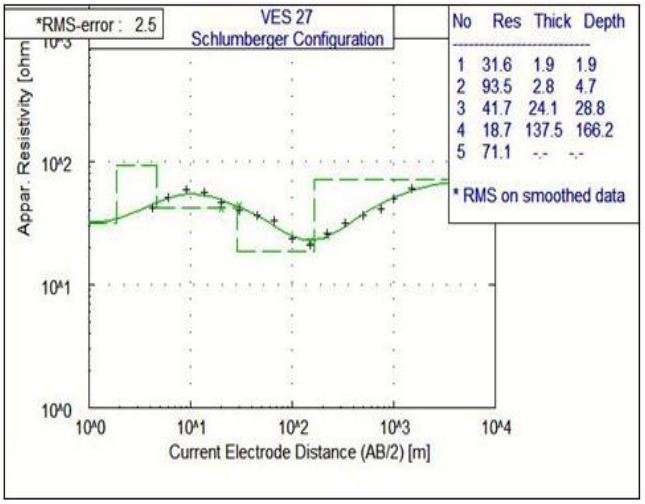
*RMS-error : 2.5
VES 27
Schlumberger Configuration
No Res Thick Depth
1 31.6 1.9 1.9
2 93.5 2.8 4.7
3 41.7 24.1 28.8
4 18.7 137.5 166.2
5 71.1 -.- -.-
* RMS on smoothed data
Appar. Resistivity [ohm]
Current Electrode Distance (AB/2) [m]

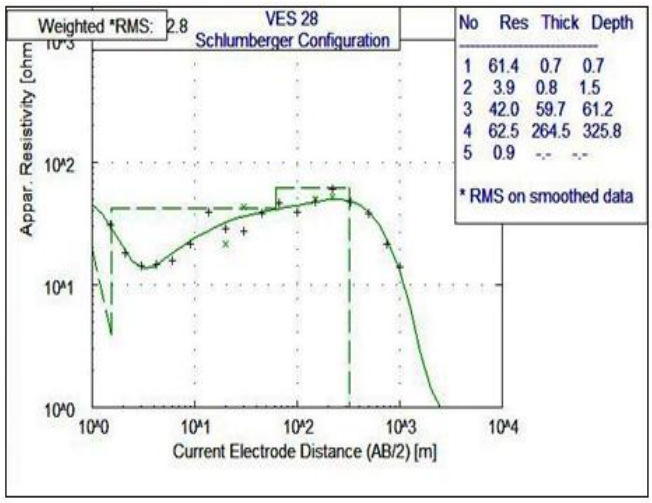
Weighted *RMS: 2.8
VES 28
Schlumberger Configuration
No Res Thick Depth
1 61.4 0.7 0.7
2 3.9 0.8 1.5
3 42.0 59.7 61.2
4 62.5 264.5 325.8
5 0.9 -.- -.-
* RMS on smoothed data
Appar. Resistivity [ohm]
Current Electrode Distance (AB/2) [m]

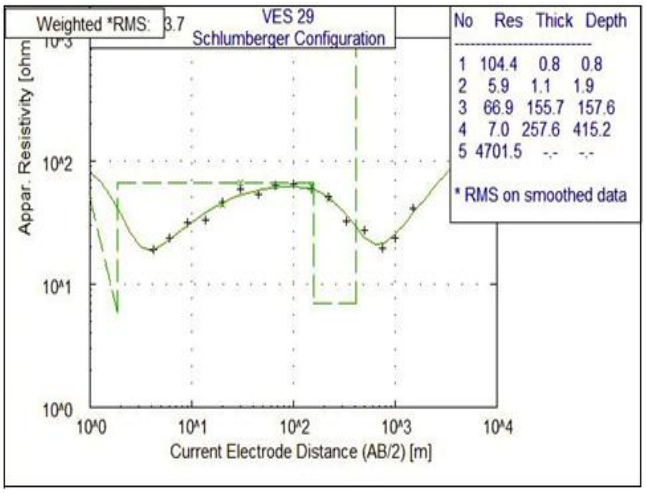
Weighted *RMS: 3.7
VES 29
Schlumberger Configuration
No Res Thick Depth
1 104.4 0.8 0.8
2 5.9 1.1 1.9
3 66.9 155.7 157.6
4 7.0 257.6 415.2
5 4701.5 -.- -.-
* RMS on smoothed data
Appar. Resistivity [ohm]
Current Electrode Distance (AB/2) [m]

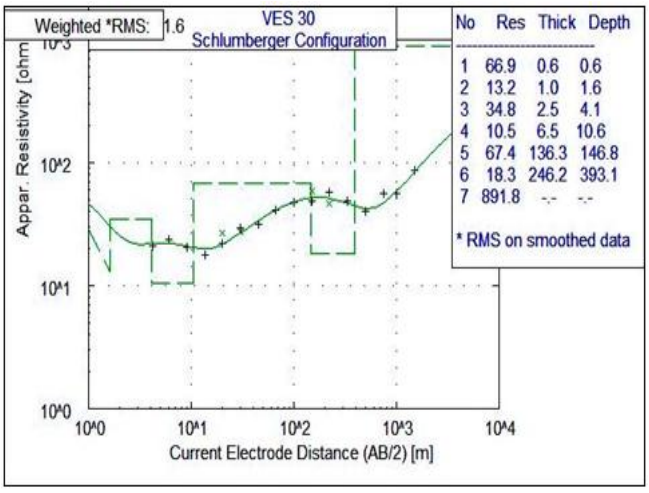
Weighted *RMS: 1.6
VES 30
Schlumberger Configuration
No Res Thick Depth
1 66.9 0.6 0.6
2 13.2 1.0 1.6
3 34.8 2.5 4.1
4 10.5 6.5 10.6
5 67.4 136.3 146.8
6 18.3 246.2 393.1
7 891.8 -.- -.-
* RMS on smoothed data
Appar. Resistivity [ohm]
Current Electrode Distance (AB/2) [m]

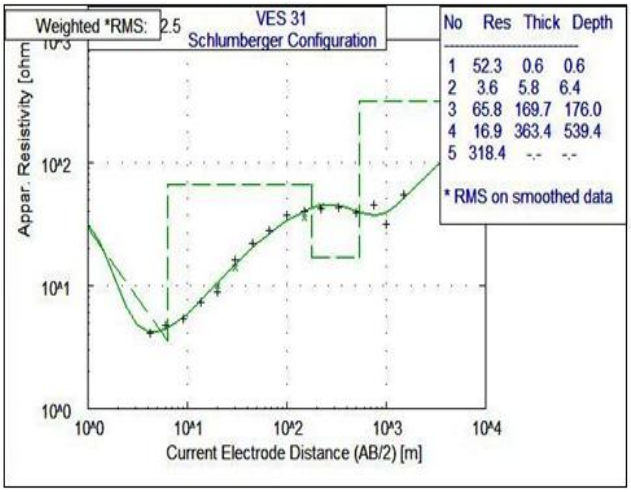
Weighted *RMS: 2.5
VES 31
Schlumberger Configuration
No Res Thick Depth
1 52.3 0.6 0.6
2 3.6 5.8 6.4
3 65.8 169.7 176.0
4 16.9 363.4 539.4
5 318.4 -.- -.-
* RMS on smoothed data
Appar. Resistivity [ohm]
Current Electrode Distance (AB/2) [m]

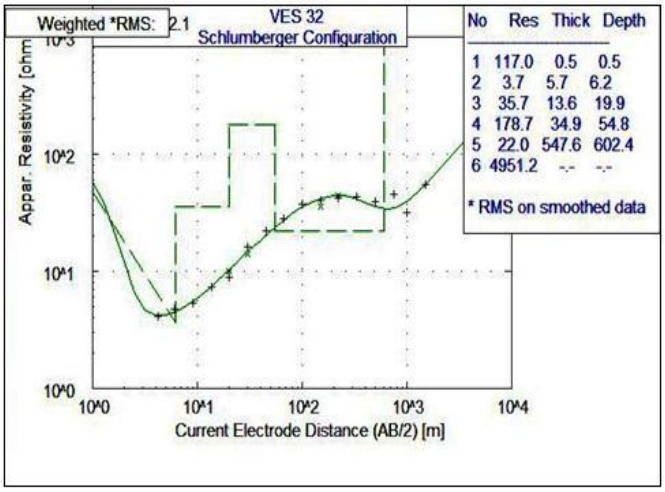
Weighted *RMS: 2.1
VES 32
Schlumberger Configuration
No Res Thick Depth
1 117.0 0.5 0.5
2 3.7 5.7 6.2
3 35.7 13.6 19.9
4 178.7 34.9 54.8
5 22.0 547.6 602.4
6 4951.2 -.- -.-
* RMS on smoothed data
Appar. Resistivity [ohm]
Current Electrode Distance (AB/2) [m]

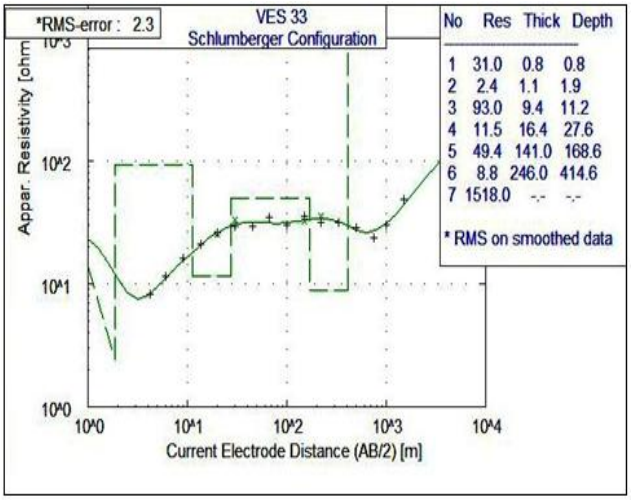
*RMS-error : 2.3
VES 33
Schlumberger Configuration
No Res Thick Depth
1 31.0 0.8 0.8
2 2.4 1.1 1.9
3 93.0 9.4 11.2
4 11.5 16.4 27.6
5 49.4 141.0 168.6
6 8.8 246.0 414.6
7 1518.0 -.- -.-
* RMS on smoothed data
Appar. Resistivity [ohm]
Current Electrode Distance (AB/2) [m]

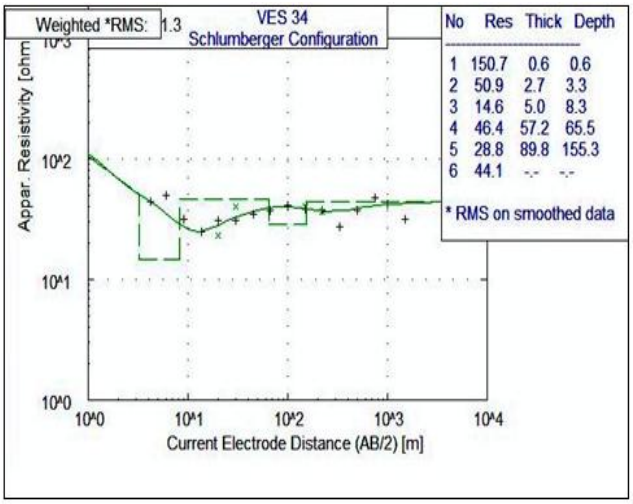
Weighted *RMS: 1.3
VES 34
Schlumberger Configuration
No Res Thick Depth
1 150.7 0.6 0.6
2 50.9 2.7 3.3
3 14.6 5.0 8.3
4 46.4 57.2 65.5
5 28.8 89.8 155.3
6 44.1 -.- -.-
* RMS on smoothed data
Appar. Resistivity [ohm]
Current Electrode Distance (AB/2) [m]

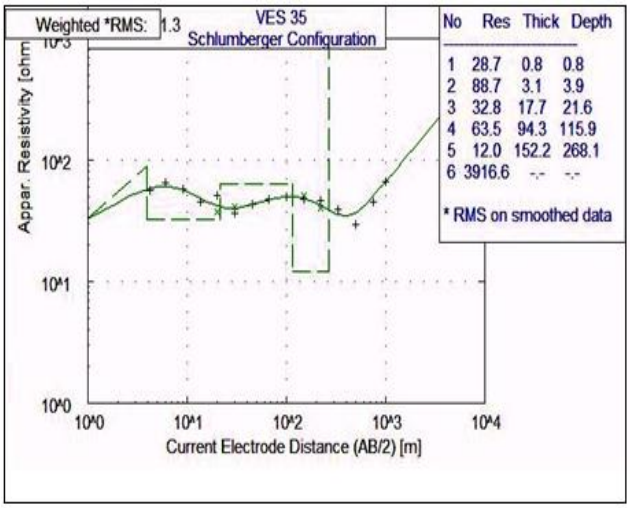
Weighted *RMS: 1.3
VES 35
Schlumberger Configuration
No Res Thick Depth
1 28.7 0.8 0.8
2 88.7 3.1 3.9
3 32.8 17.7 21.6
4 63.5 94.3 115.9
5 12.0 152.2 268.1
6 3916.6 -.- -.-
* RMS on smoothed data
Appar. Resistivity [ohm]
Current Electrode Distance (AB/2) [m]

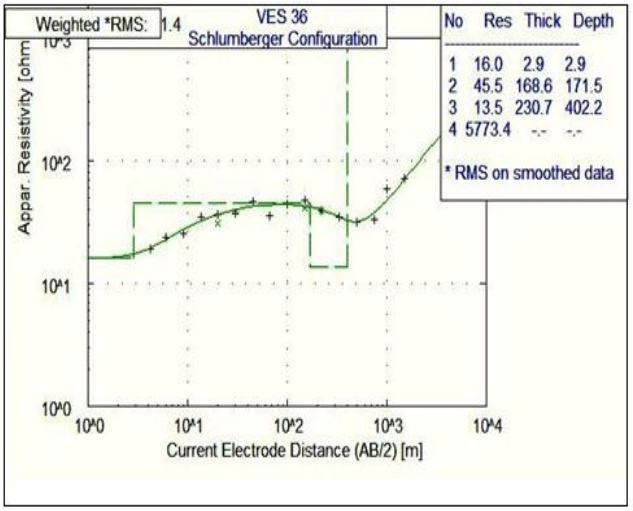
Weighted *RMS: 1.4
VES 36
Schlumberger Configuration
No Res Thick Depth
1 16.0 2.9 2.9
2 45.5 168.6 171.5
3 13.5 230.7 402.2
4 5773.4 -.- -.-
* RMS on smoothed data
Appar. Resistivity [ohm]
Current Electrode Distance (AB/2) [m]

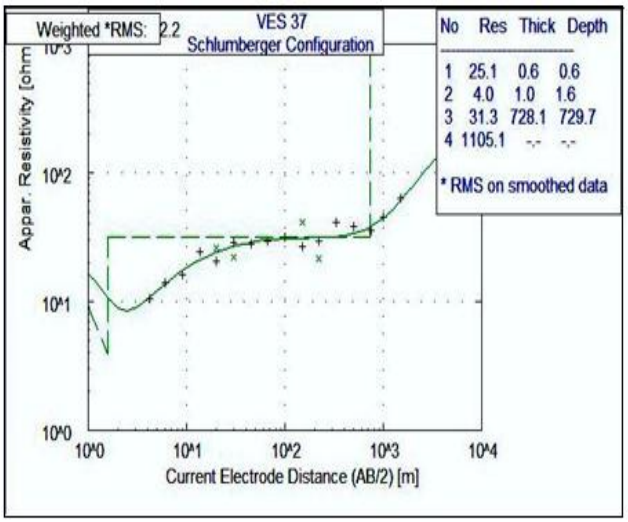
Weighted *RMS: 2.2
VES 37
Schlumberger Configuration
No Res Thick Depth
1 25.1 0.6 0.6
2 4.0 1.0 1.6
3 31.3 728.1 729.7
4 1105.1 -.- -.-
* RMS on smoothed data
Appar. Resistivity [ohm]
Current Electrode Distance (AB/2) [m]

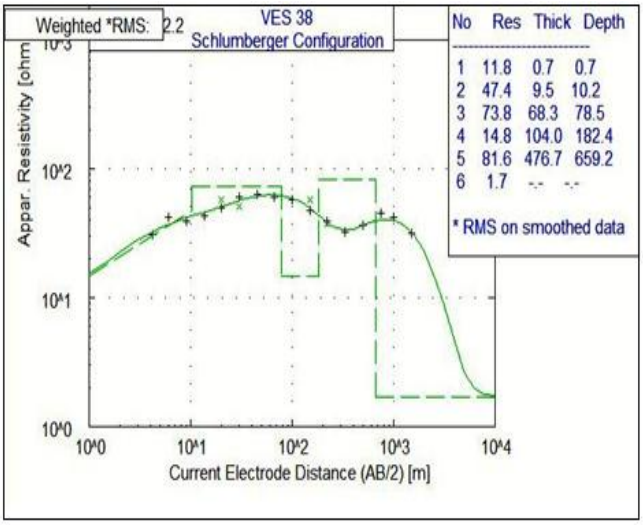
Weighted *RMS: 2.2
VES 38
Schlumberger Configuration
No Res Thick Depth
1 11.8 0.7 0.7
2 47.4 9.5 10.2
3 73.8 68.3 78.5
4 14.8 104.0 182.4
5 81.6 476.7 659.2
6 1.7 -.- -.-
* RMS on smoothed data
Appar. Resistivity [ohm]
Current Electrode Distance (AB/2) [m]

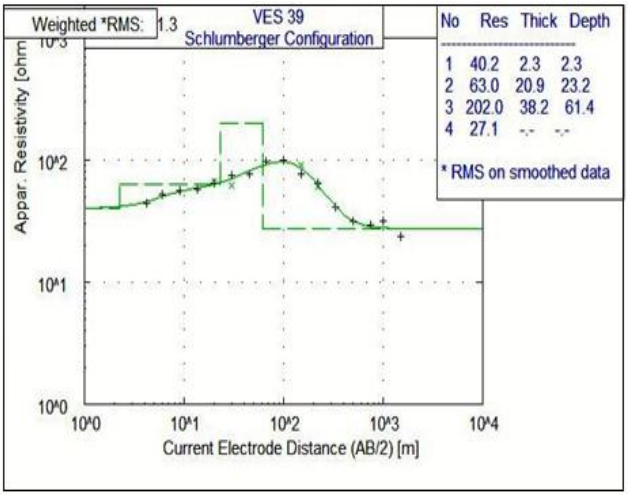
Weighted *RMS: 1.3
VES 39
Schlumberger Configuration
No Res Thick Depth
1 40.2 2.3 2.3
2 63.0 20.9 23.2
3 202.0 38.2 61.4
4 27.1 -.- -.-
* RMS on smoothed data
Appar. Resistivity [ohm]
Current Electrode Distance (AB/2) [m]

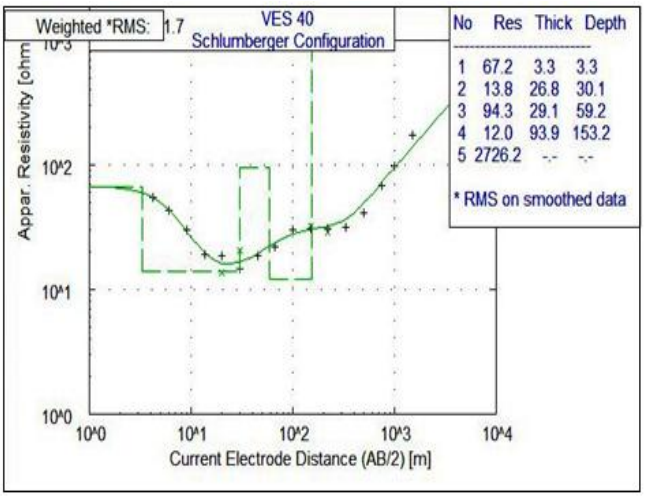
Weighted *RMS: 1.7
VES 40
Schlumberger Configuration
No Res Thick Depth
1 67.2 3.3 3.3
2 13.8 26.8 30.1
3 94.3 29.1 59.2
4 12.0 93.9 153.2
5 2726.2 -.- -.-
* RMS on smoothed data
Appar. Resistivity [ohm]
Current Electrode Distance (AB/2) [m]

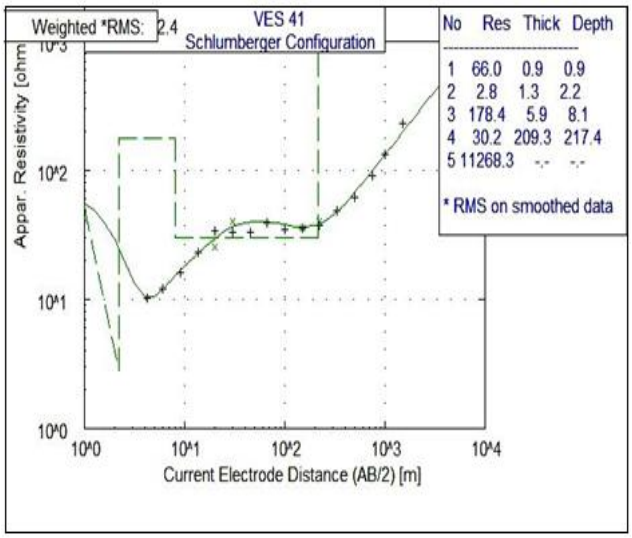
Weighted *RMS: 2.4
VES 41
Schlumberger Configuration
No Res Thick Depth
1 66.0 0.9 0.9
2 2.8 1.3 2.2
3 178.4 5.9 8.1
4 30.2 209.3 217.4
5 11268.3 -.- -.-
* RMS on smoothed data
Appar. Resistivity [ohm]
Current Electrode Distance (AB/2) [m]

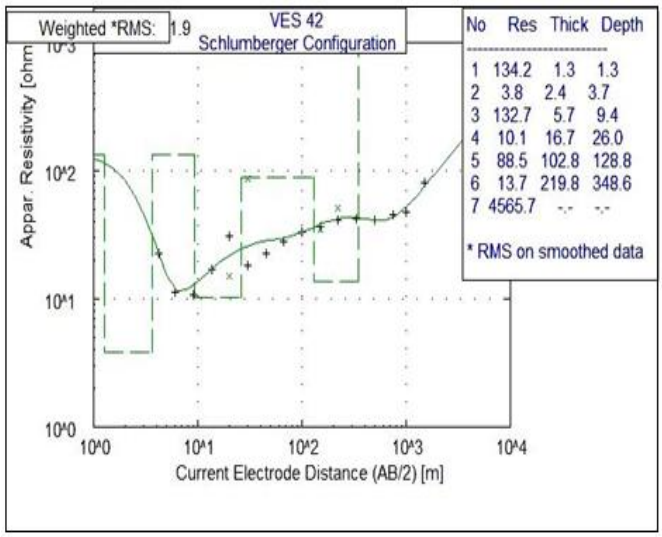
Weighted *RMS: 1.9
VES 42
Schlumberger Configuration
No Res Thick Depth
1 134.2 1.3 1.3
2 3.8 2.4 3.7
3 132.7 5.7 9.4
4 10.1 16.7 26.0
5 88.5 102.8 128.8
6 13.7 219.8 348.6
7 4565.7 -.- -.-
* RMS on smoothed data
Appar. Resistivity [ohm]
Current Electrode Distance (AB/2) [m]

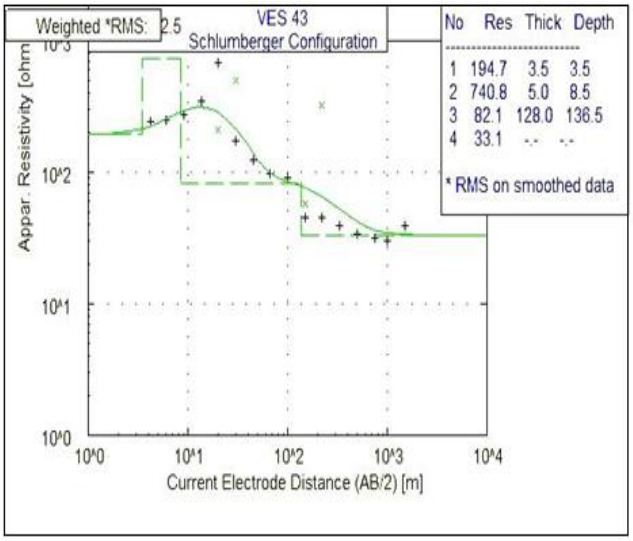
Weighted *RMS: 2.5
VES 43
Schlumberger Configuration
No Res Thick Depth
1 194.7 3.5 3.5
2 740.8 5.0 8.5
3 82.1 128.0 136.5
4 33.1 -.- -.-
* RMS on smoothed data
Appar. Resistivity [ohm]
Current Electrode Distance (AB/2) [m]

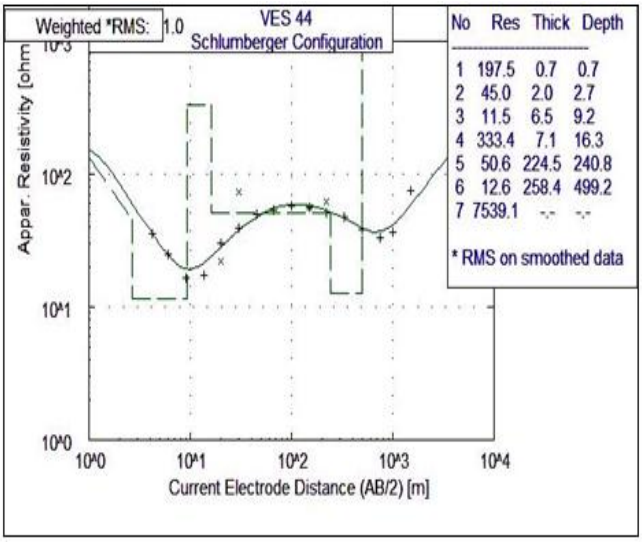
Weighted *RMS: 1.0
VES 44
Schlumberger Configuration
No Res Thick Depth
1 197.5 0.7 0.7
2 45.0 2.0 2.7
3 11.5 6.5 9.2
4 333.4 7.1 16.3
5 50.6 224.5 240.8
6 12.6 258.4 499.2
7 7539.1 -.- -.-
* RMS on smoothed data
Appar. Resistivity [ohm]
Current Electrode Distance (AB/2) [m]

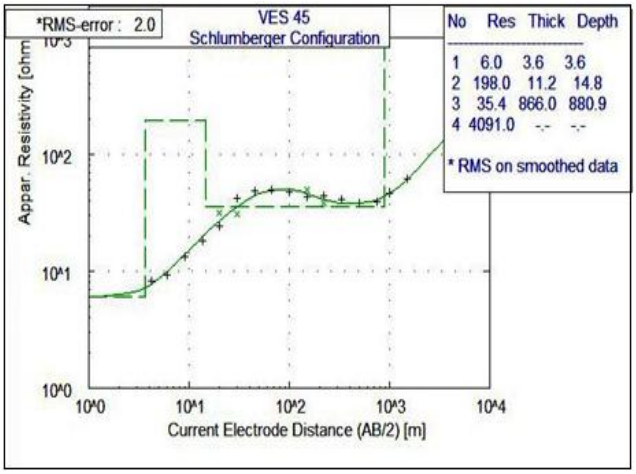
*RMS-error : 2.0
VES 45
Schlumberger Configuration
No Res Thick Depth
1 6.0 3.6 3.6
2 198.0 11.2 14.8
3 35.4 866.0 880.9
4 4091.0 -.- -.-
* RMS on smoothed data
Appar. Resistivity [ohm]
Current Electrode Distance (AB/2) [m]

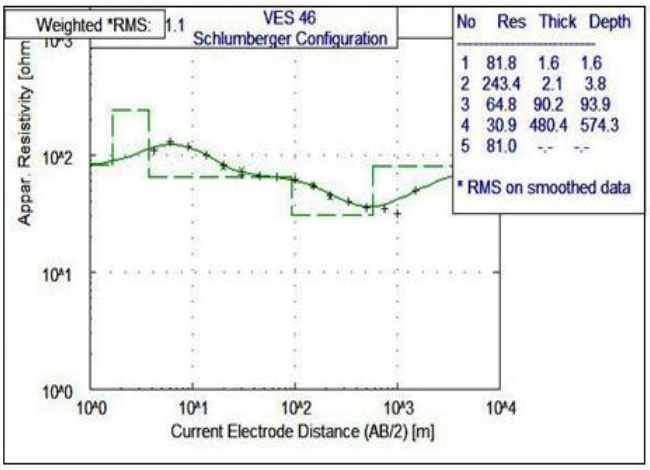
Weighted *RMS: 1.1
VES 46
Schlumberger Configuration
No Res Thick Depth
1 81.8 1.6 1.6
2 243.4 2.1 3.8
3 64.8 90.2 93.9
4 30.9 480.4 574.3
5 81.0 -.- -.-
* RMS on smoothed data
Appar. Resistivity [ohm]
Current Electrode Distance (AB/2) [m]

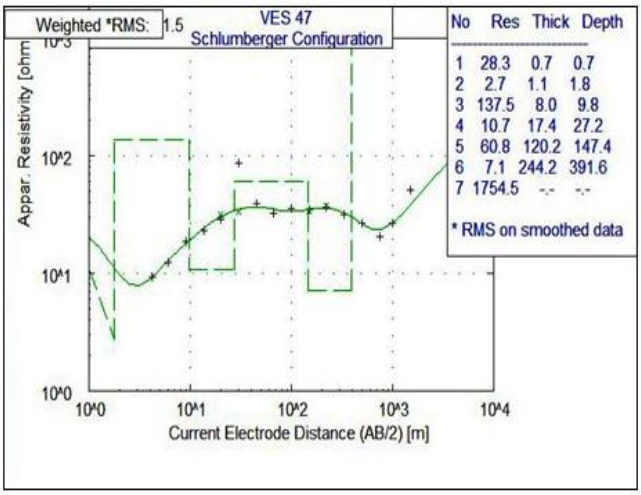
Weighted *RMS: 1.5
VES 47
Schlumberger Configuration
No Res Thick Depth
1 28.3 0.7 0.7
2 2.7 1.1 1.8
3 137.5 8.0 9.8
4 10.7 17.4 27.2
5 60.8 120.2 147.4
6 7.1 244.2 391.6
7 1754.5 -.- -.-
* RMS on smoothed data
Appar. Resistivity [ohm]
Current Electrode Distance (AB/2) [m]

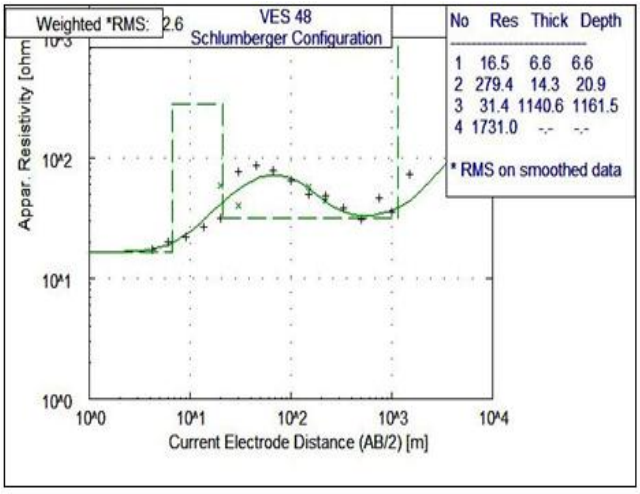
Weighted *RMS: 2.6
VES 48
Schlumberger Configuration
No Res Thick Depth
1 16.5 6.6 6.6
2 279.4 14.3 20.9
3 31.4 1140.6 1161.5
4 1731.0 -.- -.-
* RMS on smoothed data
Appar. Resistivity [ohm]
Current Electrode Distance (AB/2) [m]

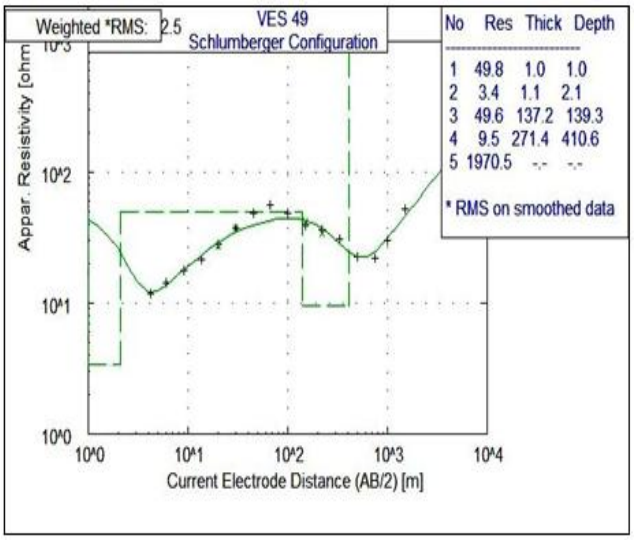
Weighted *RMS: 2.5
VES 49
Schlumberger Configuration
No Res Thick Depth
1 49.8 1.0 1.0
2 3.4 1.1 2.1
3 49.6 137.2 139.3
4 9.5 271.4 410.6
5 1970.5 -.- -.-
* RMS on smoothed data
Appar. Resistivity [ohm]
Current Electrode Distance (AB/2) [m]

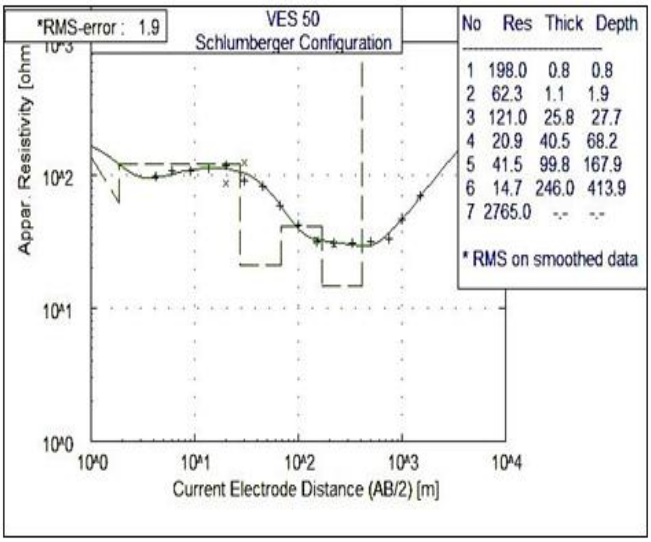
*RMS-error : 1.9
VES 50
Schlumberger Configuration
No Res Thick Depth
1 198.0 0.8 0.8
2 62.3 1.1 1.9
3 121.0 25.8 27.7
4 20.9 40.5 68.2
5 41.5 99.8 167.9
6 14.7 246.0 413.9
7 2765.0 -.- -.-
* RMS on smoothed data
Appar. Resistivity [ohm]
Current Electrode Distance (AB/2) [m]

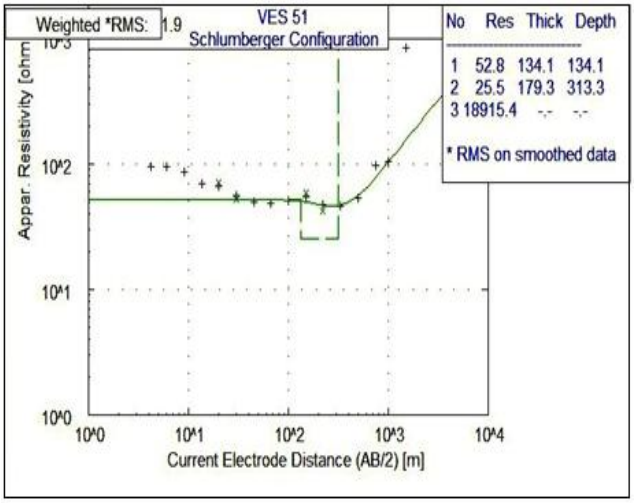
Weighted *RMS: 1.9
VES 51
Schlumberger Configuration
No Res Thick Depth
1 52.8 134.1 134.1
2 25.5 179.3 313.3
3 18915.4 -.- -.-
* RMS on smoothed data
Appar. Resistivity [ohm]
Current Electrode Distance (AB/2) [m]

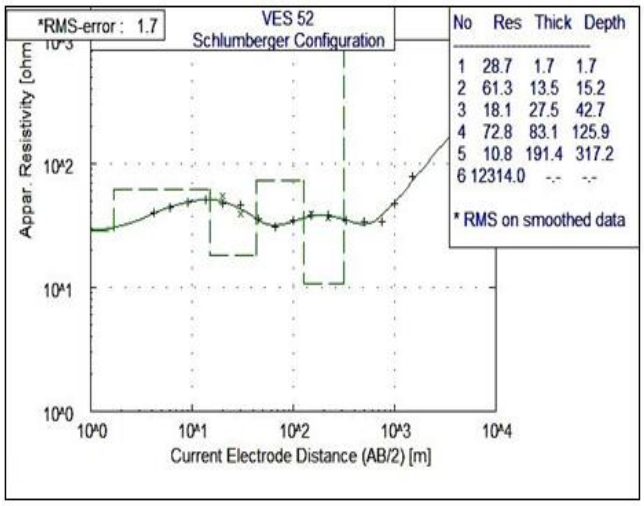
*RMS-error : 1.7
VES 52
Schlumberger Configuration
No Res Thick Depth
1 28.7 1.7 1.7
2 61.3 13.5 15.2
3 18.1 27.5 42.7
4 72.8 83.1 125.9
5 10.8 191.4 317.2
6 12314.0 -.- -.-
* RMS on smoothed data
Appar. Resistivity [ohm]
Current Electrode Distance (AB/2) [m]

Appendix 3 Resistivity of some common rocks, minerals and soils (Loke, 2004)

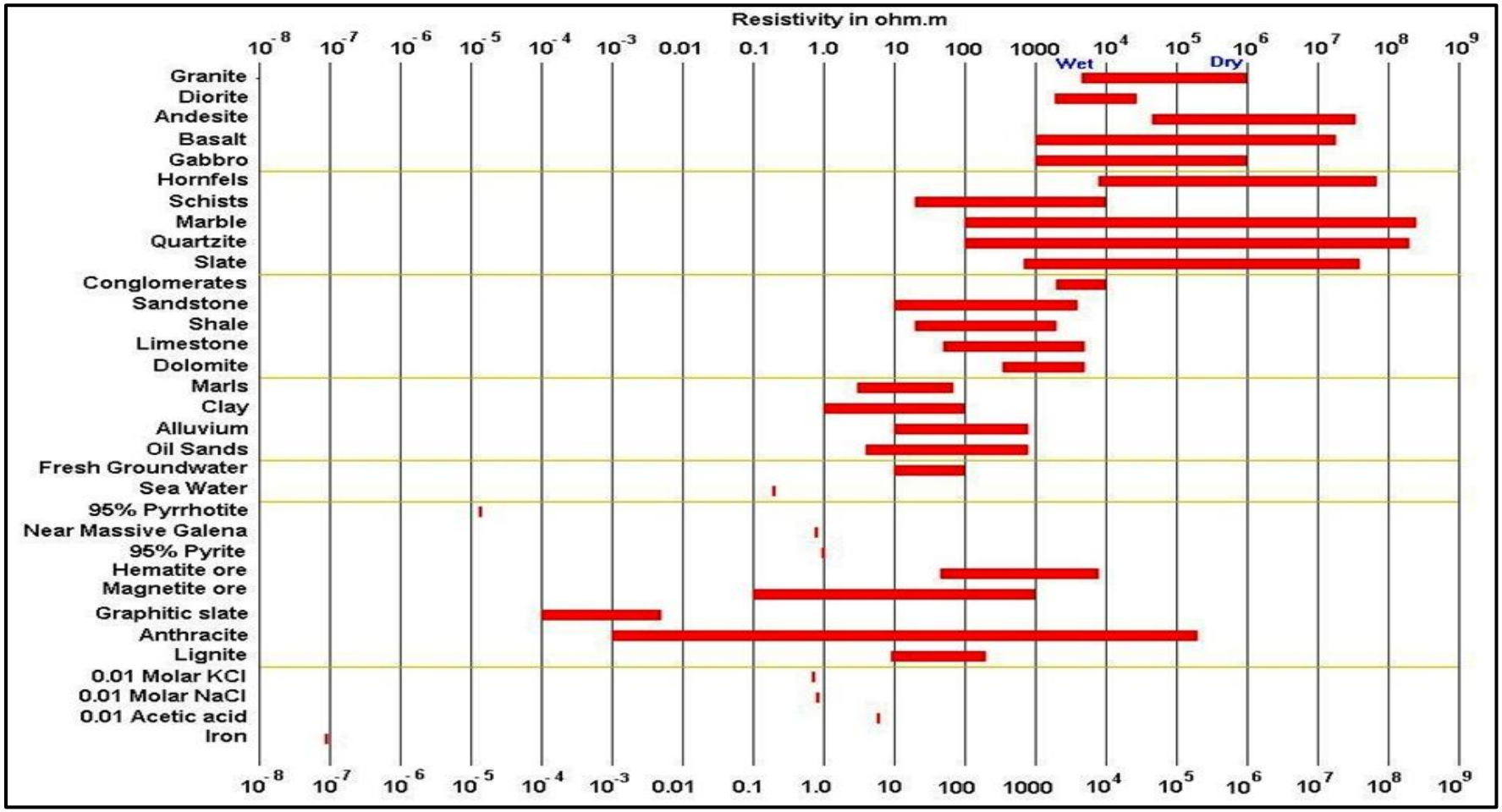

Appendix 4 Lithological description of bore hole (WWDSE, 2008)

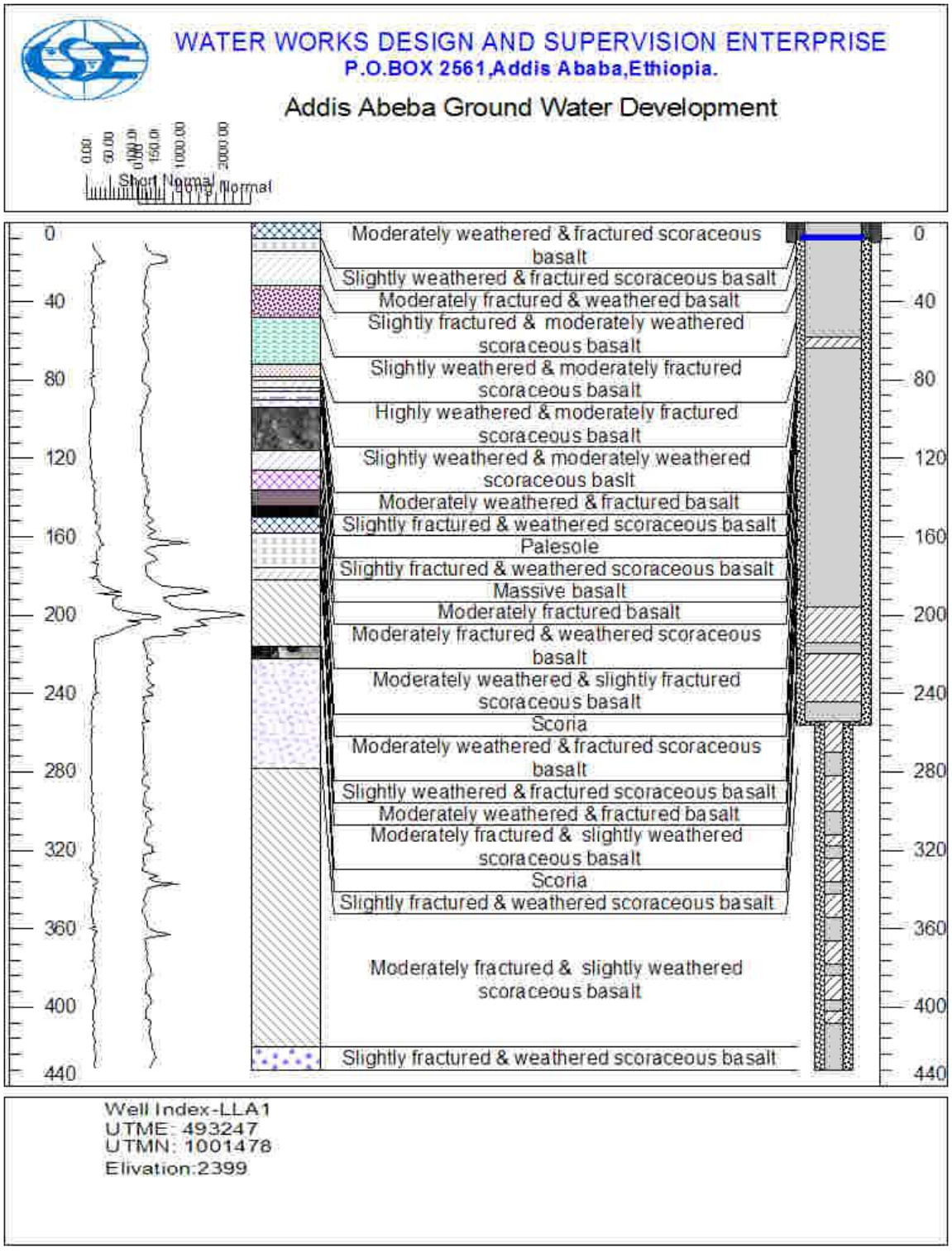

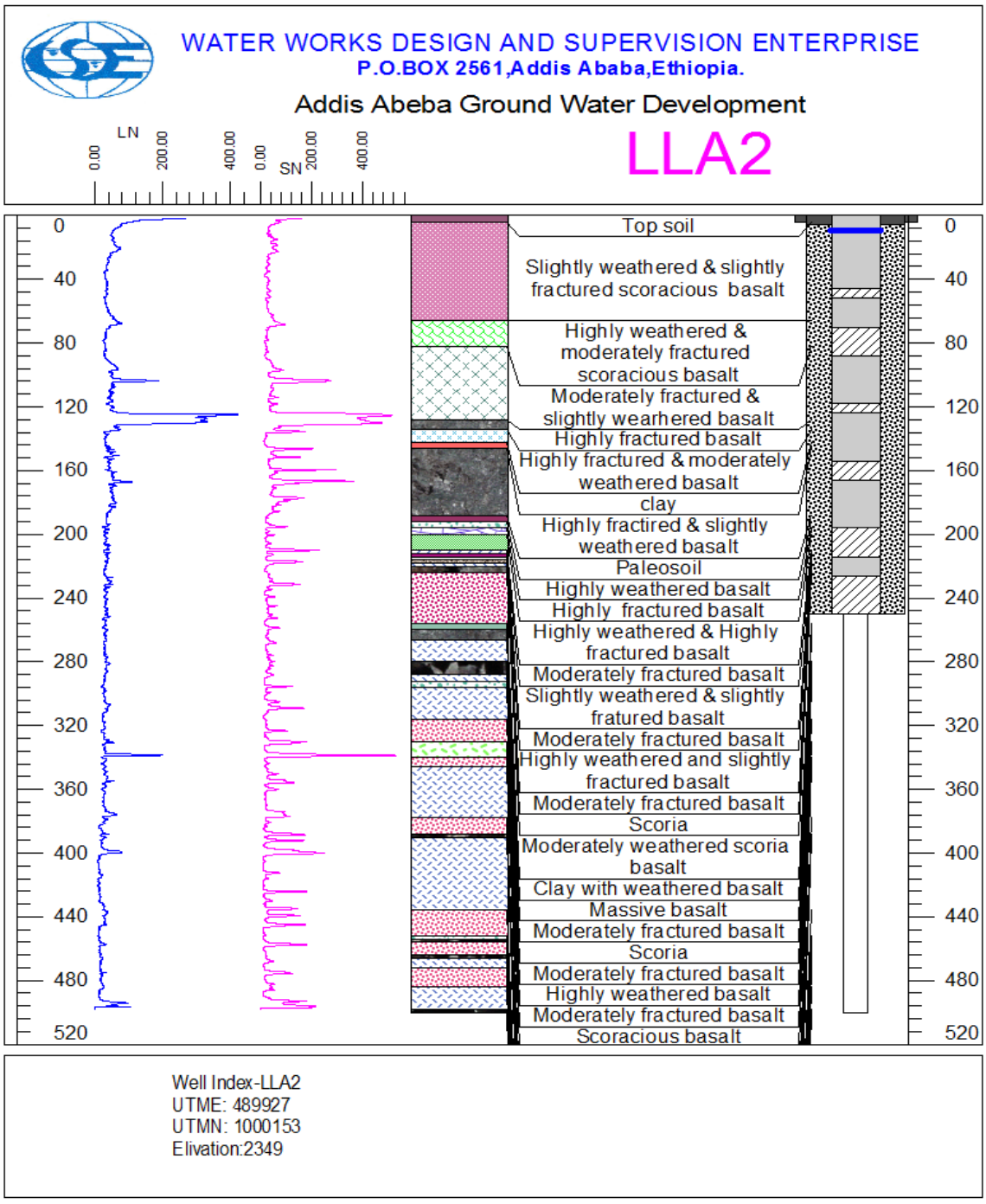
WATER WORKS DESIGN AND SUPERVISION ENTERPRISE
P.O.BOX 2561,Addis Ababa,Ethiopia.
Addis Abeba Ground Water Development
LLA2
LN
SN
0.00
200.00
400.00
0.00
200.00
400.00
0
40
80
120
160
200
240
280
320
360
400
440
480
520
Top soil
Slightly weathered & slightly fractured scoracious basalt
Highly weathered & moderately fractured scoracious basalt
Moderately fractured & slightly wearhered basalt
Highly fractured basalt
Highly fractured & moderately weathered basalt
clay
Highly fractired & slightly weathered basalt
Paleosoil
Highly weathered basalt
Highly fractured basalt
Highly weathered & Highly fractured basalt
Moderately fractured basalt
Slightly weathered & slightly fratured basalt
Moderately fractured basalt
Highly weathered and slightly fractured basalt
Moderately fractured basalt
Scoria
Moderately weathered scoria basalt
Clay with weathered basalt
Massive basalt
Moderately fractured basalt
Scoria
Moderately fractured basalt
Highly weathered basalt
Moderately fractured basalt
Scoracious basalt
Well Index-LLA2
UTME: 489927
UTMN: 1000153
Elivation:2349

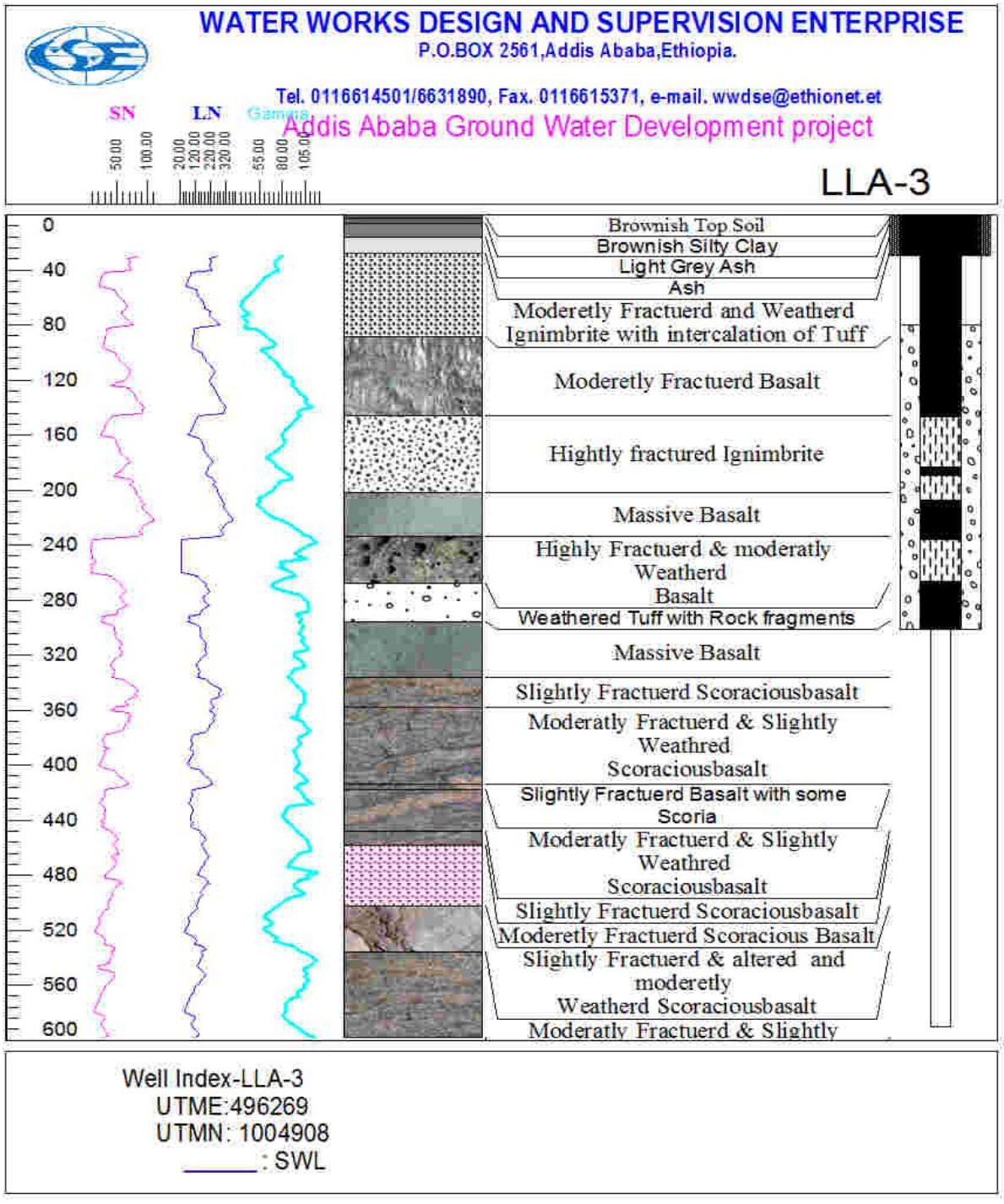
WATER WORKS DESIGN AND SUPERVISION ENTERPRISE
P.O.BOX 2561,Addis Ababa,Ethiopia.
Tel. 0116614501/6631890, Fax. 0116615371, e-mail. wwdse@ethionet.et
Addis Ababa Ground Water Development project
SN
LN
Gamma
LLA-3
0
40
80
120
160
200
240
280
320
360
400
440
480
520
560
600
Brownish Top Soil
Brownish Silty Clay
Light Grey Ash
Ash
Moderetly Fractuerd and Weatherd Ignimbrite with intercalation of Tuff
Moderetly Fractuerd Basalt
Hightly fractured Ignimbrite
Massive Basalt
Highly Fractuerd & moderatly Weatherd Basalt
Weathered Tuff with Rock fragments
Massive Basalt
Slightly Fractuerd Scoraciousbasalt
Moderatly Fractuerd & Slightly Weathred Scoraciousbasalt
Slightly Fractuerd Basalt with some Scoria
Moderatly Fractuerd & Slightly Weathred Scoraciousbasalt
Slightly Fractuerd Scoraciousbasalt
Moderetly Fractuerd Scoracious Basalt
Slightly Fractuerd & altered and moderetly Weatherd Scoraciousbasalt
Moderatly Fractuerd & Slightly
Well Index-LLA-3
UTME:496269
UTMN: 1004908
: SWL

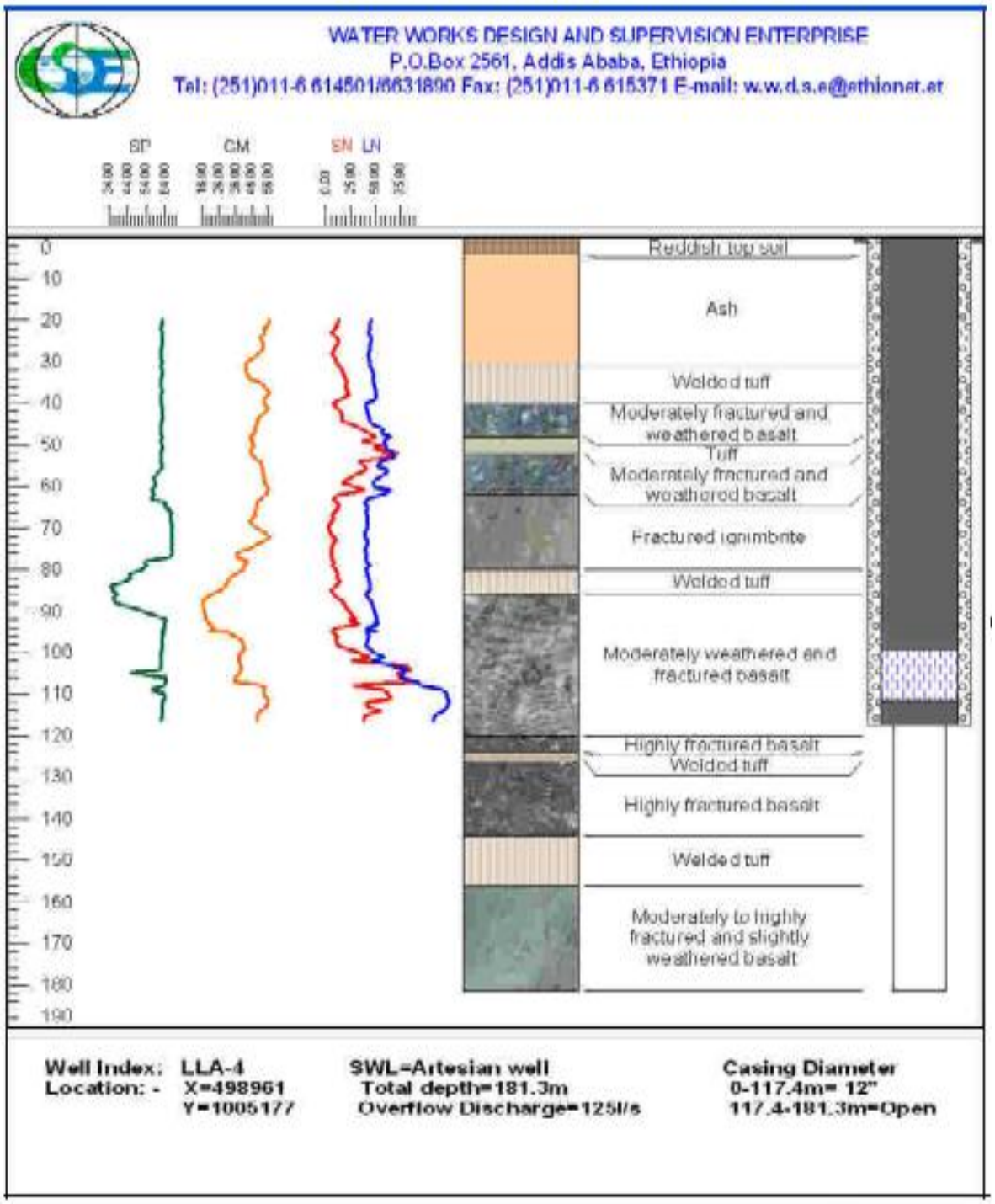
WATER WORKS DESIGN AND SUPERVISION ENTERPRISE
P.O.Box 2561, Addis Ababa, Ethiopia
Tel: (251)011-6 614501/6631890 Fax: (251)011-6 615371 E-mail: w.w.d.s.e@ethionet.et
SP
CM
SN
LN
Reddish top soil
Ash
Welded tuff
Moderately fractured and weathered basalt
Tuff
Moderately fractured and weathered basalt
Fractured ignimbrite
Welded tuff
Moderately weathered and fractured basalt
Highly fractured basalt
Welded tuff
Highly fractured basalt
Welded tuff
Moderately to highly fractured and slightly weathered basalt
Well Index: LLA-4
Location: - X=498961
Y=1005177
SWL=Artesian well
Total depth=181.3m
Overflow Discharge=12l/s
Casing Diameter
0-117.4m= 12"
117.4-181.3m=Open

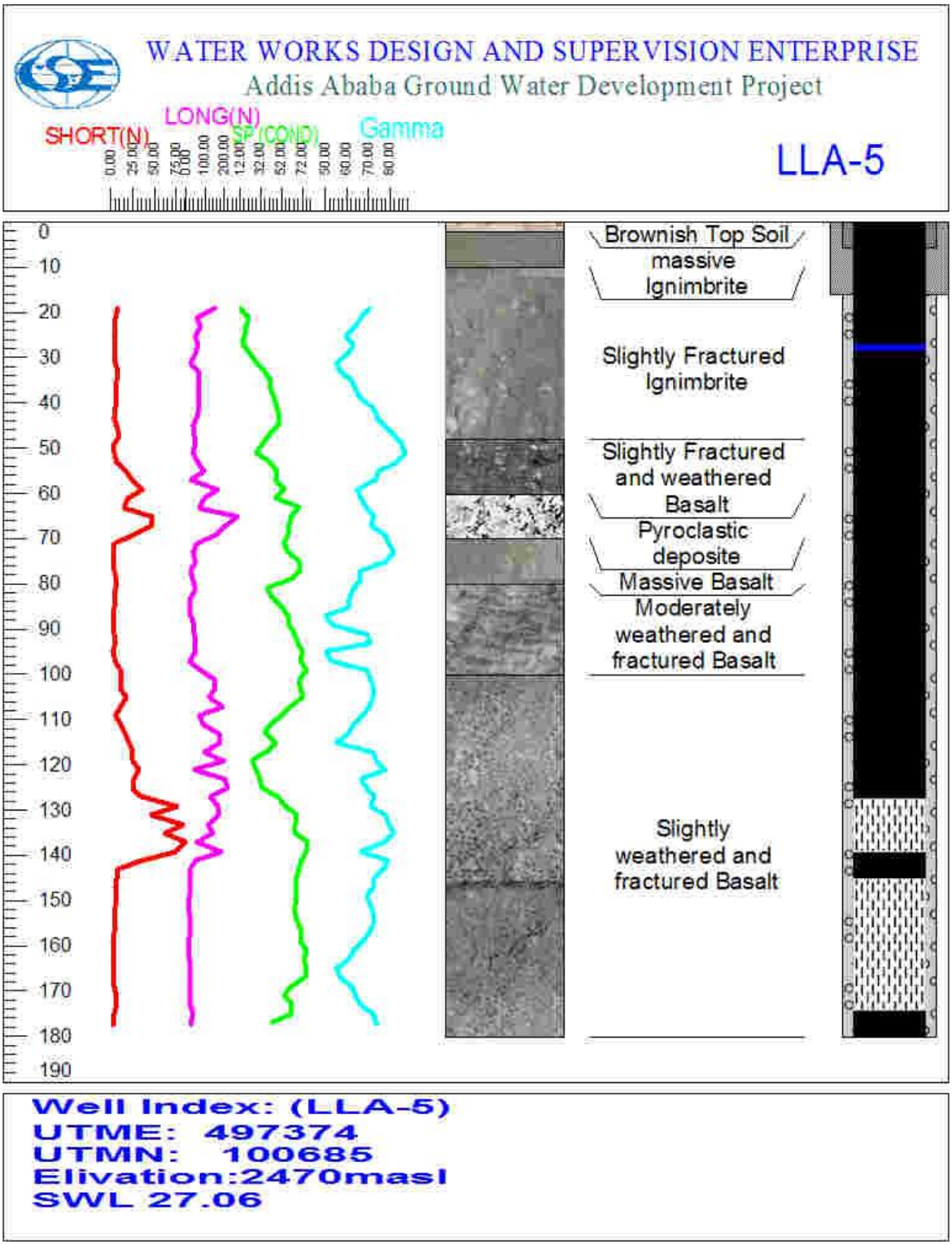
WATER WORKS DESIGN AND SUPERVISION ENTERPRISE
Addis Ababa Ground Water Development Project
SHORT(N)
LONG(N)
SP (COND)
Gamma
LLA-5
0
10
20
30
40
50
60
70
80
90
100
110
120
130
140
150
160
170
180
190
Brownish Top Soil
massive Ignimbrite
Slightly Fractured Ignimbrite
Slightly Fractured and weathered Basalt
Pyroclastic deposite
Massive Basalt
Moderately weathered and fractured Basalt
Slightly weathered and fractured Basalt
Well Index: (LLA-5)
UTME: 497374
UTMN: 100685
Elivation:2470masl
SWL 27.06

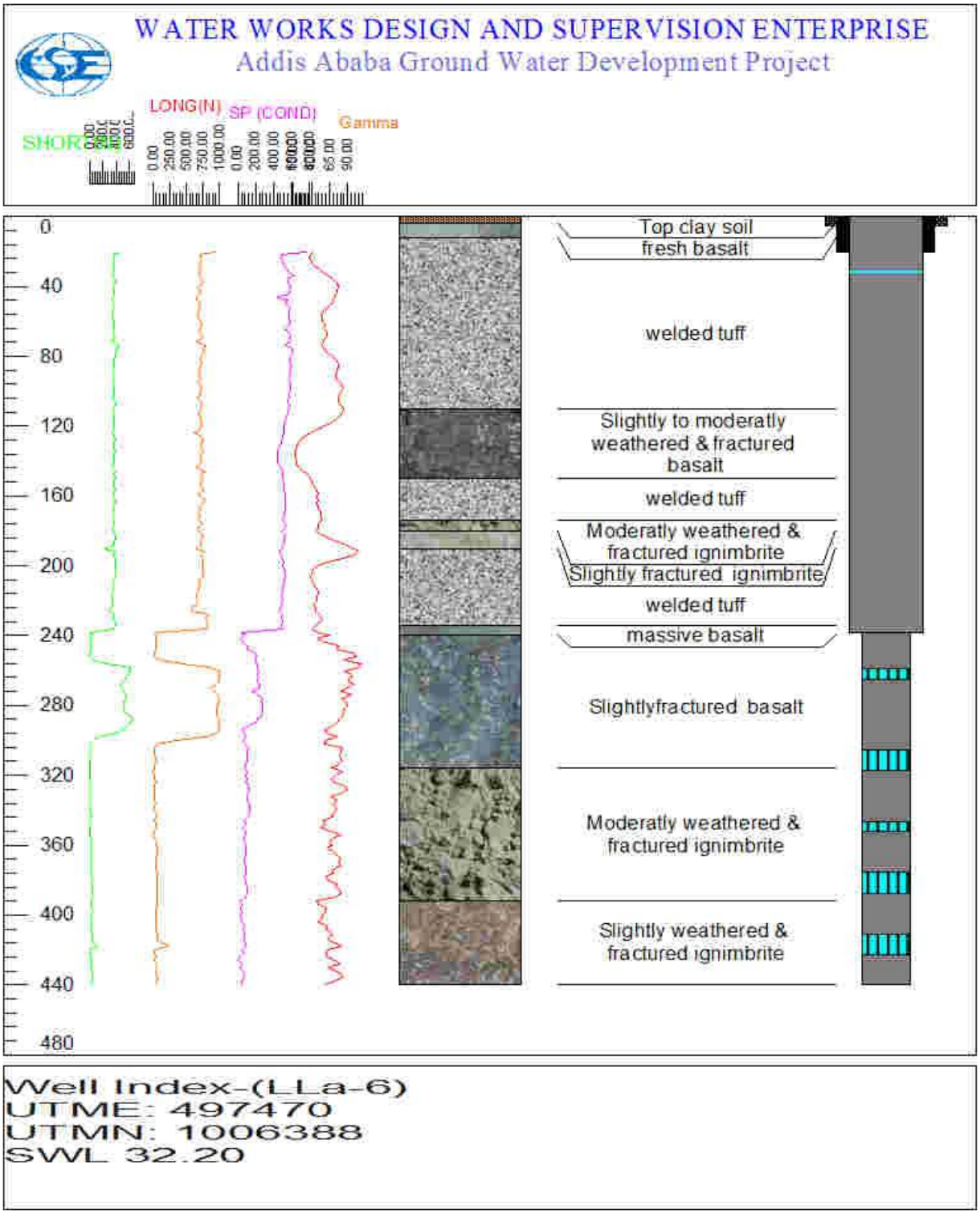
WATER WORKS DESIGN AND SUPERVISION ENTERPRISE
Addis Ababa Ground Water Development Project
LONG(N)
SP (COND)
Gamma
SHOR
0.00
250.00
500.00
750.00
1000.00
0.00
200.00
400.00
65.00
90.00
0
40
80
120
160
200
240
280
320
360
400
440
480
Top clay soil
fresh basalt
welded tuff
Slightly to moderatly weathered & fractured basalt
welded tuff
Moderatly weathered & fractured ignimbrite
Slightly fractured ignimbrite
welded tuff
massive basalt
Slightlyfractured basalt
Moderatly weathered & fractured ignimbrite
Slightly weathered & fractured ignimbrite
Well Index-(LLa-6)
UTME: 497470
UTMN: 1006388
SWL 32.20

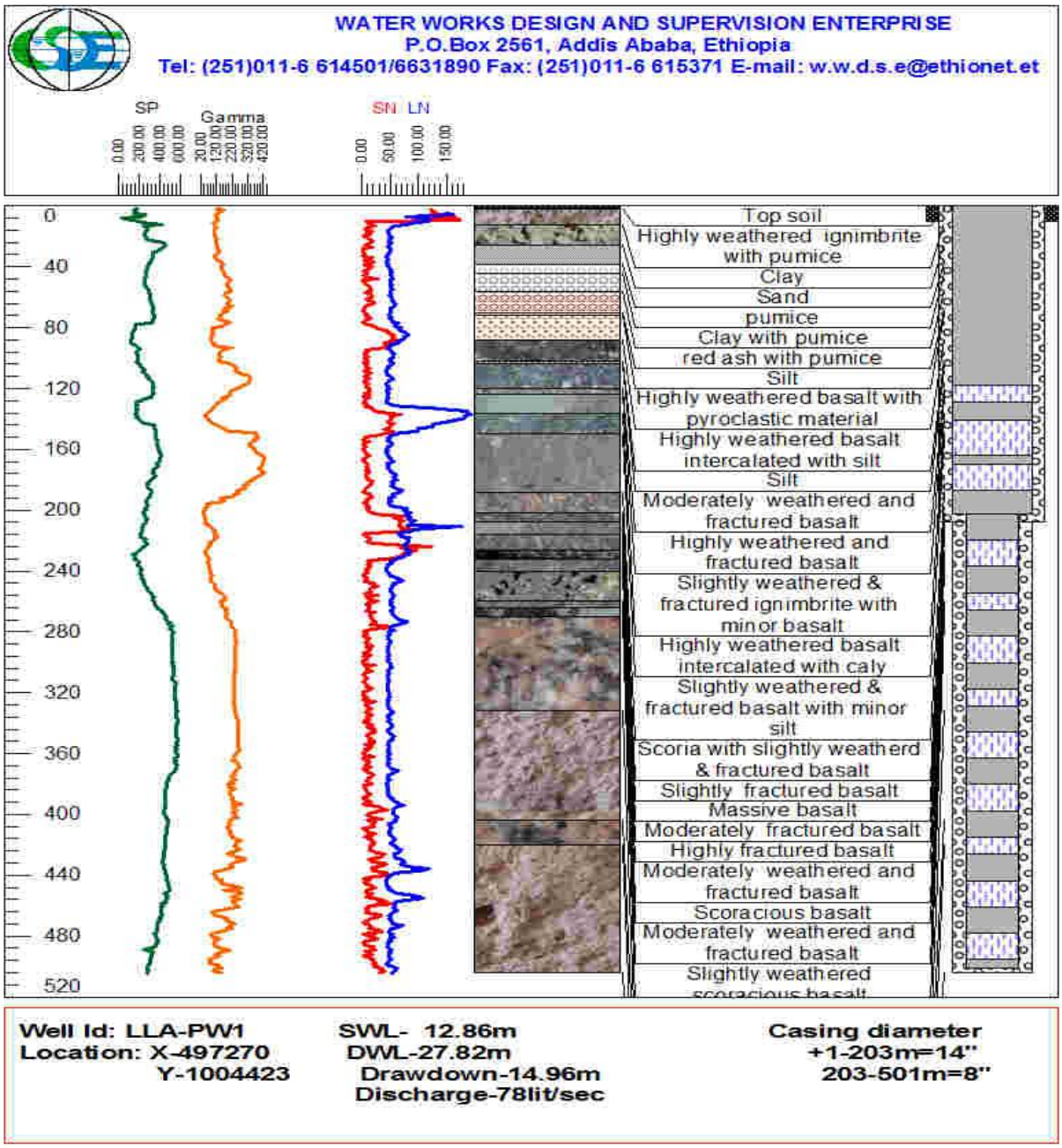
WATER WORKS DESIGN AND SUPERVISION ENTERPRISE
P.O.Box 2561, Addis Ababa, Ethiopia
Tel: (251)011-6 614501/6631890 Fax: (251)011-6 615371 E-mail: w.w.d.s.e@ethionet.et
SP
Gamma
SN LN
0.00 200.00 400.00 600.00
20.00 120.00 220.00 320.00 420.00
0.00 50.00 100.00 150.00
0 40 80 120 160 200 240 280 320 360 400 440 480 520
Top soil
Highly weathered ignimbrite with pumice
Clay
Sand
pumice
Clay with pumice
red ash with pumice
Silt
Highly weathered basalt with pyroclastic material
Highly weathered basalt intercalated with silt
Silt
Moderately weathered and fractured basalt
Highly weathered and fractured basalt
Slightly weathered & fractured ignimbrite with minor basalt
Highly weathered basalt intercalated with caly
Slightly weathered & fractured basalt with minor silt
Scoria with slightly weatherd & fractured basalt
Slightly fractured basalt
Massive basalt
Moderately fractured basalt
Highly fractured basalt
Moderately weathered and fractured basalt
Scoracious basalt
Moderately weathered and fractured basalt
Slightly weathered
Well Id: LLA-PW1
Location: X-497270
Y-1004423
SWL- 12.86m
DWL-27.82m
Drawdown-14.96m
Discharge-78lit/sec
Casing diameter
+1-203m=14"
203-501m=8"

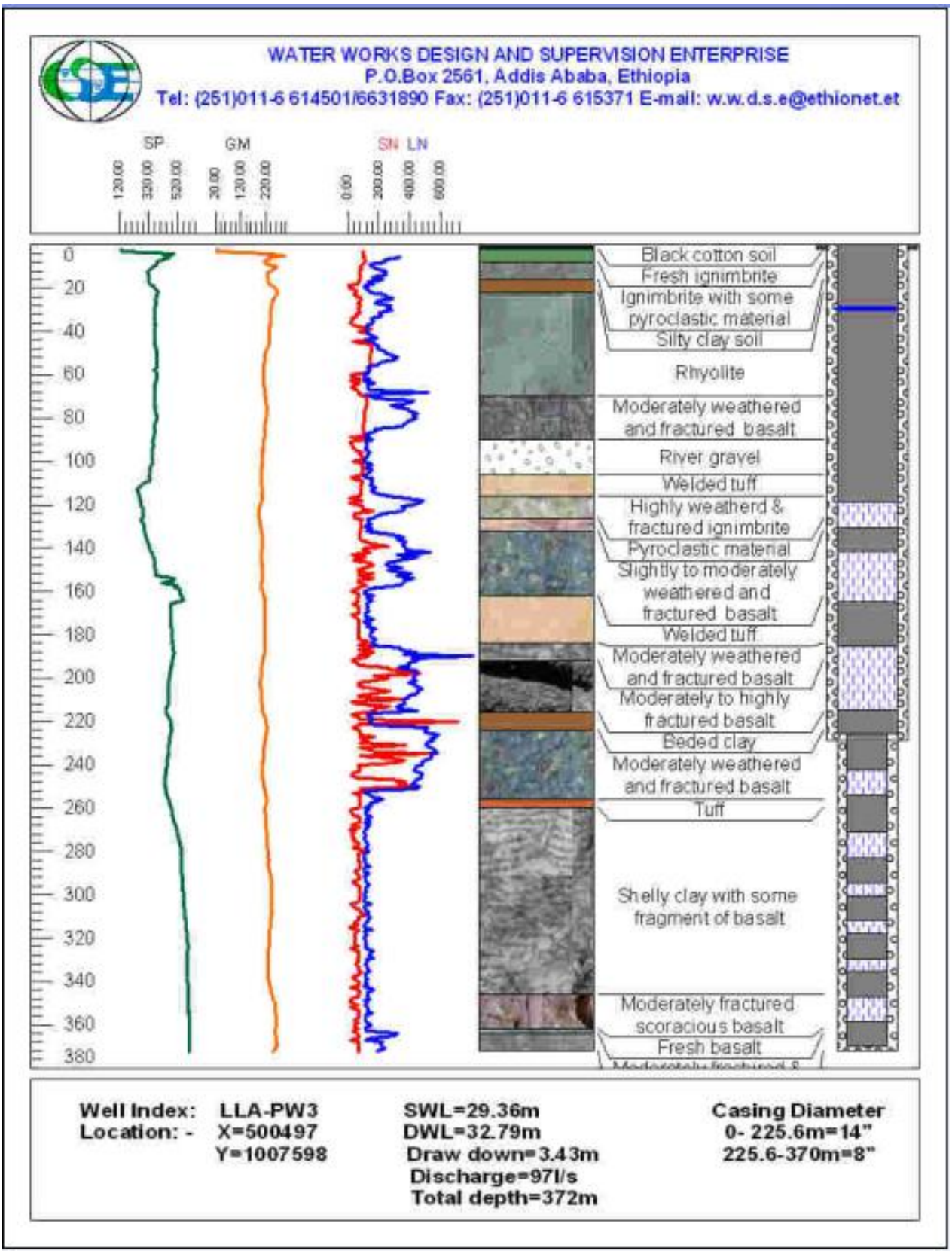
WATER WORKS DESIGN AND SUPERVISION ENTERPRISE
P.O.Box 2561, Addis Ababa, Ethiopia
Tel: (251)011-6 614501/6631890 Fax: (251)011-6 615371 E-mail: w.w.d.s.e@ethionet.et
SP
GM
SN LN
120.00 320.00 520.00
30.00 120.00 220.00
0.00 200.00 400.00 600.00
0 20 40 60 80 100 120 140 160 180 200 220 240 260 280 300 320 340 360 380
Black cotton soil
Fresh ignimbrite
Ignimbrite with some pyroclastic material
Silty clay soil
Rhyolite
Moderately weathered and fractured basalt
River gravel
Welded tuff
Highly weatherd & fractured ignimbrite
Pyroclastic material
Slightly to moderately weathered and fractured basalt
Welded tuff
Moderately weathered and fractured basalt
Moderately to highly fractured basalt
Beded clay
Moderately weathered and fractured basalt
Tuff
Shelly clay with some fragment of basalt
Moderately fractured scoracious basalt
Fresh basalt
Well Index: LLA-PW3
Location: - X=500497
Y=1007598
SWL=29.36m
DWL=32.79m
Draw down=3.43m
Discharge=97l/s
Total depth=372m
Casing Diameter
0- 225.6m=14"
225.6-370m=8"

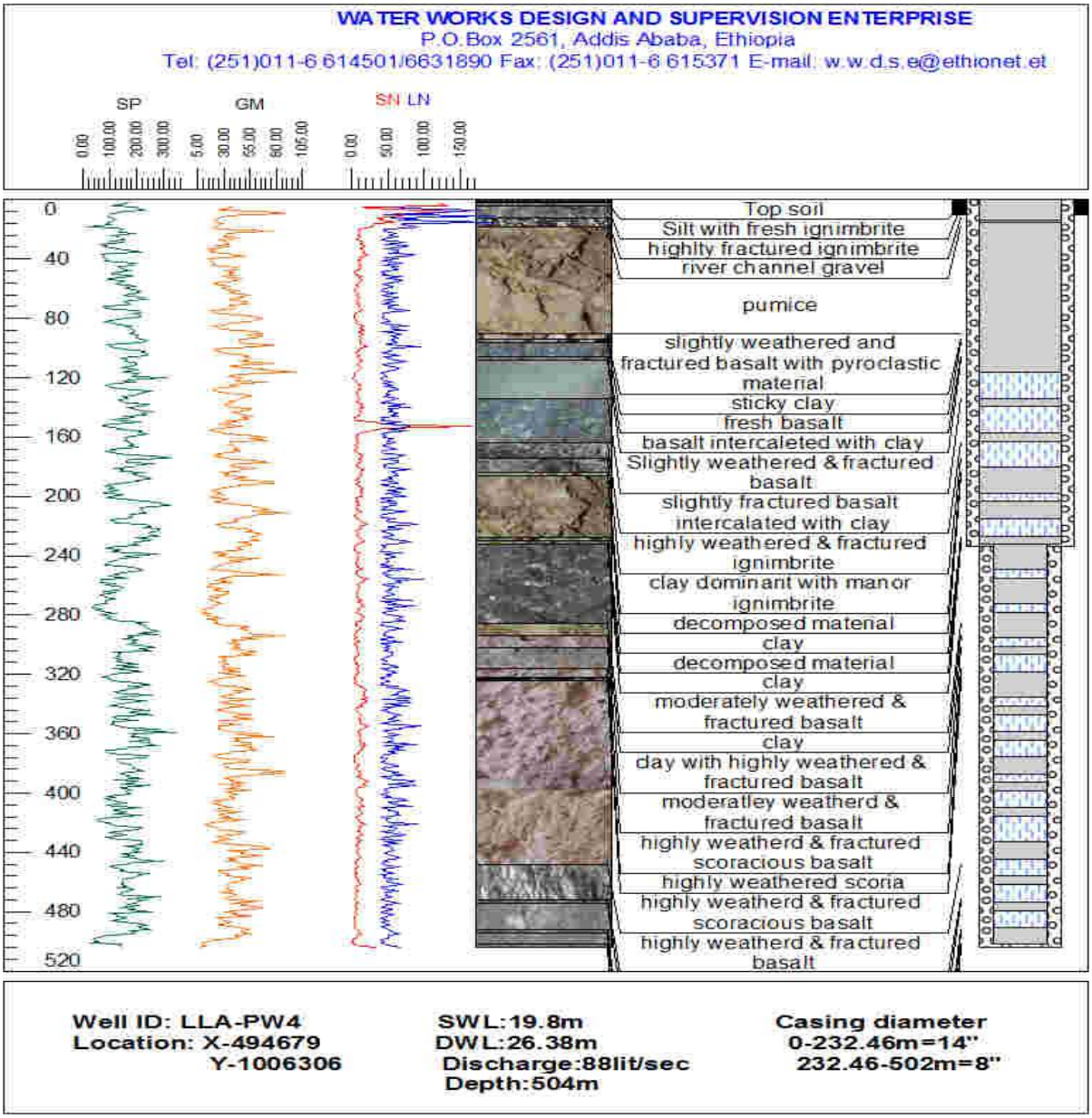
WATER WORKS DESIGN AND SUPERVISION ENTERPRISE
P.O.Box 2561, Addis Ababa, Ethiopia
Tel: (251)011-6 614501/6631890 Fax: (251)011-6 615371 E-mail: w.w.d.s.e@ethionet.et
SP
GM
SN LN
0
40
80
120
160
200
240
280
320
360
400
440
480
520
Top soil
Silt with fresh ignimbrite
highly fractured ignimbrite
river channel gravel
pumice
slightly weathered and fractured basalt with pyroclastic material
sticky clay
fresh basalt
basalt intercaleted with clay
Slightly weathered & fractured basalt
slightly fractured basalt intercalated with clay
highly weathered & fractured ignimbrite
clay dominant with manor ignimbrite
decomposed material
clay
decomposed material
clay
moderately weathered & fractured basalt
clay
day with highly weathered & fractured basalt
moderatley weatherd & fractured basalt
highly weatherd & fractured scoracious basalt
highly weathered scoria
highly weatherd & fractured scoracious basalt
highly weatherd & fractured basalt
Well ID: LLA-PW4
Location: X-494679
Y-1006306
SWL:19.8m
DWL:26.38m
Discharge:88lit/sec
Depth:504m
Casing diameter
0-232.46m=14"
232.46-502m=8"

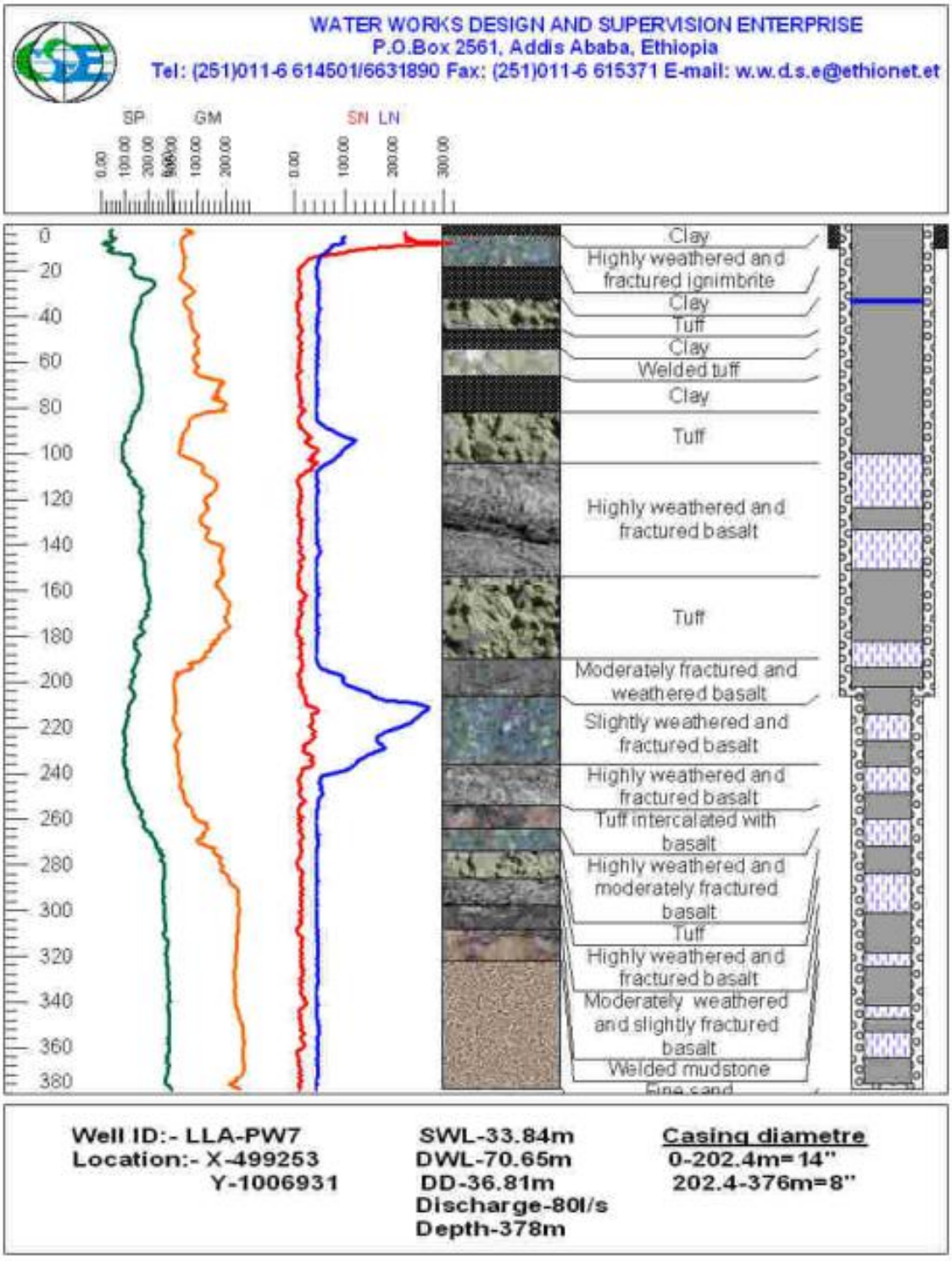
WATER WORKS DESIGN AND SUPERVISION ENTERPRISE
P.O.Box 2561, Addis Ababa, Ethiopia
Tel: (251)011-6 614501/6631890 Fax: (251)011-6 615371 E-mail: w.w.d.s.e@ethionet.et
SP
GM
SN
LN
Clay
Highly weathered and fractured ignimbrite
Clay
Tuff
Clay
Welded tuff
Clay
Tuff
Highly weathered and fractured basalt
Tuff
Moderately fractured and weathered basalt
Slightly weathered and fractured basalt
Highly weathered and fractured basalt
Tuff intercalated with basalt
Highly weathered and moderately fractured basalt
Tuff
Highly weathered and fractured basalt
Moderately weathered and slightly fractured basalt
Welded mudstone
Fine sand
Well ID:- LLA-PW7
Location:- X-499253
Y-1006931
SWL-33.84m
DWL-70.65m
DD-36.81m
Discharge-80l/s
Depth-378m
Casing diametre
0-202.4m=14"
202.4-376m=8"

Appendix 5 Magnetic **Susceptibilities of Rocks and Minerals**

Rock types	Maximum Volume Susceptibility (SI Units)
Igneous Rocks	
Andesite	0.17
Basalt	0.18
Dolerite	0.062
Diabase	0.16
Diorite	0.13
Gabbro	0.09
Norite	0.09
Dacite	0.05
Granite	0.05
Granodiorite/Tonalite	0.062
Peridotite	0.2
Quartz porphyries/Quartz-feldspar porphyries	0.00063
Pyroxenite/Hornblendite (Alaskan Type)	0.25
Rhyolite	0.038
Dunite	0.125
Trachyte/Syenite	0.051
Monzonite	0.1
Phonolite	0.0005
Spilites	0.0013
Avg. Igneous Rock	0.27
Avg. Acidic igneous rock (pegmatites)	0.082
Avg. Basic igneous rock (komatiites, tholeiite)	0.12

Metamorphic Rocks			
Amphibolite			0.00075
Gneiss			0.025
Granulite			0.03
Acid granulite			0.03
Basic granulite			0.1
Phyllite			0.0016
Quartzite			0.0044
Schist			0.003
Serpentine			0.018
Slate			0.038
Marble			0.025
Metasediments			0.024
Migmatites			0.025
Charnockite (pyroxene granulite)			0.03
BIF (anisotropic) hematite rich (~7% magnetite)			0.25
Magnetite rich (>20% magnetite)			1.8
Magnetite Skarn			1.2
Avg. Metamorphic Rock			0.073
Magnetite	~	0.1 %	0.0034
	~	0.5 %	0.018
	~	1 %	0.034
	~	5 %	0.175
	~	10 %	0.34
	~	20 %	0.72

Sedimentary Rocks	
Clay	0.00025
Coal	0.000025
Silt/Carbonates	0.0012
Dolomite	0.00094
Limestone	0.025
Red sediments	0.0001
Sandstone	0.0209
Shale	0.0186
Tuffs	0.0012
Conglomerate/arkose/pelites	0.0012
Arenites/Breccia	0.0012
Avg. Sedimentary rock	0.05